Evolution of the fresh water lens of Veermansplaat

A field and modelling investigation of the influence of a restricted tide on the evolution of a fresh water lens using Hydrogeosphere

A thesis presented
by

Freek Huijser
4261445

In partial fulfilment of the requirements
for the Master's degree of
Earth Sciences

Utrecht university
Utrecht, The Netherlands

Supervisor: prof. dr. Jasper Griffioen (Environmental Sciences)
2nd reader: dr. Thilo Behrends (Earth Sciences)

9 August 2019

Abstract

The Veermansplaat, located at the middle of saltwater lake Grevelingen in the Netherlands, has formed a fresh water lens since the embankment of lake Grevelingen in 1971. Rijksstructuurvisie Grevelingen en Volkerak-Zoommeer (RSV) has suggested a mitigation plan to stop the increasing anoxic concentrations in the former deep tidal channels by introducing a restricted tide of 50 cm in lake Grevelingen. This research investigates the historical and the future evolution of the fresh groundwater lens below Veermansplaat in a non-tidal and tidal system from 1971 to 2025 by conducting a field and model study using the fully integrated, physically based hydrological model Hydrogeosphere. The purpose of this research is to indicate the effect of a restricted tide on the evolution of the fresh water lens of Veermansplaat compared to the evolution without a tidal system. The first step of this research involves the analysis of infiltration rate, depth of the fresh-saline groundwater interface, chemical composition of the groundwater, the hydraulic head an historical data by using single ring infiltration, electrical resistivity tomography, groundwater sampling and automated groundwater level registration. The second step involves modelling the evolution of the fresh water lens for a tidal and non-tidal system using Hydrogeosphere. The fieldwork and historical data show a fresh water infiltration depth of -12 m NAP in 2019 and a varying infiltration depth along the island due to surface infiltration rate, vegetation and elevation variability. The models show a future lens shaped evolution of the fresh water lens between 2019 and 2025 for a non-tidal boundary condition. The introduction of a restricted tide will increase the mixing zones of the fresh water lens and will start a salinization of the coastline. The RSV is advised to take caution and to conduct further research of the effects on a restricted tide on the evolution of the fresh water lens of Veermansplaat using other modelling programs.

Keywords: Fresh water lens, Veermansplaat, Hydrogeosphere, restricted tide

Acknowledgement

I thank Jasper Griffioen for supervision, comment and suggestions on this research. Special thanks to Martin van der Weiden for his cooperation during the fieldwork and lab work. Further, I want to thank Marios Karaoulis from Deltares for the post-processing of the ERT data and Rijksstructuurvisie Grevelingen en Volkerak-Zoommeer for the opportunity to be part of the mitigation work sessions. My sincere thanks go to the personal at the Aquanty helpdesk for their fast and in-depth feedback on Hydrogeosphere related questions.

Table of Contents

List of figures

List of Tables

1. Introduction

The North Sea flood of 1953 caused by a spring tide and a European windstorm resulted in approximately 1836 deaths and major collateral damage in the South-western Netherlands (Gerritsen, 2005). This tragedy initiated the establishment of the Delta commission, which implemented the Delta Plan to negate the possibility of water-induced catastrophes (van den Hengel, 2006). One of the measures of this plan included the enclosure of the estuaries in the province of Zeeland (Blauw, Haas & Adriaanse, 2004). The closing of the estuaries in Zeeland resulted in an attenuation of the tides and a reduction of the intertidal area (Slim & Zonneveld, 2004). Although these measures brought benefits regarding the safety of the Netherlands, the passing of time also has shown the disadvantages of closing the estuaries of Zeeland. The natural processes and dynamics caused by the tidal influences of the sea became non-existing due to the embankments. This comes with the change in sedimentation and erosional patterns, an increase in the turbidity of the water column, eutrophication and the loss of estuarial specific habitats, flora and fauna (Slim & Zonneveld, 2004). The increase in nature and environmental consciousness of the Netherlands resulted in the 1970s in the adjustment of the Delta Plan in which the Oosterschelde remained an estuary with a flexible construction (Bijker, 2002). Starting 2004, 50 years after the North Sea flood, the negative effects of the Delta works have been recognized by the provinces of South-Holland, North-Brabant and Zeeland and it was decided to bring back the hydrological dynamics in the Delta (Blauw et al., 2004).

One of the closed estuaries of Zeeland is the “Grevelingen”. The major problem induced by the occlusion of the sea in Grevelingen is the occurrence of oxygen-free waters in the former, deep tidal channels. The “Rijksstructuurvisie Grevelingen en Volkerak-Zoommeer” (RSV) has started a research on mitigation measures to tackle this problem. This has resulted into the “Programma Ontwikkeling Grevelingen en Volkerak-Zoommeer” (POGV). The mitigation plan created by the RSV has been approved by the cabinet on October 2014 in which the following development perspective was projected for the Grevelingen: the Grevelingen will be reintroduced to a restricted tide of 50 cm by the passage of the Brouwersdam which connects the Grevelingen with the North Sea. The State additionally gives the opportunity to private parties for sustainable tidal energy (Tangelder et al., 2018).

Four major islands are present within the Grevelingen: Hompelvoet, Veermansplaat, Stampersplaat and Dwars in Den Weg. Each island has its own flora and fauna, including protected species. The current vegetation cover of the islands thrives on the fresh water lenses under these islands (Tangelder et al., 2018). These fresh water lenses have steadily grown over the years due the absence of tidal influences and the presence of abundant yearly rainfall (Stuyfzand Oskam & Van Loon, 2014). However, the fresh water lenses will become exposed to a hydraulically dynamic system due to the reintroduction of a restricted tide. This could lead to changes in the ecohydrology of the islands and thus the vegetation and fauna on the islands can also change.

The transition from a non-tidal to a tidal system for an inhabited island in a salt body of water is a rare research subject. Research on the evolution of fresh water lenses primarily focuses on islands already affected by a tidal system (Fetter Jr, 1972; White & Falkland, 2010; Pauw et al., 2012; Sulzbacher et al., 2012; Holding & Allen, 2015). Research involving the change of the tidal system primarily focus on the effect of sea-level rise (Pauw et al., 2012; Sulzbacher et al., 2012) or wave overwash (Holding & Allen, 2015) on the fresh water lenses. Therefore, this research can give new insight on the hydro(geo)logical principles of the evolution of fresh water lenses.

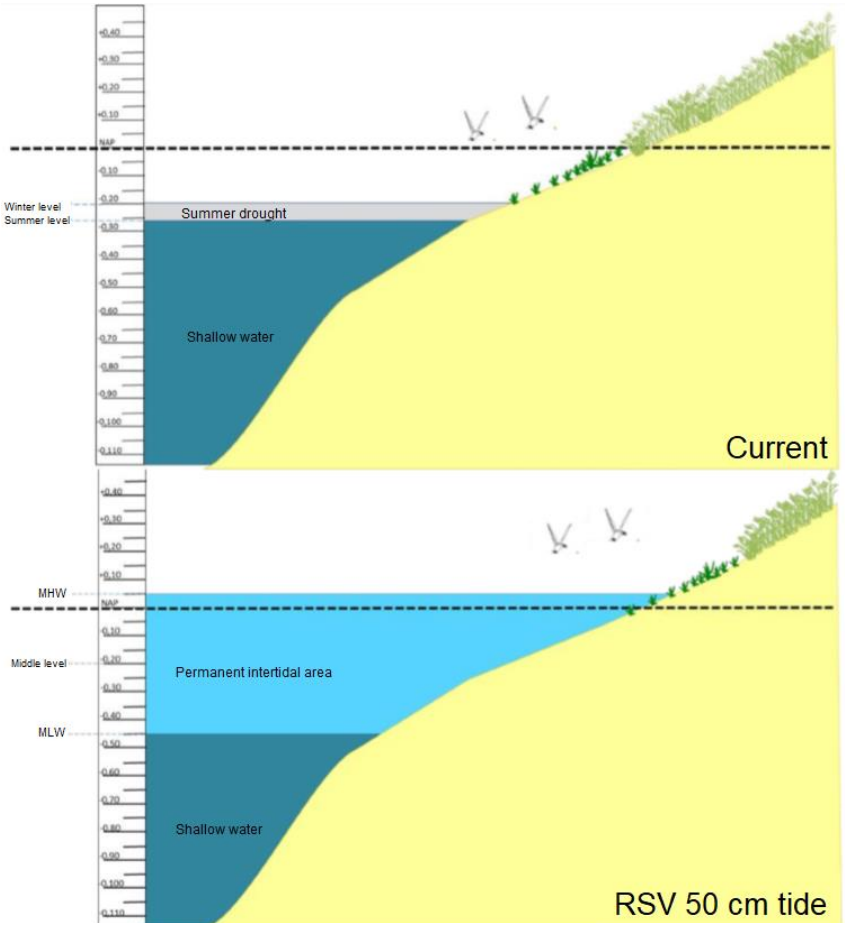

Figure 1, Tidal scenario of the Rijksstructuurvisie Grevelingen en volkerak-zoommeer (RSV) (Tangelder et al. 2018)

To predict the changes of the fresh water lenses of the islands in the Grevelingen as induced by the reintroduction of a restricted tide of 50 cm (figure 1), a hydrological study should be done at Veermansplaat. The aim is to define the evolution of the fresh water lens from 1972 to 2019 due to the enclosure of the Grevelingen and to predict the future change of the fresh water lens induced by the reintroduction of a restricted tide of 50 cm.

This research has the following research question and sub questions:

What is the influence of the reintroduction of a restricted tide on the fresh water lens of Veermansplaat in the Grevelingen, the Netherlands?

- How much has the fresh water lens of Veermansplaat evolved in the period of 1971-2019?
  - What is evolution of the fresh water lens according to historical data?
  - What is the current shape of the fresh water lens according to field measurements?
  - What is the shape of the fresh water lens using Hydrogeosphere?

- How will the fresh water lens of Veermansplaat evolve in the period of 2019-2025?

This research involves fieldwork, lab work and modelling. To predict the evolution of the fresh water lens the modelling program Hydrogeosphere was used. The change in the fresh-saline groundwater interface was the focus of this research.

2. Background information

This chapter provides information on fresh water lenses and the study area. This information serves as a base to understand the method and results of this research.

2.1. Fresh water lenses

A fresh water lens is defined by a convex body of fresh groundwater underlain by groundwater with a significant higher salinity (Pauw, 2015). Although a fresh water lens is an 3D structure, often a cross sectional view is used to visualize the lens as depicted in figure 2. A fresh water lens (figure 2) is bounded by a draining feature (e.g. stream, canal or marine water) which indicates the width of the fresh water lens (L). The fresh water lens, the mixing zone and salt water body can be defined using the salinity of the groundwater. The thickness of the fresh water lens (H) is defined by the depth of fresh groundwater relative to the sea level and consist of only fresh water (Pauw, 2015). The thickness of the fresh water lens is primary controlled by the ratio of the recharge rate and the hydraulic conductivity of the island when the fresh water lens is not in equilibrium (Schneider & Kruse, 2005).

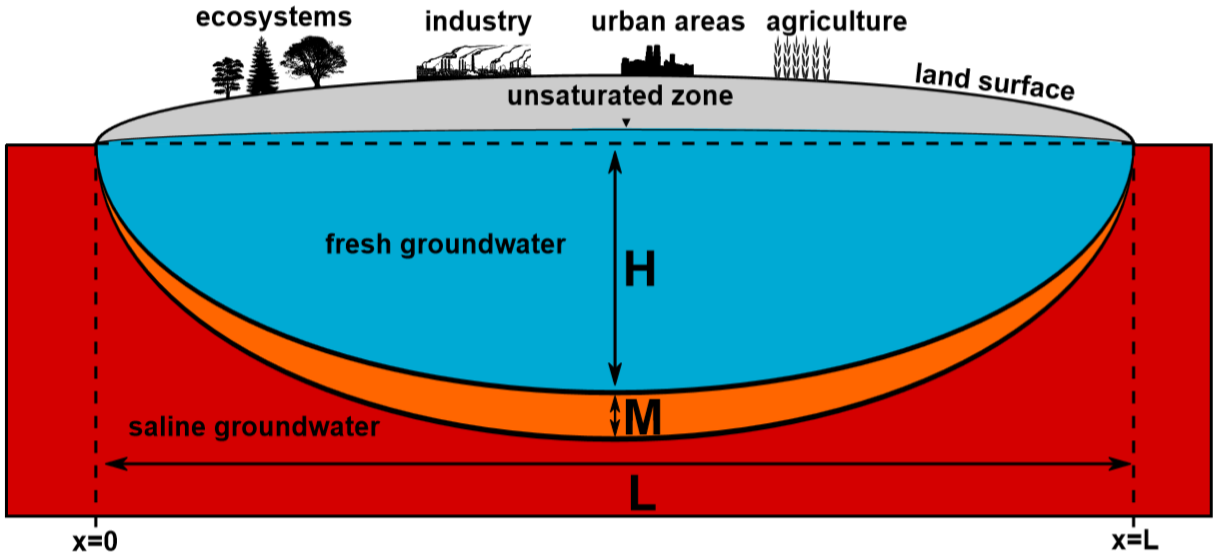

Figure 2, Vertical cross section of a fresh water lens (Pauw, 2015)

The transition zone (M) is positioned between the fresh water lens and the salt water body, where the groundwater salinity increases from fresh groundwater to the maximum salinity of the saline groundwater. Ideally, the saline groundwater has a homogeneous and maximum salinity and is positioned around the transition zone and fresh water lens (Pauw, 2015). In the 19th and early 20th century, Du Commun (1828), Badon Ghyben (1889) and Herzberg (1901) formulated the principle of fresh groundwater floating on top of a salt water body with the Ghyben-Herzberg equation (figure 3; equation 1). The Ghyben-Herzberg principle estimates the depth of the fresh water lens at equilibrium relative to the sea level (H). Therefore, it uses the groundwater level relative to the sea level (h) and the densities of fresh (ρ_f) and saline water (ρ_s).

$$h_\infty = \frac{\rho_s - \rho_f}{\rho_f} H_\infty \qquad (1)$$

where h_∞ is the elevation of the groundwater level in equilibrium over an infinite time [m], H_∞ is the depth of the fresh water lens in equilibrium over an infinite time [m], ρ_s is the density of saline water [kg m^{-3}] and ρ_f is the density of fresh water [kg m^{-3}].

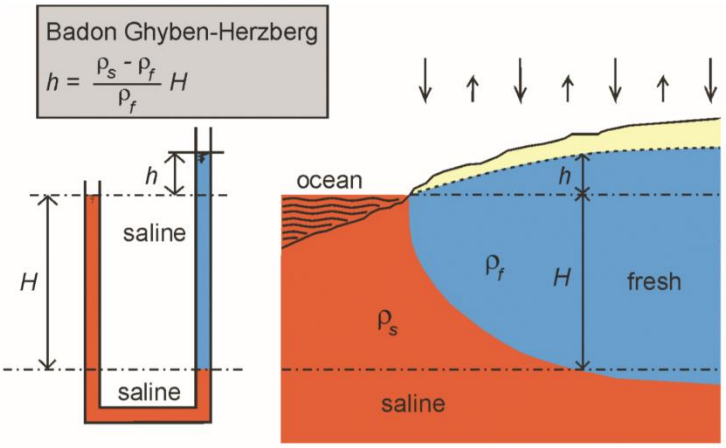

Figure 3, Visualization of the Ghyben-Herzgerg principle (Pauw, De Louw & Oude-Essink, 2012)

The Ghyben-Herzberg equation estimates the depth of a sharp fresh-salt groundwater interface which does not occur in reality. Dispersion along the fresh-salt groundwater interface is the primary cause for the origin of the transition zone. The dispersion is activated by (a) normal circulation patterns of the fresh water lens, (b) natural changes of the salt groundwater flow, (c) natural changes in the shape of the fresh water lens due to erosion, accretion of the surface structure and long term sea level or precipitation changes due to climate change and (d) anthropogenic interference (Stuyfzand, 1993).

2.2. Hydrogeosphere

Hydrogeosphere is a fully integrated, physically based hydrological model. To accomplish an integrated hydrological analysis, Hydrogeosphere couples a two-dimensional (2D), depth integrated diffusion-wave approximation of the Saint Venant equation for surface water flow (Viessman & Lewis, 1996) and a three-dimensional (3D) saturated and unsaturated approximation by using a modified form of the Richards equation for subsurface flow (Aquanty inc., 2016; Brunner & Simmons, 2012; Erler et al., 2019). Hydrogeosphere originates from the code FRAC3DVS, developed by R. Therrien at University of Wageningen (Therrien, 1992). Hydrogeosphere is written in FORTRAN and can be used on Linux and Windows operation 32- and 64-bit systems. Hydrogeosphere does not use a graphical user interface, but instead uses a three-step process executable. This involves the pre-processor program GROK, Hydrogeosphere and the postprocessor program HSPLOT (Brunner & Simmons, 2012).

Hydrogeosphere is capable to simulate the fluid flow including the hydrological cycle by using an integrated code with the physics of surface and subsurface flow. This includes the accounting of all the components of the water budget, water levels, unsaturated flow, delayed yield, ponding, seepage and vertical flow. The inclusion of mass and thermal energy transport in Hydrogeosphere makes it possible to compute and simulate the transport of non-reactive and reactive chemicals, including straight or branching decay chains and the interaction of chemicals with the surface and subsurface (Aquanty inc., 2016; Brunner & Simmons, 2012). The calculation of temperatures for surface and subsurface is driven by air temperatures and solar radiation. The programming of Hydrogeosphere results in multiple numerical methods that can be used. This involves the possibility of strong interactions between hydrological systems due to the fully-implicit coupling approach, advanced computational algorithms, balance tracking and adaptive time stepping (Aquanty inc., 2016).

2.3. Single ring infiltration

Single ring infiltration is a method to measure the field-saturated conductivity and matrix flux potential at field saturation. Single ring infiltration measures the infiltration rate of a column water in a cylindrical ring which is partly inserted into the ground. Traditionally the single ring infiltration uses a constant ponded head and steady state flow conditions. A constant ponded head is easy to maintain and the analysis of the measurement is not complex, but this approach needs the value of the field-saturated conductivity or matrix flux potential at field saturation to be known. Another approach is by using a falling head to measure the infiltration rate. This approach does not need the field-saturated conductivity or matrix flux potential at field saturation to be known. However, this method is less suitable to estimate the matrix flux potential at field saturation (Elrick et al., 2014; Stewart & Abou Najm, 2018).

Equations 2 and 3 (Stewart & Abou Najm, 2018) and the cumulative infiltration approach (Di Prima et al., 2019; Zhang, 1997) can be used to calculate the field-saturated soil hydraulic conductivity from the infiltration rates using single ring infiltration with a falling head. This method uses a fixed value of λ = 150 mm, excluding the need to measure the macroscopic capillary length (Di Prima et al., 2019), which can be interpreted as the measure of the effects of capillarity as opposed to gravity in the field (Saefuddin, Saito & Šimůnek, 2019).

$$K_{fs} = \frac{c_2}{a\left(\frac{h_{source}+\lambda}{G*}+1\right)} \qquad (2)$$

$$G^* = d + \frac{r_d}{2} \qquad (3)$$

where K_{fs} is the field-saturated soil conductivity [m s^{-1}], c_2 is the infiltration coefficient of the cumulative infiltration against the squared time [-], a is the dimensionless constant (0.45), h_{source} is the established ponding depth of the water in the infiltration test tube, λ is the macroscopic capillary length [m], d is the ring insertion depth into the soil [m], r_d is the inner radius of the ring [m] and G* is the ring geometry of the infiltration setup [m].

2.4. Research area

Veermansplaat is positioned in the centre of Lake Grevelingen in the south western Netherlands (figure 4). During the Roman period, the sea level rise flooded the former peat channels and large rivers in the Grevelingen, which resulted in the Grevelingen becoming an estuary. For centuries, the rivers transported sand and clay to the Grevelingen where the tidal currents induced the deposition locations. This system caused the creation of multiple tidal flats and salt marshes (Hoeksema, 2002). The fluvial and tidal influence on the Grevelingen stopped since the construction of the Grevelingendam in 1965 (southeast of the Grevelingen, stopping the fluvial influences) and the Brouwersdam in 1971 (west of the Grevelingen, stopping the tidal influences). The absence of tides caused the tidal flats and salt marshes to transition from an intertidal to a non-tidal situation. A sluice was installed in the Brouwersdam in 1979 to prevent the freshening of the lake water due to a precipitation surplus.

Lake Grevelingen has a water surface area of 10800 ha and a volume of $575*10^6$ m^3 (Hoeksema, 2002). The average depth of the lake is 5.4 m and the maximum depth is 48 m in the fairway (Hoeksema, 2002; Withagen, 2000). The water level is regulated at -0.20 m NAP (Normaal Amsterdams Peil; a vertical datum based on the sea level) with a lowering to -0.26 m during the summer period to stimulate nestling of birds in the Grevelingen (Hoeksema, 2002; MLNV, 2017; Tangelder et al., 2018).

Lake Grevelingen is a stagnant saltwater lake and therefore regulated to meet the pre-determined norm on chloride concentration in the lake. The salt concentration is kept at a minimum of 16 g Cl/L. Oxygen, nitrogen and phosphate concentration are measured on daily to monthly base (Hoeksema, 2002).

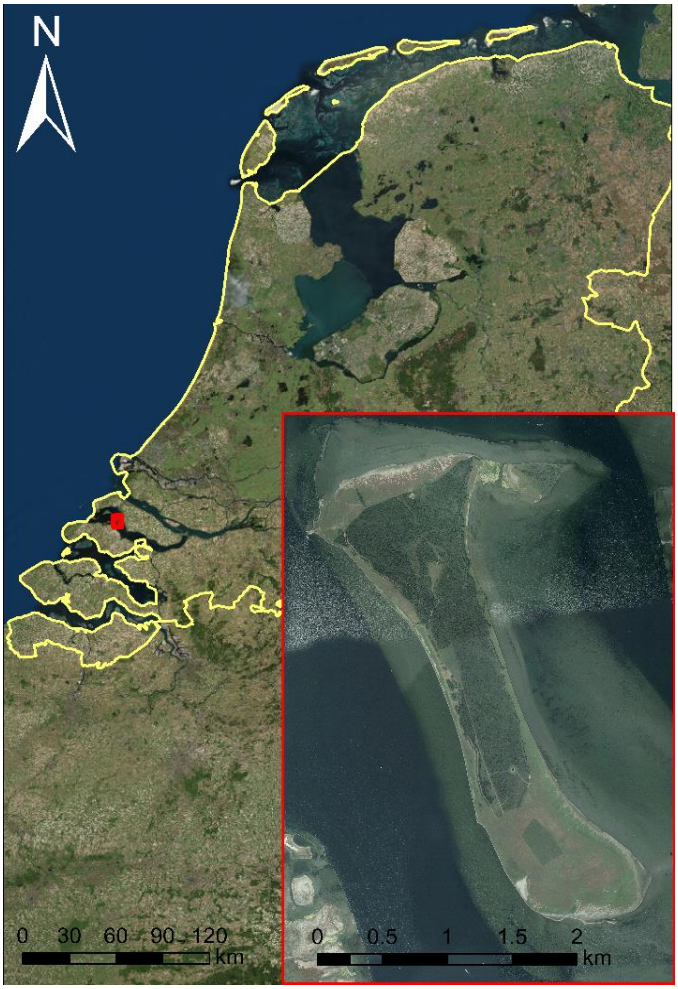

Figure 4, Location of Veermansplaat in The Netherlands

The research takes place on Veermansplaat, one of the four major islands within the Grevelingen. Veermansplaat is an uninhabited island with a length of approximately 4000 m, a width ranging from 530 to 1400 m and a surface area of 3,700,000 m^2. The surface height of the island varies between -0.20 m NAP and 0.65 m NAP with the exception of several sand dikes of c. 2.5 m NAP. Veermansplaat has a sea climate with soft winters and timid summers. The temperature averages between 10.5 – 10.8 °C through the year with an average maximum between 6.9 – 7.2°C and an average minimum between 13.8 – 14.1°C (KNMI as cited in Stuyfzand et al., 2014).

The island is a fixed sandbar with some silt and clay layers (figure 5; Slager en Visser, 1990). The soil formation on Veermansplaat consists of the accumulation of biomass and presence of small peat formation between the sand ridges (Stuyfzand et al., 2014). Due to the tidal system before 1971, Veermansplaat originally has a calcium carbonate content of approximately 4.2 - 5.5 % within the upper 15 cm of the subsurface. However, since the closing of lake Grevelingen in 1971 the surplus of rainfall on the island slowly leaches the calcium carbonate in the soil (Visser, 1995). At the border of Veermansplaat, upward seepage causes the deposition of secondary calcium carbonate (Van Haperen,

2009), which favours the growth of young dune slack vegetation and Fen orchid (Van de Haterd et al., 2010).

The specific hydrogeological situation of Veermansplaat where fresh and saline water is present which results in a varied distribution of fresh- and brackish-favourable water vegetation. The north and south side of the island have a brackish environment with rainfall, upward fresh water seepage, salt spray and wind set-up (Van Haterd, 2010). Therefore, we see low-standing, halophilic pioneer vegetation at these locations. The inland of Veermansplaat is bordered by an aeolian sand ridge and is defined by high thicket (De Kraker, 2012).

Although Veermansplaat is an uninhabited island, multiple fortifications and management by humans have been executed over the lifetime of the island. To prevent erosion of the island by waves due to wind surges and lake currents, a foreshore defence was built in the 1990s (Van de Haterd, 2010). After the absence of tide, wind erosion took place which was counteracted by the placement of aeolian sand ridges in the centre of the island and weaving straw into the ground at the south of the island (Hoeksema, 2002), which both are still visible on the island. Furthermore, the entire island has always been grazed by oxen and/or horses and is annually mowed at the south side of Veermansplaat (Hoeksema, 2002; Van Haperen, 2009).

The hydrological base of Veermansplaat is located at -215 m NAP at the top of the Mid Oligocene Rupel Formation. The low permeable Late Oligocene and Early Pliocene Breda and Late Miocene and Pliocene Oosterhout Formations are situated on top of the Rupel Formation ranging from c. -90 to -215 m NAP and consist of marine silty sand and clay layers. The Early Pleistocene Maassluis and Pleistocene Peize Formation are situated between c. -90 to -30 m with on top the Holocene Naaldwijk Formation which continues to the ground surface of Veermansplaat. The Maassluis, Peize and Naaldwijk Formations consist mainly of sand with discontinuous loam and clay layers between -50 to -60 m NAP and -30 to -35 m NAP (Stuyfzand et al., 2014; TNO, 2019a; TNO, 2019b). Research by Stuyfzand et al. (2014), shows an alternation of fine to moderately coarse sand with a corresponding median grain size of 245 µm for the Naaldwijk Formation. Figure 5 shows the presence of local clay and mud layers within the first 2 m of the subsurface along the coastline of Veermansplaat as the result of the tidal system on Veermansplaat (Slager & Visser, 1990).

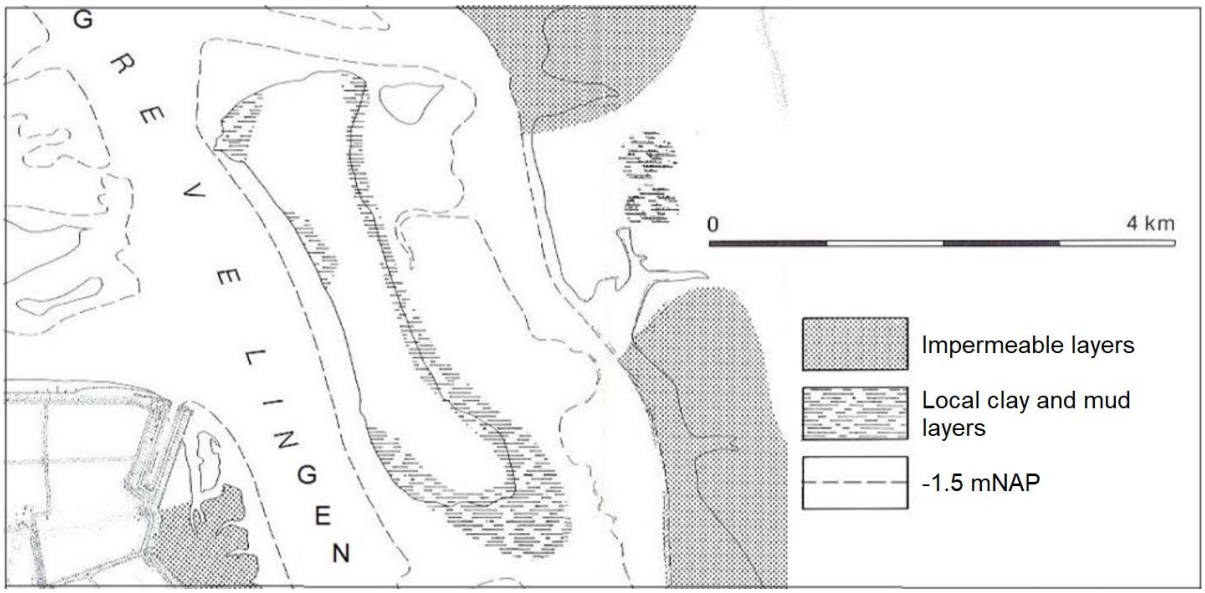

Figure 5, Distribution of impermeable layers and local clay and mud layers on Veermansplaat (Slager & Visser, 1990)

3. Method

This chapter describes the approach, datasets, measuring methods and model setup used for this research

3.1. Approach

To make a time-based model of Veermansplaat, historical and present data is used to calibrate the Hydrogeosphere models. The historical datasets are publicly available for personal or academic use. The data set of the present situation is achieved by conducting fieldwork on Veermansplaat in the months of February and March 2019. Data is gathered on the current surface infiltration rate, the depth of the fresh-saline groundwater interface, the groundwater compositions and the hourly hydraulic head change by doing infiltration tests, electrical resistivity tomography measurements, groundwater sampling and hydraulic head measurements (figure 6).

Figure 6, Field measurement locations on Veermansplaat

3.2. Research data

This subchapter describes the use and collection method of the data for this research.

3.2.1. Historical and general data

To model the evolution of the fresh water lens, input data is needed. This includes the historical precipitation, historical evaporation, historical and future water levels, altitude, geological properties of the subsurface and scenario-based changes on the precipitation and evaporation (table 1). The historical data of the daily sum of precipitation is retrieved from the weather station at the Brouwersdam (KNMI, 2019a) 9 km from Veermansplaat. Due to a scarce availability of monitoring stations for evaporation, the historical daily actual evaporation data is retrieved from the weather station in Vlissingen (KNMI, 2019b) 44 km from Veermansplaat. The historical daily water levels of lake Grevelingen are retrieved from an observation buoy near Bommenende (Rijkswaterstaat, 2019) 2 km from Veermansplaat. The future water levels are retrieved from the imposed restricted tide of 50 cm by the RSV (Tangelder et al., 2018). The altitude of the research area consists of a merged map of three individual maps: a single beam boxing (SBB) data map (2014), the third version of the current topographic map of the Netherlands (AHN3) (2017) and a Real Time Kinematic (RTK) measurement map (2018). The geological properties of the subsurface are retrieved from DINOLOKET (TNO, 2017), an open-source data source for the subsurface by the Netherlands Organization for Applied Scientific Research (TNO). The subsurface model used for this research is GeoTOP v1.3 and consist of geological properties per 0.5 m of the subsurface with a maximum depth of 50 m. The data for future precipitation and evaporation are estimated by extrapolating the historical precipitation and evaporation values of the years 2017 and 2018.

Table 1, Location, period and source of the input data for the model

Data	Location	Period	Description	Source
Historical Precipitation	Brouwersdam	1971-2019	KNMI daily values for precipitation	KNMI, 2019a
Historical Surface Evaporation	Vlissingen	1971-2019	KNMI daily values for evaporation	KNMI, 2019b
Water levels	Bommenende	1971-2019	Rijkswaterstaat daily values for the water levels of the Grevelingen lake	Rijkswaterstaat, 2019
	Grevelingen lake	2020-future	Restricted tide of 50 cm imposed by the RSV	Tangelder et al., 2018
Altitude	Netherlands	2014, 2017, 2018	Combined 5x5 m map of AHN3, SBB and RTK	"Surface height", 2019
Geological properties subsurface	Netherlands	2016	100x100m map of GeoTOP v1.3 with geological properties per 0.5 m of the subsurface with a maximum depth of 50 m	TNO, 2017

3.2.2. Infiltration rate

A single ring infiltration method (Ch. 2.3) was chosen to measure the infiltration rate along the coastline of Veermansplaat. This method is useful for this research considering the high number of infiltration tests, a limited timeframe and limited financial resources (Di Prima et al., 2019). The depth of the groundwater is close to the surface at the coastline of Veermansplaat, which results to none or a slight horizontal flow during a single ring infiltration test. The limited resources of transport during the fieldwork also asked for a simple approach compared to a double ring infiltration test. The setup consisted of a 32.5 cm inner diameter and c. 50 cm length tube made of PVC, a buoyant disk with a diameter of 30 cm, a measuring stick of 95 cm and a holder for the measuring stick (figure 7). The tubes were placed in a pre-sawed groove in the ground and hammered down to a depth of approximately 13 cm. The infiltration tests were executed in single, duplicate or triplicate (duplicate setup most common) depending on the available time during the fieldwork. After placement, the tubes were filled with a column of approximately 56 cm saline water (retrieved from lake Grevelingen) with the buoyant disk initially at the bottom to prevent disturbance of the ground due to the downpour of the water. During the filling of the tube the buoyant disk stays at the surface of the water due its buoyancy. After filling of the tube, the measuring stick and holder were placed on the floating buoyant disk. The height on the measuring stick was recorded every 3 minutes for a period of 1 hour, thereafter 1 or 2 measurements were taken after the first hour with an interval of a half to a full hour (figure 8). Hereafter, the field-saturated hydraulic conductivity was calculated using equation 2 and 3 and the cumulative infiltration approach (Ch. 2.3).

Figure 8, Infiltration test setup: Three jerry cans with saline water, tube, buoyant disk, holder and measuring stick

Figure 7, Side view infiltration test during the measurement

3.2.3. Depth fresh-saline groundwater interface

The depth of the fresh-saline groundwater interface is measured by using electrical resistivity tomography (ERT) and groundwater samples from a series of monitoring wells on the island (Ch. 3.2.4.). ERT is a direct current continuous characterization of the electrical resistivity of the subsurface and uses multiple electrodes driven into the soil in an array and an automatic Data Acquisition System (DAS; figure 9; Dahlin, 1993). To visualize the fresh-salt groundwater interface along the coastline and inland, 4 ERT lines were established. Each ERT line consists of multiple reels of 40 m with 21 electrodes and were placed using the roll-along method (Okpoli, 2013). This roll-along method uses measurements along a line in which always 3 reels are connected to the DAS and every new measurement results in disconnecting a reel at one side and the addition of one at the other side. By using this method an optimal resolution and a depth of 32 m can be achieved (Loke, 2000). The measured apparent resistivities from the ERT lines were deconvolved by Deltares using geoelectrical modelling.

Figure 9, ERT setup with the DAS, reels and electrodes

3.2.4. Chemical composition ground- and surface water

The chemical composition of the ground- and surface water is evaluated using 4 lake water samples, 3 hollestelle (artificial drinking water basins) samples and 78 groundwater samples of 10 observation wells each containing 8 to 9 screens (figure 10). The lake water and hollestelle samples were collected by filling 10-liter jerry cans after rinsing the jerry cans three times with the sampled water. The

Figure 10, Monitoring well B42F0077 comprising eight tubes with varying filter depths

Figure 11, Field setup for the chemical sampling of the groundwater

groundwater was sampled using a 4-step process: (1) measuring water level, (2) flushing tubes, (3) sampling tubes and (4) re-measuring water level.

1. Measuring the water level

First, the distance between the top of the casing of the observation well and the concrete foundation (presumable the original surface elevation) was measured. Secondly, the distance between the top of the tubes and the top of the casing of the observation well was measured. Lastly, the water level relative to the top of each tube was measured using a plopper (manual acoustic indicator) with an accuracy of 5 mm.

2. Flushing the tubes

The protocol of flushing the tubes three times their volume by SIKB (2007) was used to be sure that the sampled groundwater is representative for the chemical water composition at the screen depth. The water in each tube was pumped up three times using a motorized pump filling a maximum of 23 jerry cans of 10 L. Between the pumping of each tube, the pump hose was dried with a towel to prevent cross contamination between tubes.

3. Sampling the tubes

Water samples of the flushed tubes were taken using a new sampling tube with a length of 5 m and inner diameter of 6 mm per individual tube driven by a peristaltic pump (figure 11). Before sampling the tubes, the pH, temperature (°C), Electrical Conductivity (µS/cm) and the O_2 concentration (mg/l) were measured using a combined EC-meter and pH-meter. These measurements were executed by filling a beaker of 500 ml. Hereafter, every tube was sampled for 11 containers with a conservation measure depending on the analytical technique employed (table 2). Each sample was taken using a large syringe and filtering through a new 0.45 µm filter.

4. Re-measuring the water level

The water levels in the tubes were re-measured after sampling the tubes using the same method as the first time to compare the water level of the tubes before and after flushing.

All the groundwater samples were analysed in the lab on electrical conductivity, pH, alkalinity, anions, cations, NH_4, NO_3, NO_2, PO_4, H_2S, Dissolved Organic Carbon (DOC), and stable isotopes of water in the laboratory at the University Utrecht (table 2). Ion Chromatography (IC), Inductively Coupled Plasma - Optical Emission Spectrometry (ICP-OES), AutoAnalyzer3 (AA3), Mass Spectrometer (MS) and titration were used to analyse these samples.

Table 2, Overview of samples and their analysis technique

Nr	Field / Lab	Analysis	Technique	Container	Volume container (ml)	Volume sample (ml)	Conservation
1	Field	pH	Field titration	Greiner tube	25	25	
2		*Reserve 1*		Greiner tube	15	15	
3	Lab	EC+pH+Alk		Greiner tube	15	15	
4		Anions	IC	Greiner tube	15	15	
5		Cations	ICP-OES	Greiner tube	15	14	140 µl HNO_3
6		NH_4, NO_3, NO_2	AA3	Greiner tube	15	14	Deep freezing (-18°C)
7		PO_4	AA3	Greiner tube	15	14	140 µl HCl
8		H_2S	Titration	Greiner tube	15	9	6 ml Zn Acetate
9		DOC		Glass bottle	25	25	250 µl HCl
10		Isotopes (δ^2H and $\delta^{18}O$)	MS	Glass bottle	10	10	
11		*Reserve 2*		Greiner tube	15	15	

3.2.5. Hydraulic head

The hydraulic head of groundwater at the island is highly dependable on the rainfall, evaporation and the water level of lake Grevelingen. The hydraulic heads were measured with Autonomous Data Collectors (ADCs) of the DCX-22-AA data logger series (figure 12) manufactured by KELLER (Swiss manufacturer of isolated pressure transducers and transmitters). The hydraulic heads were measured at 4 monitoring wells on Veermansplaat with screens at a depth of -6.1 to -28.9 m NAP (table 3; figure 13). The monitoring wells used for this measurement consist of three monitoring wells at the north of Veermansplaat with a southwest to northeast alignment and a single monitoring well at the south of Veermansplaat (figure 6). The measurements took place over the period of 6 March 2019 to 15 April 2019.

Figure 13, DCX-22-AA Autonomous Data Collector by KELLER

Figure 12, Monitoring well B2F0072 with three ADCs installed for screen number 3, 6 and 9 (screen 9 is below the monitoring well mantle)

The water head was calculated from the pressure data and water densities by using equation 4 (KELLER AG für Druckmesstechnik, 2014).

$$WC = \frac{P_w - P_a}{\rho_w \cdot g} \qquad (4)$$

where WC is the length of the water column above the pressure sensor [m], P_w is the water pressure 5 m below the top of the well tube at the depth of the sensor [$kgm^{-1}s^{-2}$], P_a is the air pressure at the top of the well tube [$kgm^{-1}s^{-2}$], g is the gravitational acceleration [ms^{-2}] and ρ_w is the water density [kg/m^3].

After measurement, the data was corrected for the surface level of the monitoring wells and compared to the precipitation and evaporation data.

Table 3, Locations and depths of monitoring screens, used for hydraulic head measurements

Monitoring well	X-coordinate (RD)	Y-coordinate (RD)	Screen number	Screen depth bottom (m NAP)	Screen depth top (m NAP)	Start (date)	End (date)
B2F0072	58582	418960	3	-6.1	-5.9	8-3-2019	15-4-2019
B2F0072	58582	418960	6	-17.2	-17.0	8-3-2019	15-4-2019
B2F0072	58582	418960	9	-28.9	-28.7	11-3-2019	15-4-2019
B2F0073	59660	416574	4	-12.2	-12.0	6-3-2019	15-4-2019
B2F0078	58760	419045	3	-6.4	-6.2	8-3-2019	15-4-2019
B2F0079	58409	418861	3	-6.5	-6.3	11-3-2019	15-4-2019

3.3. Model phases

The modelling of the fresh groundwater lens of Veermansplaat follows two phases (figure 14). These phases include modelling the fresh water lens from its origin in 1971 till 2019 with historical values for precipitation and evaporation and calibrating the model based on measurements from the field (phase 1) and running the model from 2019 to 2025 for a non-tidal system and a tidal system starting in 2022 with extrapolated parameters for rainfall and evaporation (phase 2).

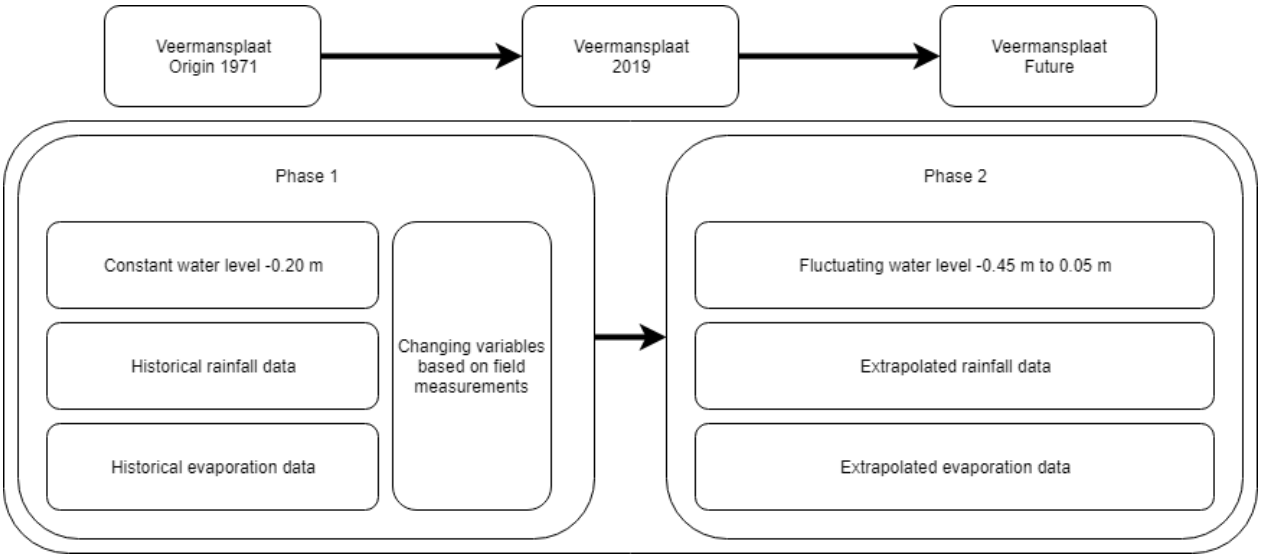

Figure 14, Modelling phases

4. Results and discussion field data

This chapter will present and discuss the data derived from the fieldwork and external sources. The results are split into four parts: the infiltration rate and hydraulic conductivity, hydraulic head, fresh-saline groundwater interface and the chemical composition of Veermansplaat.

4.1. Infiltration rate

Infiltration tests were executed at 12 locations using single, duplicate or triplicate measurements. Figure 15 and appendix 1 show the locations of the infiltration test locations.

Figure 15, Infiltration test locations at Veermansplaat

4.1.1. Results

The graphs of the cumulative surface infiltration against time per infiltration test location on Veermansplaat (appendix 2) show the surface infiltration rate of the conducted infiltration tests. With the use of equations 2 and 3 the average hydraulic conductivity per infiltration location was calculated (figure 16 & 17).

The measured surface infiltration rates on Veermansplaat are analysed and presented as the average hydraulic conductivity of the surface layer per duplicate or triplicate infiltration setup (figure 16). The hydraulic conductivities vary between 0.15 and 2.17 m d^{-1} with a standard deviation between 0.04 and 0.36 m d^{-1}. INFIL VV, 17, 20, 21, 25 and 26 show a standard deviation of 0.10 m d^{-1} or lower. INFIL 5 and INFIL 6 do not have a standard deviation due to a single execution of the infiltration test. Figure 16 shows hydraulic conductivity values higher than 1.0 m d^{-1} for the northern infiltration test with an exception for INFIL 2 and lower values than 1 m d^{-1} for the southern infiltration tests. The standard deviations of INFIL 2, 8, 9 and 18 are considerably higher as the other infiltration setups.

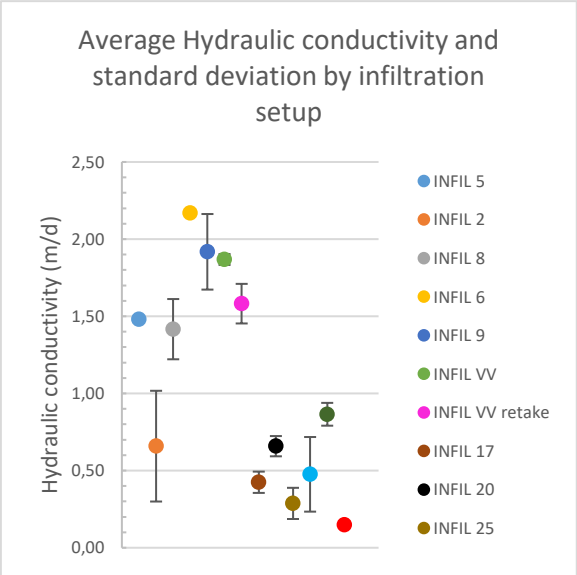

Figure 16, Average hydraulic conductivity by infiltration test location

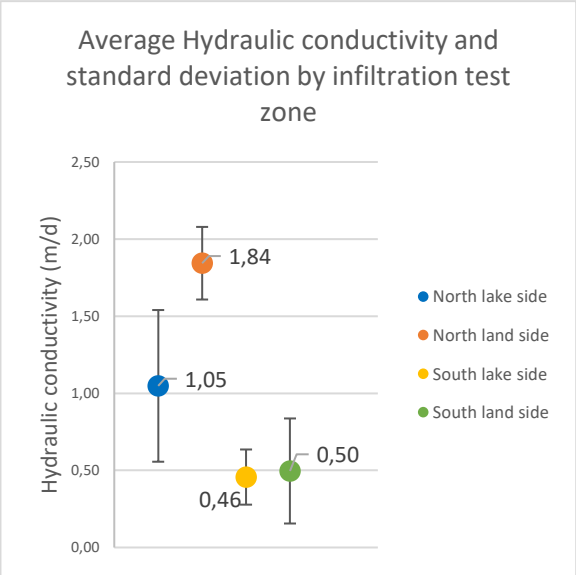

Figure 17, Average hydraulic conductivity by zonal area of Veermansplaat

Figure 17 shows the mean average hydraulic conductivities of the surface layer per studied area. The north lake side consists of INFIL 2, 5 and 8; the northern land side consists of INFIL 6, 9, VV and VV retake; the south lake side consists of INFIL 17, 20 and 25 and the south land side consists of INFIL 18, 21 and 26. The hydraulic conductivities per test zone average between 0.46 and 1.84 m d^{-1} and have a standard deviation ranging from 0.18 to 0.49 m d^{-1}. The northern infiltration zones show a difference in hydraulic conductivity of 0. 79 m d^{-1} and the southern infiltration zones show a difference of 0.04 m d^{-1}. The hydraulic conductivities at the north lake side shows the highest standard deviation.

4.1.2. Discussion

The hydraulic conductivities in the north have higher values compared to the values for the south. The low value for INFIL 2 could be related to the local increased density of vegetation at the infiltration test location and local mud and clay layers which are present in this area (figure 5; Slager & Visser, 1990). This would also explain the lower hydraulic conductivity values for the infiltration test locations at the southern border and the north-western border of Veermansplaat, which are also located in areas with local mud and clay layers. The hydraulic conductivity of the surface layer near the coastline of Veermansplaat therefore increases land inwards from 1.40 to 2.20 m d^{-1} for the areas without the presence of mud and clay layers and increases land inwards from 0.10 to 0.90 m d^{-1} for areas with the presence of mud and clay layers.

The infiltration measurements at Veermansplaat bring some uncertainty because of the time span of the measurements and a change in measuring method. INFIL 5 and 6 were measured in January, INFIL 2 in February and all the other infiltration tests in March. During this period the temperature changed from -1 to 20 °C resulting in different water temperatures of lake Grevelingen and different soil permeability due to frost and the growth of vegetation. INFIL 2, 5 and 6 were measured without the use of a buoyant disk and were instead measured using a measuring stick. However, this should not have had a great influence on the measurement, as both methods measure the change in water column over time using a reference height.

4.2. Depth fresh-saline groundwater interface

This subchapter will present and discuss the electrical resistance tomography data from the fieldwork. The depth of the fresh-saline groundwater interface was measured along 4 lines on Veermansplaat (figure 18).

Figure 18, ERT profile location on Veermansplaat

4.2.1. Results

The 4 ERT lines (figure 19-22) show the resistivity ranging from 0.3 to 93 Ωm. Values of 0.3 - 2 Ωm are considered saline, values of 2 - 10 Ωm are considered brackish and values of +10 Ωm are considered fresh. The lithology of the subsurface of Veermansplaat mainly consists of sand (appendix 4). Therefore, increased values due to clay layers can be neglected most of the time. The X-axis shows the distance from the coastline in meters and the Y-axis shows the depth in m NAP.

ERT profile II (figure 19) shows the resistivity profile for the northern coast of Veermansplaat. The resistivity ranges between 0.2 and 122 Ωm for the entire slice. The first 160 m starting at the northern border show a surface resistivity of 0.3 to 2 Ωm. Hereafter, the surface resistivity at shallow depth increases from 2 Ωm to 8 Ωm between 160 and 190 m from the border. The surface resistivity between 190 and 279 m varies between 20 and 122 Ωm of which the values of 20 Ωm are situated at a distance of 245 and 279 m. Between 190 and 245 m the fresh to brackish interface (10 Ωm) is situated at -1 m NAP, between 245 and 279 m the depth of the fresh to brackish interface increases to a depth of -5 m NAP. The brackish to saline interface (2 Ωm) is situated at -1 m NAP between a distance 160 and 190 m; increases from -1 to -5 m NAP between 190 and 240 m and increases from -5 to -15 m NAP between a distance of 245 and 179 m. The maximum infiltration depth of the fresh water lens is -4 m NAP.

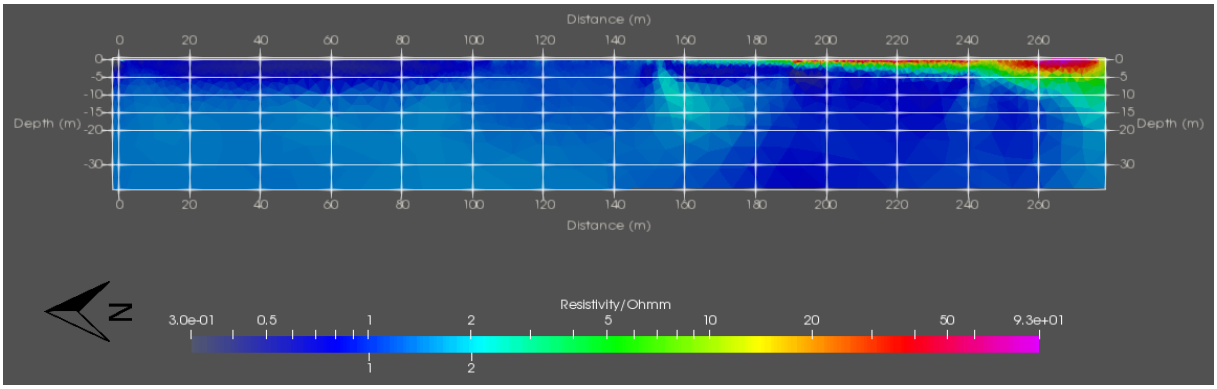

Figure 19, Resistivity (Ohm m) of ERT profile II

ERT profile VII (figure 20) shows the resistivity profile for the south coast of Veermansplaat. The resistivity ranges between 0.4 and 92 Ωm for the entire slice. The first 134 m from the southern border shows a surface resistivity of 0.4 to 8 Ωm. Between a distance of 134 and 402 m, the surface resistivity ranges between 8 and 93 Ωm. The surface resistivity increases along the distance from the coastline except for a decrease in resistivity at the distance of 180 m. The fresh to brackish interface is situated at -2 m NAP between a distance of 145 and 178 m and a depth of -3 and -10 m NAP between a distance of 185 and 385 m and increasing depth to -15 m NAP between a distance of 385 and 402 m. The brackish to saline interface is situated at a depth of 0 to -10 m NAP between a distance of 125 and 170 m; -10 m NAP between a distance of 170 and 230 m; a depth of -15 and -20 between a distance of 230 and 380 m and an increasing depth of -20 and -48 m NAP between a distance of 380 and 402 m. The maximum infiltration depth of the fresh water lens varies between -10 and -15 m NAP.

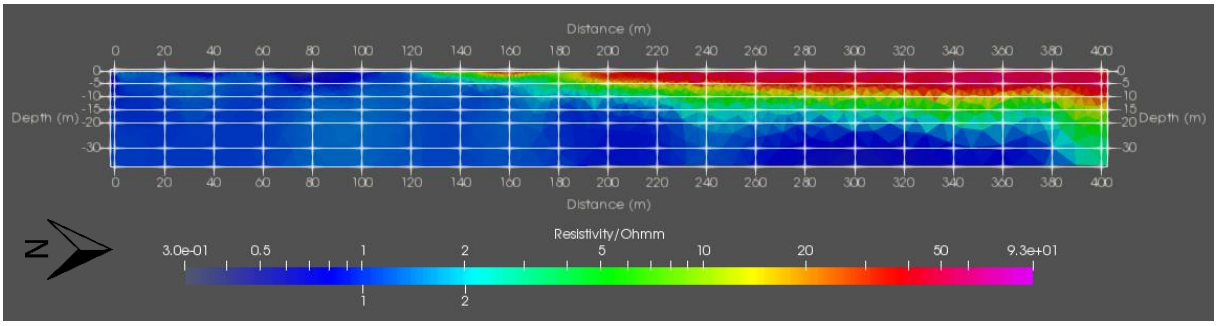

Figure 20, Resistivity (Ohm m) of ERT profile VII

ERT profile V (figure 21) shows the resistivity profile from the east to the west border of the southern part of Veermansplaat. The resistivity ranges from 0.4 to 93 Ωm for the entire slice. The surface resistivity starting from the eastern coastline to a distance of 630 m ranges from 10 to 92 Ωm. Between a distance of 630 and 641 m from the east border, the surface resistivity ranges between 10 and 0.4 Ωm. The fresh to brackish interface is situated at a depth of -10 to -15 m NAP between a distance of 0 and 220 m; a depth of -7 to -10 m NAP between 220 and 480 m and a depth of -10 to 0 m NAP between a distance of 480 and 630 from the east coastline. The brackish to saline interface is situated at a depth of -15 to -20 m NAP between a distance of 0 and 150 m; -20 and 25 m NAP between a distance of 150 and 230; a depth of -10 to -20 between a distance of 230 and 535 m; a depth of 0 to -10 m NAP between a distance of 535 and 630 m. The maximum infiltration depth of the fresh water lens varies between -7 and 15 m NAP.

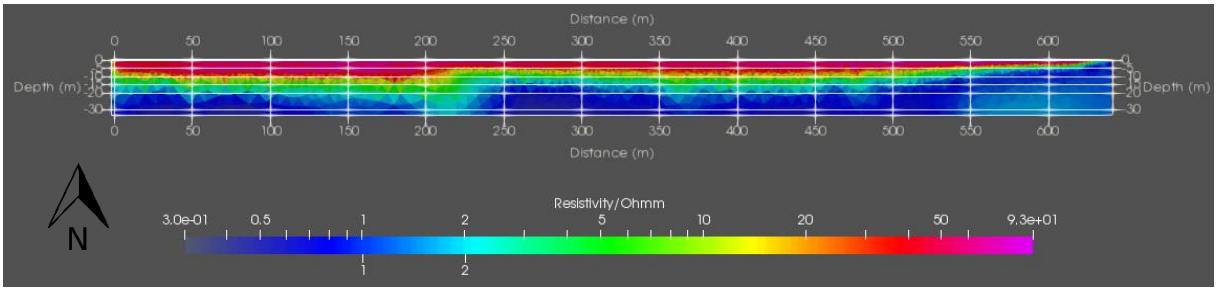

Figure 21, Resistivity (Ohm m) of ERT profile V

ERT profile X (figure 22) shows the resistivity profile from the east to the west border of the northern part of Veermansplaat. The resistivity ranges from 3 to 171 Ωm for the entire slice. The surface resistivity starting from the eastern coastline to a distance of 820 m ranges from 13 to 171 Ωm. Between a distance of 820 and 840 m from the east border the surface resistivity ranges between 5 and 8 Ωm. The fresh to brackish interface is situated at a depth of -5 to -11 m NAP between a distance

of 0 and 140 m NAP; a depth of -11 to -20 m NAP between a distance of 140 and 280 m; a depth of -25 m NAP between a distance of 280 and 350 m; a depth of -15 to -20 m NAP between 350 and 740 m with an increased depth of -48 m NAP between 540 and 610 m and between 720 and 740 m; a depth of 0 to -10 m NAP between 740 and 820 m. The brackish to saline interface is situated at a depth that is not visible in ERT profile X. The maximum infiltration depth of the fresh water lens varies between -20 and -48 m NAP.

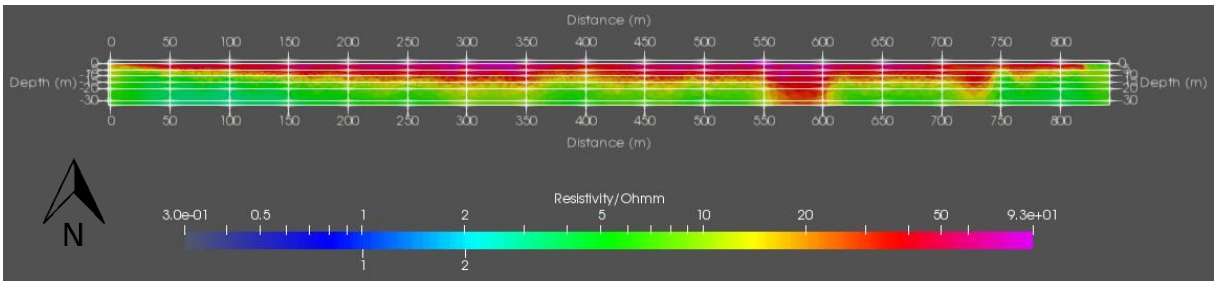

Figure 22, Resistivity (Ohm m) of ERT profile X

4.2.2. Discussion

The maximum depth of the fresh water lens of Veermansplaat varies a lot considering the data of the 4 ERT profiles. The data of ERT profile X at a distance of 575 and 725 m shows two deep fresh water infiltration columns and a high resistivity (figure 22) indicating a high infiltration depth of fresh groundwater at the location where saline water was predicted. These values could not be corrected during the post processing of the ERT profiles. The high resistivity columns are situated at locations where the reels of the ERT measurements were placed in a water pool of 20 cm. The error in ERT profile X therefore limits the validity of the measurement along the profile. Without the use of ERT profile X the maximum depth of the fresh water lens infiltration is -15 m NAP.

The shape of the fresh water lens also deviates from the standard shape of a fresh water lens (figure 2). The infiltration depth of the fresh water lens at Veermansplaat does not start at the boundary between the island and the lake but starts developing at a distance between 120 and 160 m from the north and south border of Veermansplaat (figure 19 & 20). This can be the result of salt spray and small water floods induced by wind surges. Additionally, the fresh water lens does not show the shape of a perfect lens for ERT profile V, but instead shows two separate lobes of fresh water (figure 21). The vegetation and surface level along this profile do not differ to a great extent. The lithology of the subsurface along profile V does not change either along the profile according to the lithology recovered from GeoTOP (appendix 4). However, GeoTOP estimates the lithology of Veermansplaat in a stochastic process based on 44 measurements on and nearby Veermansplaat, resulting in local uncertainties for the lithology. The uncertainty for profile V varies between 0 and 50% between surface level and -30 m NAP and varies between 50 and 80% between -30 and -40 m NAP (appendix 4). More research on the hydraulic conductivity of Veermansplaat is needed to confirm if the changes in lithological class along ERT profile V causes the irregular shape of the fresh water lens.

4.3. Chemical composition of ground and surface water

This subchapter will present and discuss the chemical composition of the groundwater samples acquired from the fieldwork on Veermansplaat (figure 23). Four lake water samples, 3 hollestelle samples and 78 groundwater samples of 10 observation wells were collected and processed.

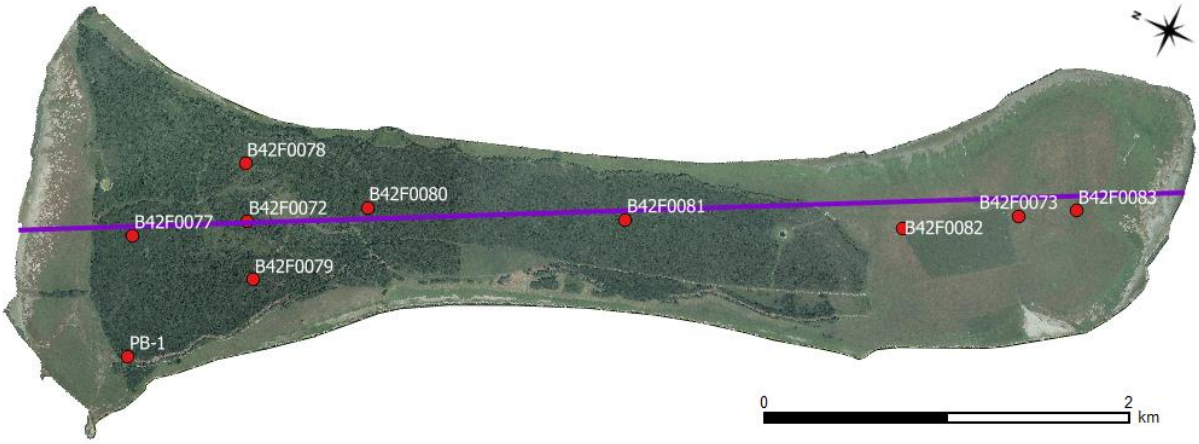

Figure 23, Monitoring well locations and north south profile of the fresh water lens on Veermansplaat

4.3.1. Results

The chloride concentrations along the north-south profile (figure 23) is plotted in figure 24, using the total dissolved solids per groundwater sample of monitoring wells 72, 73, 77, 80, 81, 82 and 83 (appendix 3). Appendix 3 shows the chemical composition of each groundwater sample taken at Veermansplaat. Figure 24 shows chloride concentrations of less than 1000 mg L^{-1} at a depth of approximately -13 m NAP at the northern part of Veermansplaat and -9 m NAP at the southern part of Veermansplaat. The mixing zone with chloride concentrations between 1000 and 13000 mg L^{-1} is visible at monitoring wells 72, 80, 81, 82 and 83 at depths between -12 and -17 m NAP.

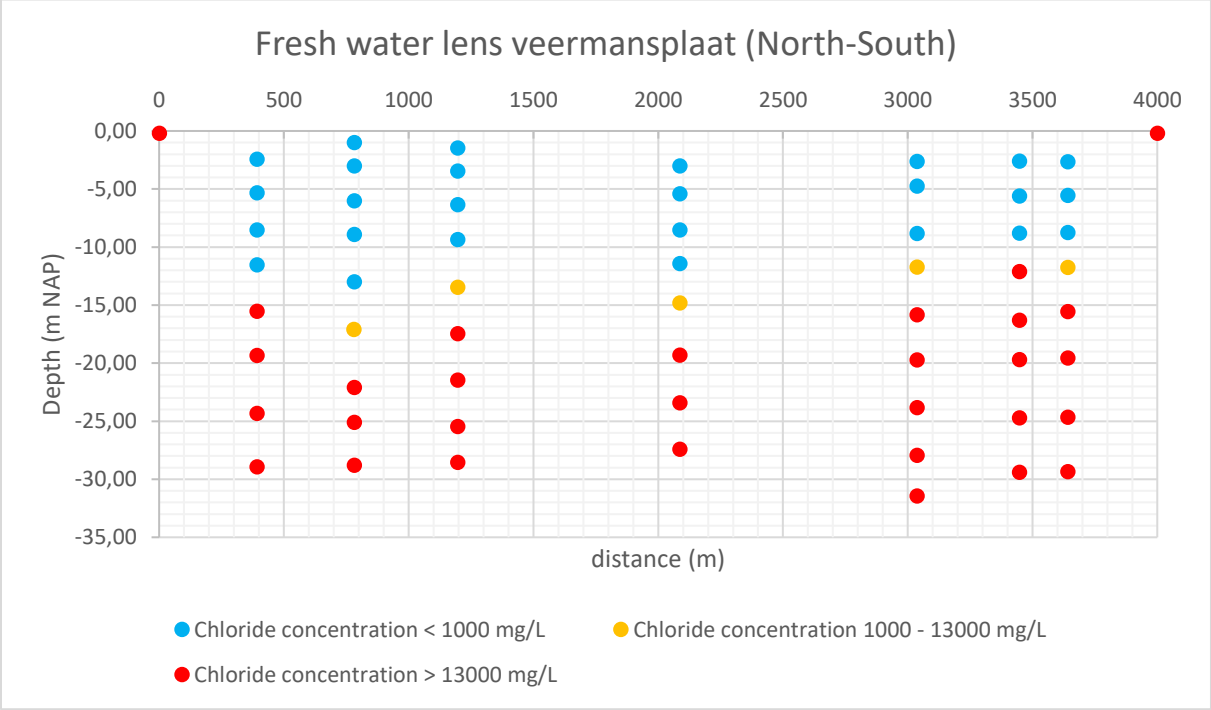

Figure 24, Chloride concentration per depth along a northwest oriented cross-section of Veermansplaat

Figure 25 shows the chloride concentration of the groundwater samples per monitoring well against the depth of the screens. All the groundwater samples show a chloride concentration between 20 and 200 mg L^{-1} for a depth down to -8 m NAP between -8 and -13 m NAP from a concentration of between 20 and 200 mg L^{-1} to a concentration between 15000 and 16000 mg L^{-1} at a depth of -15 m NAP and deeper. This chloride concentration transition differs per monitoring well. The chloride concentration transition at monitoring wells 73, 82 and 83 starts at c. -8 m NAP and ends at c. -16 m NAP; at monitoring wells 77 and 81 it starts at c. -11 m NAP and ends at c. -18 m NAP; at monitoring wells 78, 79 and 80 it starts at c. -13 m NAP and ends at c. -20 m NAP; at monitoring well 72 it starts at c. -13 m NAP and ends at c. -23 m NAP.

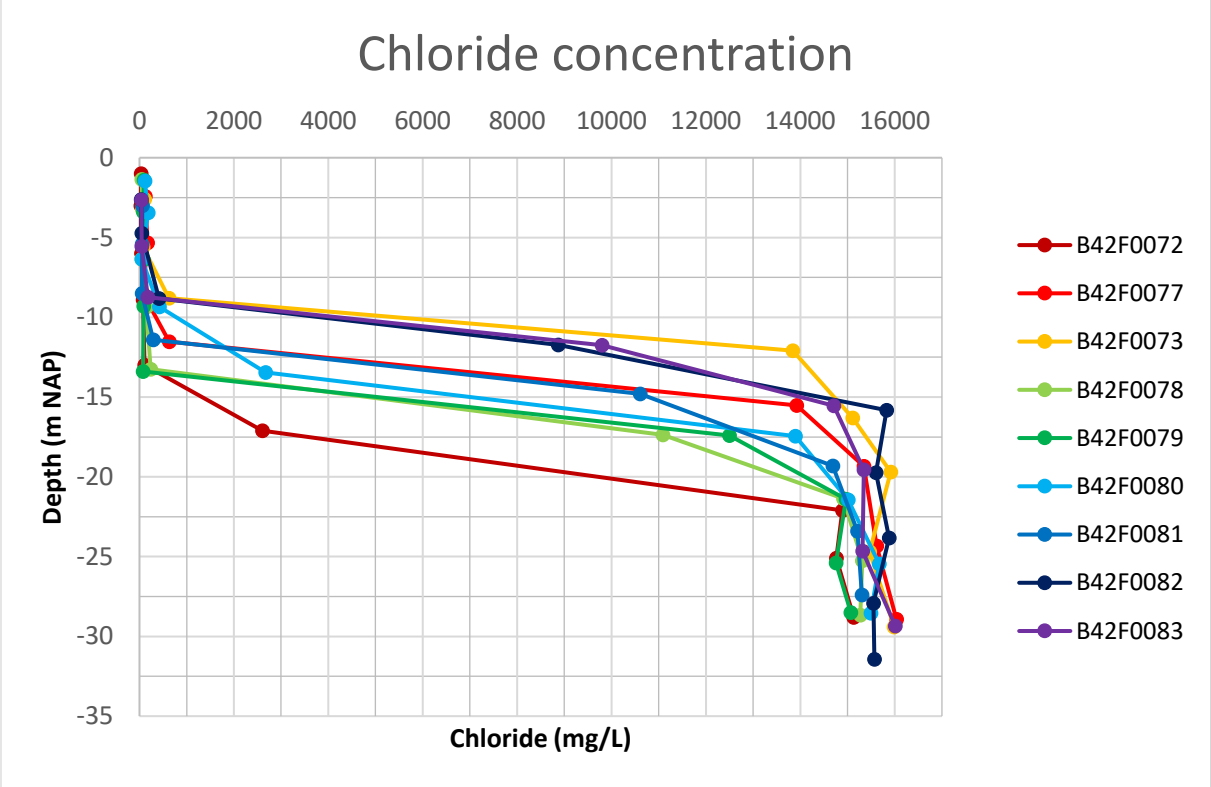

Figure 25, Chloride values against the infiltration depth

Figure 26 shows the d^2H isotope signature against $d^{18}O$ isotope signature of groundwater from the monitoring wells, hollestelle and lake water (legend: Grevelingen) samples. Additionally, the standard values for rainwater, seawater, the global meteoric water line (GMWL) and the linear plotted trend line of the groundwater samples are used as reference. The isotope signatures of the groundwater samples are positioned along the rainwater-seawater line, except for the hollestelle groundwater samples which are positioned below the rainwater-seawater line. Figure 26 shows 4 clusters along the rainwater-seawater line: the fresh groundwater samples which have a d^2H isotope signature of -48 to $-32^0/_{00}$ and a $d^{18}O$ isotope signature of -7.5 to $-5.9^0/_{00}$, a cluster of brackish groundwater samples with a d^2H isotope signature of c. $-20^0/_{00}$ and a $d^{18}O$ isotope signature of c. $-3.0^0/_{00}$, the saline groundwater samples which have a d^2H isotope signature of -16 to $-9^0/_{00}$ and a $d^{18}O$ isotope signature of -2.4 to $-1.5^0/_{00}$ and the lake groundwater samples with a d^2H isotope signature of c. $-8^0/_{00}$ and a $d^{18}O$ isotope signature of c. $-1.2^0/_{00}$.

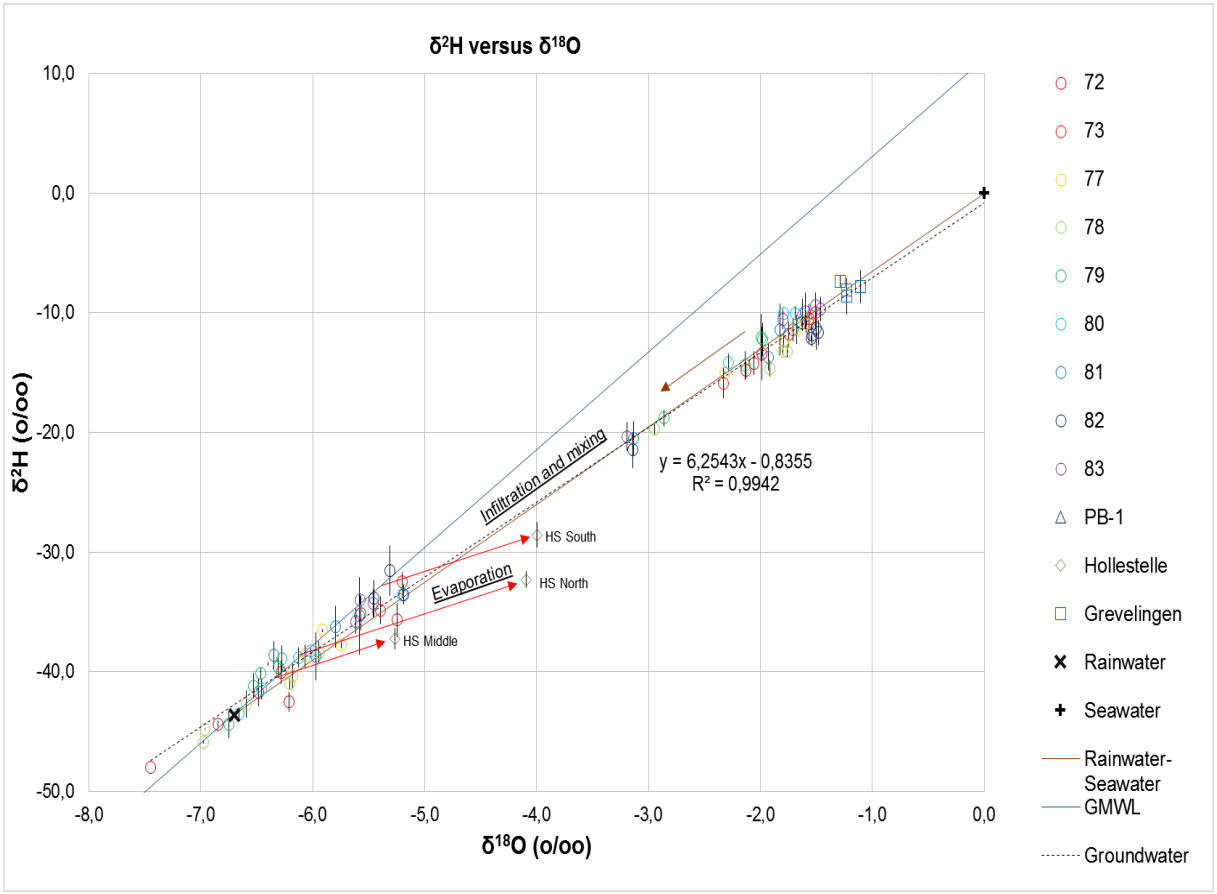

Figure 26, Stable isotopes values of the monitoring wells on Veermansplaat

Figure 27 shows the Piper diagram of the deep and shallow groundwater, lake water and hollestelle groundwater samples. The arrows follow the groundwater samples from the deep monitoring wells by decreasing depth and show the shift in the water composition along the depth at Veermansplaat. The water composition is plotted in percentage milliequivalents per litre for the anions calcium, magnesium, sodium and potassium and the anions chloride, sulphate and carbonate + bicarbonate. Figure 27 shows an increase for c. 0 to 80% in carbonate + bicarbonate and a decrease from c. 90 to 10-20% in chloride for the anions along the decreasing depth at Veermansplaat. For the cations figure 27 shows an increase for c. 0 to 30-90% in calcium; a decrease for c. 100 to 10-30% in sodium and potassium and an increase fraction of c. 0 to 40% in magnesium with an exception for monitoring wells 78 and 72 which decreases in magnesium from 40 to 10% for the shallow screens. The combined graph of the anions and cations (diamond shaped graph; figure 27) shows a transition from strong to weak acids and thereafter a transition from alkalis to alkaline earths along the decreasing depth of Veermansplaat.

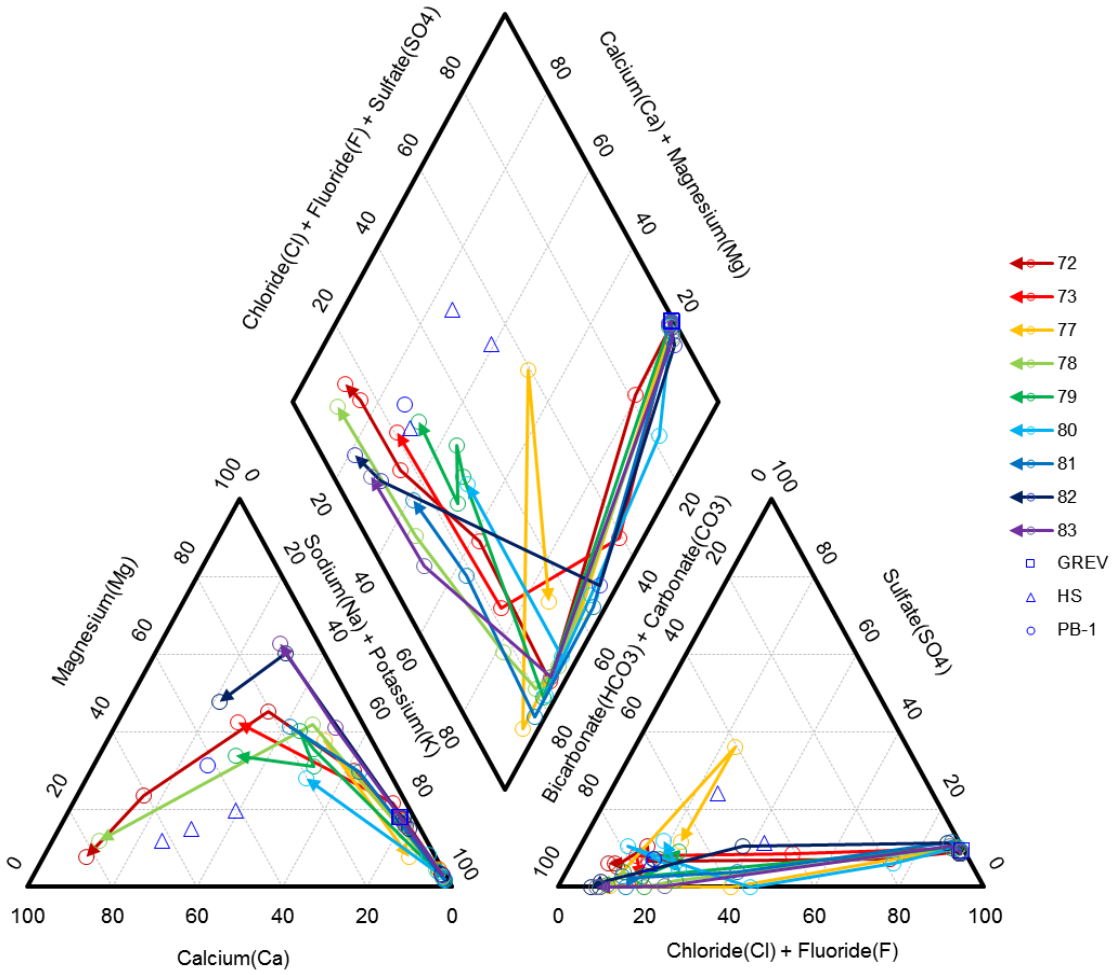

Figure 27, Piper diagram of the monitoring wells, lake and hollestelle samples of Veermansplaat

4.3.2. Discussion

The chemical composition of the groundwater shows a clear transition of fresh to saline groundwater along the depth at Veermansplaat. The chloride concentration graphs (figure 24 & 25) show a maximum infiltration depth between -10 to -13 m NAP. The chloride concentration graph along the north-south axis of Veermansplaat (figure 24) shows two infiltration lobes of which the northern lobe infiltrates deeper than the southern lobe. This irregularity is also visible in ERT profile V (Ch. 4.2). The middle to northern part of Veermansplaat is covered with shrubs and trees while the southern part is covered with grass and mowed shrubs (Ch. 2.4). The middle and northern parts of Veermansplaat also have a higher surface elevation than the southern part and are bordered by sand ridges. This results in less overland flow and the local retention of rainwater which could have a positive effect on the infiltration of fresh water. Thus, the surface elevation and vegetation along the north south axis of Veermansplaat varies a lot resulting varying infiltration rates and water retention along the axis.

The clustering of the stable isotope measurements of the fresh, brackish and saline groundwater samples along the rainwater-seawater line (figure 26) indicates a transition of fresh to saline groundwater along the depth and the mixing of fresh and saline groundwater at Veermansplaat. The deviation of the stable isotope values for the hollestelle when compared with the stable isotope values of the nearby shallow groundwater samples, can be related to evaporation of water in the hollestelle. Open water evaporation of water causes a decrease in the d ^{2}H and d ^{18}O values (Gat & Matsui, 1991).

The Piper diagram (figure 27) follows the freshening pattern where the dominant subtype changes from NaCl to $NaHCO_3$ and finally to $CaHCO_3$ (Vandenbohede & Lebbe, 2012) which is to be expected for a fresh water lens. The pattern of monitoring well 77 does not follow the pattern of the other monitoring wells. The shallow groundwater samples of monitoring well 77 show a sudden increase of carbonates together with an increase in alkalinity which is not expected compared to the other monitoring wells or due to change in soil textures. This could be a result of mistakes during the sampling or post processing of the groundwater samples.

The groundwater samples show that the chloride concentration along the depth of Veermansplaat differ depending on the location at Veermansplaat. Therefore, the number of groundwater samples along the depth could be increased to give a more precise estimation of the infiltration depth. Additionally, more monitoring wells near the east and west coastline would give more insight on the irregular shape of the fresh water lens of Veermansplaat.

4.4. Hydraulic head

This subchapter will present and discuss the data of the hydraulic head measurements acquired from fieldwork. ADC measurements were executed at 4 locations (figure 28).

4.4.1. Results

Figure 28, Hydraulic head measurement locations on Veermansplaat

The screen depth of the monitoring wells used for the measurements of the hydraulic head vary between -6.1 and -28.9 m NAP and range in salinity between 70.5 and 27335.0 mg L^{-1} (table 4). All the hydraulic heads are corrected for their corresponding density and tube width and length to represent the fresh water heads.

Table 4, Data of all hydraulic head measurement locations

Monitoring well	**72-3**	**72-6**	**72-9**	**78-3**	**79-3**	**73-4**
Height top well tube (m NAP)	1.95	1.89	1.82	1.51	1.53	1.26
Length keller (m)	5.50	5.50	5.50	5.50	5.50	5.50
Keller (m NAP)	-3.55	-3.61	-3.68	-3.99	-3.97	-4.24
Depth filter bottom (m NAP)	-6.10	-17.20	-28.90	-6.40	-6.50	-12.20
Chlorinity (mg/L)	39.00	2607.00	15131.00	44.00	84.00	13843.00
Salinity (mg/L)	70.46	4709.68	27334.91	79.49	151.75	25008.07
Density (kg/L)	997.94	1003.40	1026.00	997.83	997.82	1023.90
Average temperature (°C)	8.60	9.10	9.20	9.50	9.70	9.70

Figure 29A shows the relative change of the hydraulic heads at monitoring well 72 for tubes 3, 6 and 9 and the relative water level of lake Grevelingen relative to the hydraulic head and lake water level at 11 March 2019. The hydraulic heads of tubes 6 and 9 follow the same pattern differentiating with 0.0095 m over a period of 35 days. Tube 3 shows a pattern which deviates starting from 18 March 2019. Figure 29B shows the relative change of the hydraulic head within monitoring well 72, 78 and 79 for tube 3 and the relative water level of lake Grevelingen compared to the hydraulic head and water level at 11 March 2019. The hydraulic head of monitoring well 72 and 79 follow the same pattern until 18 March 2019. Monitoring well 78 shows a more irregular pattern than monitoring well 72 and 79 until 18 March 2019. After 18 March 2019 the hydraulic head of monitoring well 79 decreases at a faster rate compared to monitoring wells 72, while the hydraulic head in monitoring well 78 decreases at a slower rate. At 13 April 2019 both monitoring wells 72 and 79 have a relative hydraulic head of -0.27 m NAP compared to 11 March 2019. Figure 29C shows the relative change of the hydraulic head

within monitoring well 73 for tube 4 and the relative lake water level of lake Grevelingen compared to their relative hydraulic head and water level at 11 March 2019. The hydraulic head in tube 4 of monitoring well 73 increases by 0.04 m NAP between 11 and 17 March 2019. Hereafter, the relative hydraulic head lowers to -0.19 m NAP towards 1 April 2019. After an increase towards -0.12 m NAP the relative hydraulic head lowers towards -0.45 m NAP at 14 April 2019 with the same gradient as the decrease in relative hydraulic head between 17 and 1 April. 15 April 2019 shows the same value of -0.45 m NAP as the value at 14 April 2019.

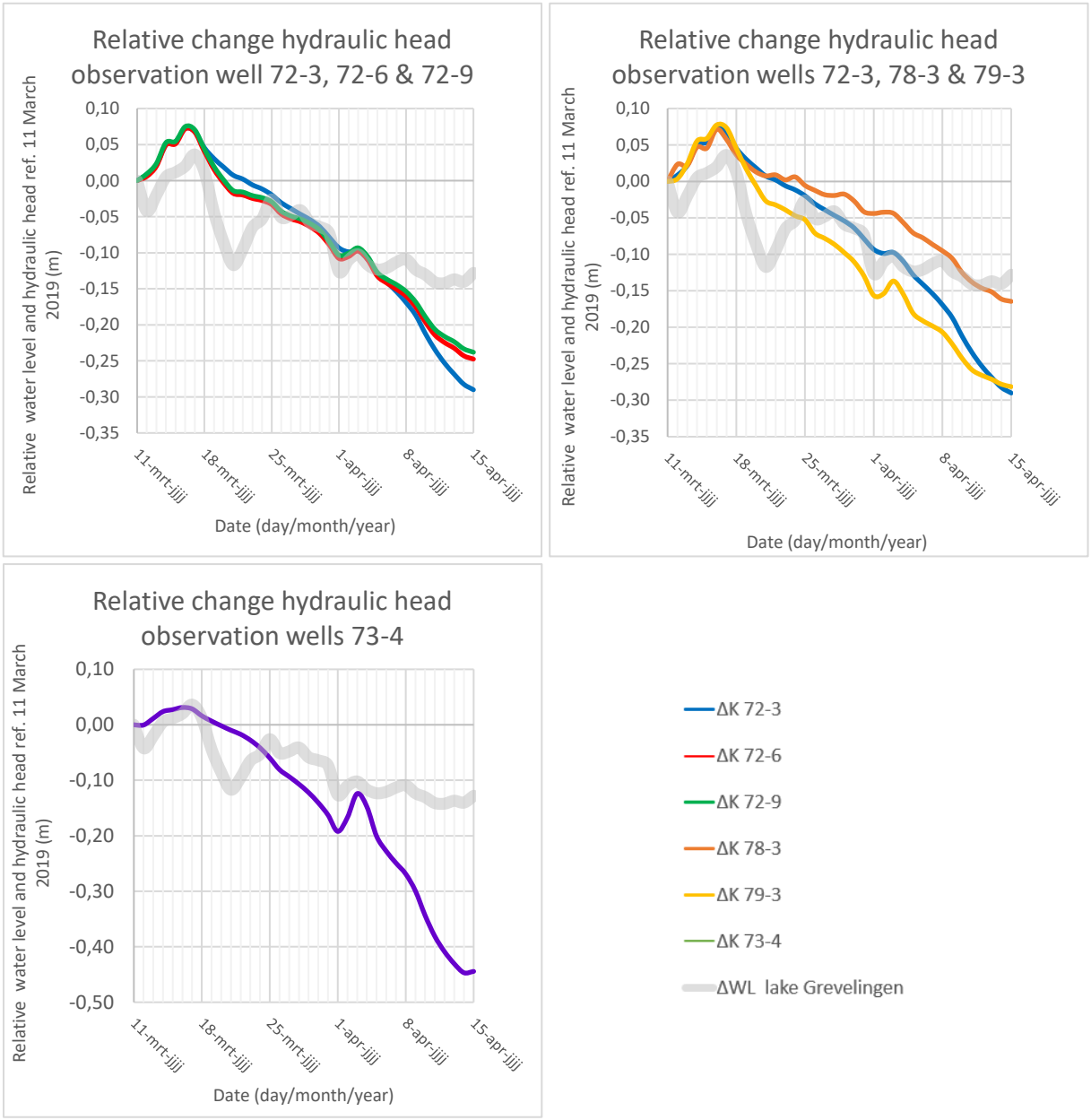

Figure 29A, B & C, The water level of lake Grevelingen compared to the change of the hydraulic head relative to 11 March 2019 for monitoring well 72 (top left, A) 72, 78 & 79 (top right, B) and 73 (bottom left, C)

Figure 30 shows the hydraulic heads of the monitoring wells per screen depth compared to the rainfall and water level of lake Grevelingen. Monitoring wells 72-6 and 79-3 both have the same pattern and vary between a hydraulic head of 0.1 and 0.5 m NAP. Monitoring wells 72-3 and 78-3 follow the same pattern between 11 to 21 April 2019 and vary with a hydraulic head between 0.2 and 0.7 m NAP during the measured period. The hydraulic head of monitoring well 72.9 varies between -0.2 and 0.1 m NAP

and monitoring well 73-4 varies between -0.9 and -0.4 m NAP. The water level of lake Grevelingen varies between -0.2 and -0.1 m NAP between 1 and 20 March 2019 and varies between -0.3 and -0.2 m NAP during the period of 21 March to 17 April 2019. The precipitation at Veermansplaat during the period of 1 March to 17 April is limited to the period of 1 to 17 March 2019. The daily rainfall in this period ranges between 0 to 0.0017 m d^{-1}.

The groundwater flow is downwards due to differences in head along the depth at monitoring well 72 and decreases in velocity starting 8 April 2019 between -17 and -6 m NAP. The difference between the hydraulic heads along a horizontal line for monitoring wells 72-2, 78-3 and 79-3 indicates a groundwater flow from the centre of Veermansplaat towards the west. Starting on 20 March 2019, groundwater also flows from the centre of Veermansplaat towards the east with an increasing velocity over time.

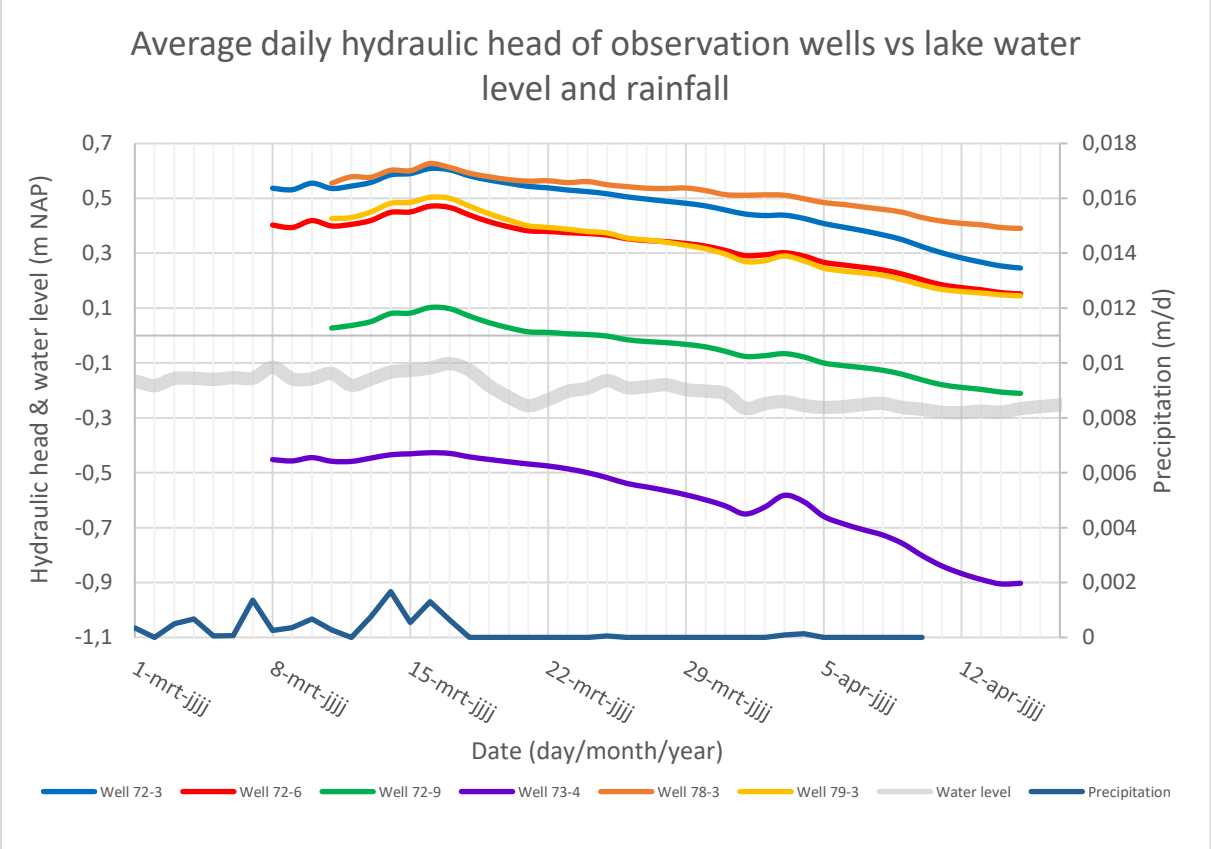

Figure 30, Daily averaged hydraulic head of the monitoring wells compared to the water level of lake Grevelingen together with the daily precipitation at Brouwershaven

4.3.2. Discussion

Figures 29 and 30 show a fast and positive feedback on the hydraulic head of Veermansplaat by the precipitation and the water level of lake Grevelingen for the hydraulic heads in the tubes of the monitoring wells. The influence of the precipitation on the hydraulic head has a larger influence compared to the water level of lake Grevelingen. During the period of precipitation, the hydraulic heads increase and during the period without precipitation the hydraulic heads decreases. The daily changes in water level of lake Grevelingen are small and are relative constant over a longer period. Figure 30 shows a change in the average water level of lake Grevelingen, which can be related to the lowering of the lake water level with 6 cm by Rijkswaterstaat during the breeding season (Ch. 2.4). The lowering of the water level of the lake and the absence of precipitation takes place around the same

period which makes it difficult to estimate how much the decrease in hydraulic head is caused by the change in precipitation or the change of the water level of lake Grevelingen.

The remarkably low hydraulic head values for monitoring well 73 and its positioning below the lake water level can be caused due to coiling of the connector cord during placement of the ACDs resulting in a wrong correction for the measuring depth. The relative short period of measurements and the absence of multiple precipitation periods makes it difficult to correlate the effect of the precipitation and the lake water level on the hydraulic heads in the monitoring wells. Data covering a longer period is needed to correlate this effect.

5. Results hydrological models

This chapter will describe the results of the modelling of the fresh water lens below Veermansplaat with Hydrogeosphere. The results are based on three models: The evolution of the fresh water lens for the years 1971 to 2025 without a tidal system (models 1 & 2) and the evolution of the fresh water lens for the years 1971 to 2023 with a tidal system starting at 2022 (model 3; table 5). The K scaling of the models translates to the multiplying factor for the hydraulic conductivities of the entire model.

Table 5, Overview Model information

Model name	K scaling	Duration	Tide	Start tide
Model 1	0.1	1971-2025	NO	-
Model 2	0.033	1971-2025	NO	-
Model 3	0.3	1971-2023	YES	2022

The evolution of the fresh water lens of Veermansplaat is modelled for a 2D slice at the centre of the island with an east to west orientation (figure 31). The slice covers a length of 700 m and a depth down to -50 m NAP.

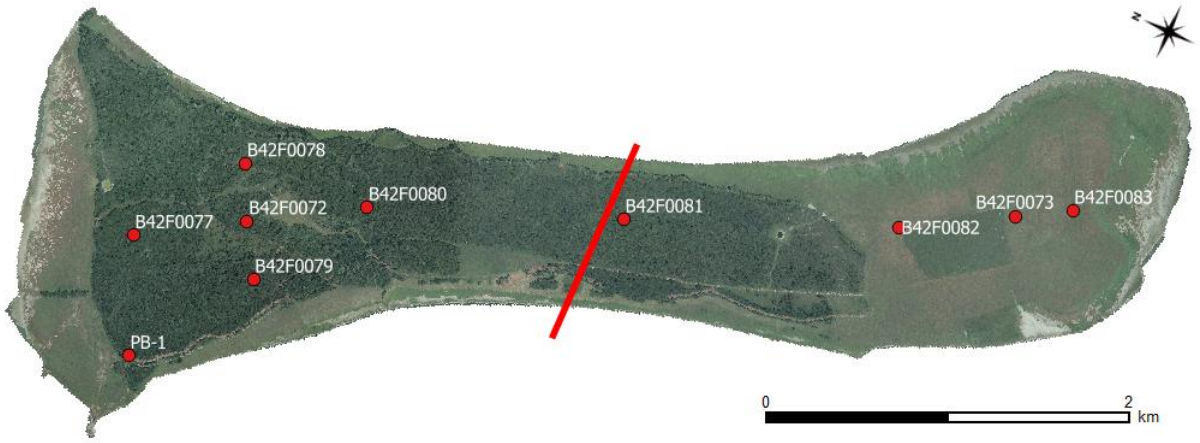

Figure 31, Location of the Hydrogeosphere model and deep monitoring wells on Veermansplaat

5.1. Model inputs

Hydrogeosphere makes use of multiple boundary conditions and parameter values to run the models. All the models use the same boundary conditions and initial conditions. The parameter values of the models do differ depending on the presence of a tidal system.

5.1.1. Boundary conditions

Multiple boundary conditions are used to calibrate the model (figure 32). The water level of lake Grevelingen is controlled by the fluid transfer and hydraulic head boundary conditions. The fluid transfer boundary condition controls the fluid flow towards the sides of the model for a given hydraulic head for the top nodes of the boundary condition. The hydraulic head boundary condition controls the lake water level by assigning a hydraulic head to the top nodes of the model at the bottom of the lake. The rainfall and evaporation boundary condition covers the surface of Veermansplaat. The salt concentration boundary condition controls the salinity of the sides of the model. Observation points

are located along the depth in the middle of the slice to analyse the exact salt concentration at the points. This column of monitoring points is used to visualize yearly trends and to compare with measured values at observation well B42F0081.

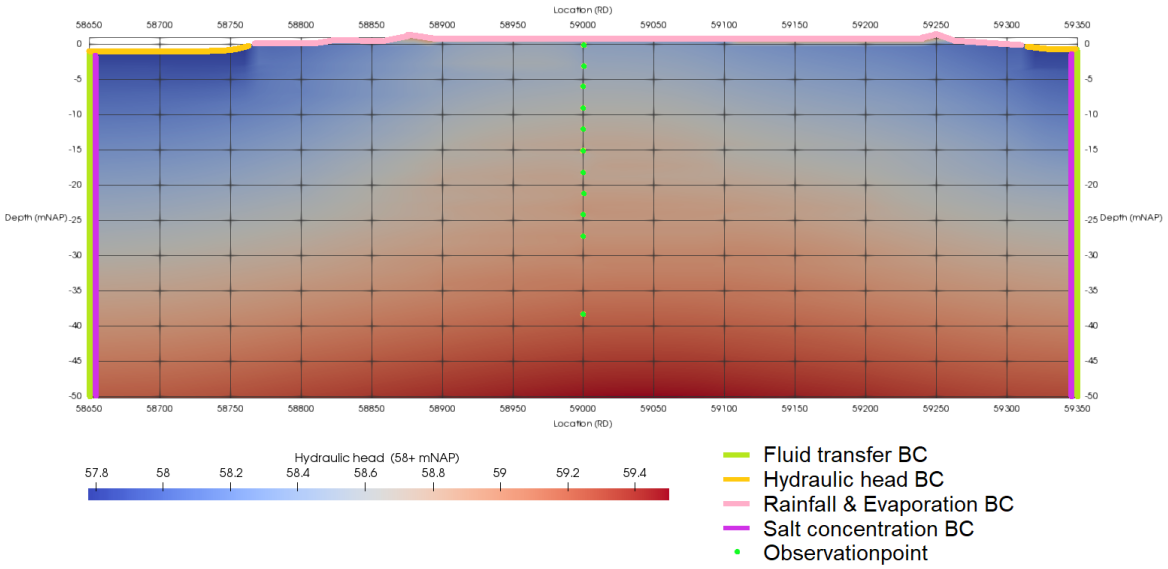

Figure 32, Initial hydraulic head and boundary conditions of the Hydrogeosphere model

5.1.2. Parameter values

Hydrogeosphere uses multiple parameters to calculate the transport of salt. The runtime of the models depends on the time interval and range of these values. Therefore, the parameter values of the historical data and fieldwork are adjusted for the model to decrease runtime. The daily rainfall and evaporation values are averaged for every 15 days and are based on the historical data (Ch. 3.2.1.). The values for rainfall and evaporation for the runs towards the year 2027 are extrapolated using the averaged 15 daily rainfall of the years 2017 and 2018. The hydraulic head value to control the water level of lake Grevelingen is fixed at -0.20 m NAP for the models in a non-tidal system and alternates daily between -0.45 and 0.05 m NAP resulting in a diurnal tidal cycle for the model in a tidal system. The initial value for the hydraulic head of the model (figure 32) is made using a spin-up of 50 years with constant, averaged rainfall of 0.0022 m d^{-1} and evaporation of 0.0017 m d^{-1} based on the historical data of the year 1971 to 2019. The hydraulic conductivity is corrected for depth of the model, resulting in an addition of 58 meter to the hydraulic heads (figure 32). Hydraulic conductivity values used for the spin-up and real-time modelling use the Geo-TOP values (figure 33; TNO, 2019b). Figure 33 shows the lithological classes and their corresponding hydraulic conductivity of the 2D slice where *k* is clay; *kz* is mixed clay and sand; *zf* is fine sand; *zm* is medium sand and *zg* is coarse sand. The grid size for Geo-TOP is 100x100x0.5 m.

The initial salt concentration for the model amounts a salinity of 30 kg m^{-3} for the entire model starting at 1 January 1971. Hydrogeosphere uses salinity to model salt transport which is converted to chloride concentration using equation 5 (Wooster et al., 1970).

$$S‰ = 1.80655CL‰ \qquad (5)$$

where S‰ is the salinity of the water [kg m^{-3}] and CL‰ is the chloride concentration of the water [kg m^{-3}].

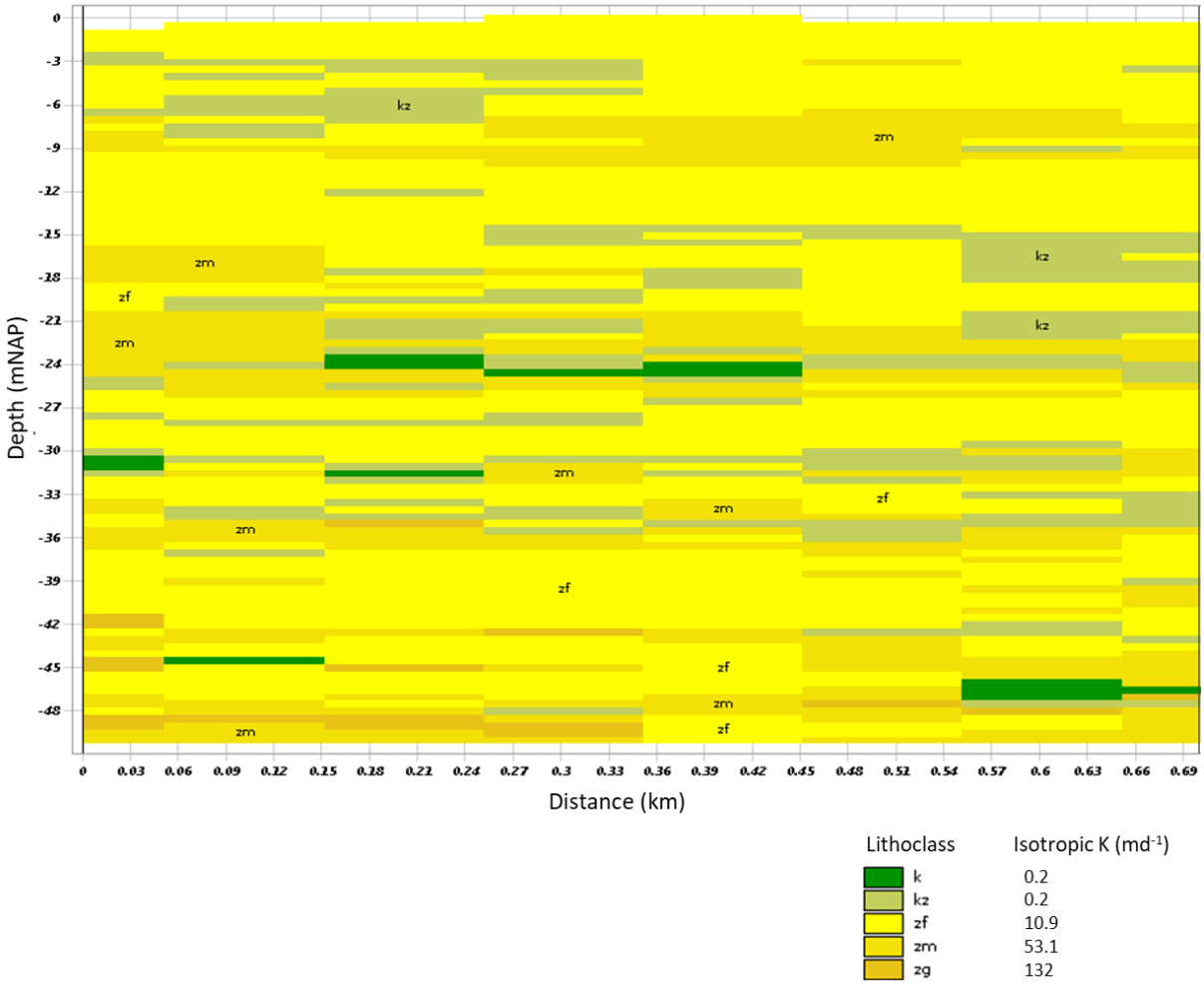

Figure 33, Isotropic hydraulic conductivity of the models (TNO, 2019b)

5.2. Fresh water lens in a non-tidal system 1971-2025

This section shows the results of the evolution of the fresh water lens of Veermansplaat from 1971 to 2025 in a non-tidal system. Model 1 uses a K scaling of 0.1 and model 2 uses a K scaling of 0.033. The salinity visualization of the models shows the salt concentrations of the models where the dark blue areas represent fresh water, the light blue to yellow areas represent brackish water and the red areas represent saline water.

5.2.1. Model 1

Figure 34 shows the salinity of model 1 for the evolution of the fresh water lens of Veermansplaat for the years 1976, 1986, 1996, 2006 and 2019 for a non-tidal system. In 2019, the average fresh water infiltration depth of model 1 reached a value of -20 m NAP at the centre of the island with a brackish water zone (mixing zone) thickness ranging between 1 and 5 m. The increase of infiltration depth of fresh water does not change at the same rate along the entire island. The fresh water infiltration is absent 50 m land inward from the west and east border for years 1971-1976. Rainwater infiltration at the west border starts between the year 1976 and 1986 and infiltration at the east border starts between 1986 and 1996. The shape of the fresh water lens changes around 1996 from an angled shape to a lens shape. Model 1 shows the growth of a fresh west oriented water lobe, an increase in infiltration depth at three locations at the bottom of the fresh water lens and the encapsulating of a saline water part at the eastern border starting at 1996. The model shows the extension of the lobe towards the western border. The fresh groundwater lobe in the west forms around local sandy clay layers (figure 33). Starting in 2006, the downwards growth of the fresh water lens stagnates in the eastern part of the model at a depth of -15 m NAP. This stagnation takes place at another local sandy clay layer (figure 33). The increased infiltration depth spikes at the bottom of the fresh water lens increase in size over time along the gridlines with the exception of the western one which decreases over time. The saline groundwater part at the eastern border decreases in size over time and is further encapsulated by fresh and brackish groundwater.

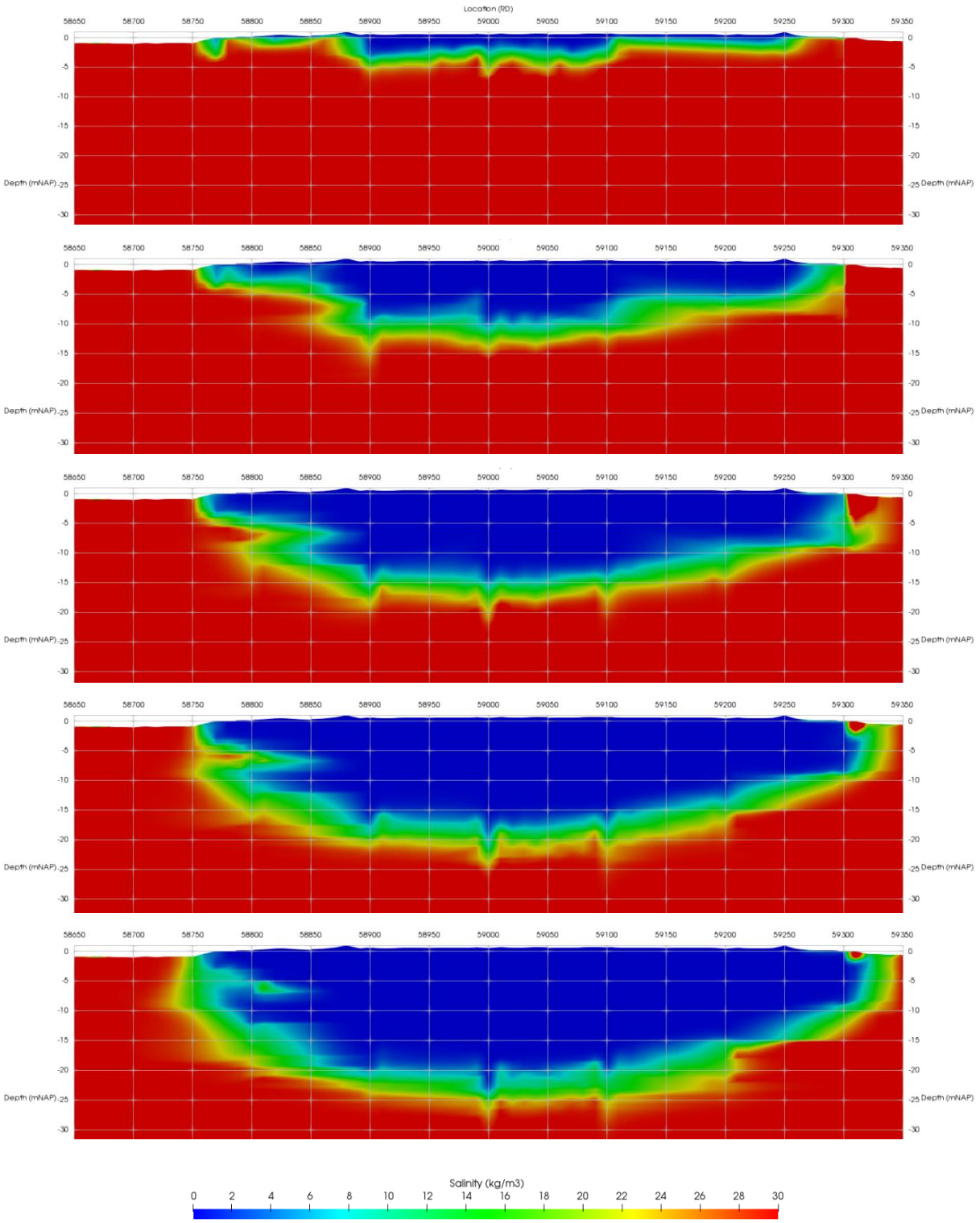

Figure 34, Salt concentration of groundwater for model 1 for the years 1976, 1986, 1996, 2006 and 2019 (from top to bottom)

Figure 35 shows the model results for the evolution of the fresh water lens of Veermansplaat for the years 2019, 2021, 2023 and 2025 for a non-tidal system. Through the course of these 6 years the average fresh water infiltration depth increases from -20 to -21 m NAP with an unchanged thickness for the mixing zone ranging between 1 and 5 m. The western fresh water lobe further extends towards the west and upwards resulting in the encapsulation a brackish water part at a depth of -6 m NAP and 50 m from the west border. The stagnation of infiltration in the east at -15 m NAP due to the presence of local sandy clay layers continues towards 2025. The saline water part in the east of the model further decreases in size over the course of this 6 years.

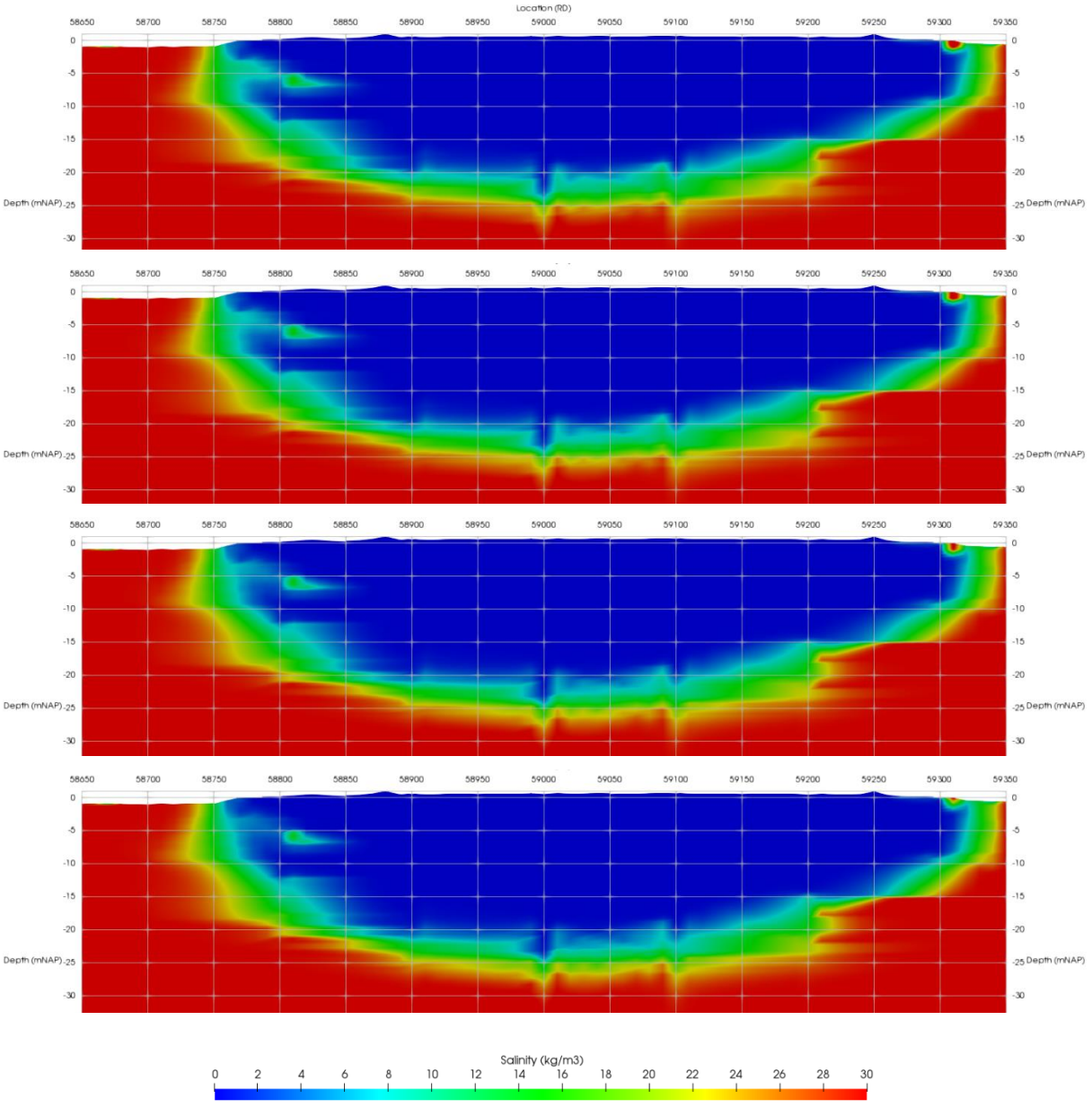

Figure 35, Salt concentration of groundwater for model 1 without tide for the years 2019, 2021, 2023 and 2025 (from top to bottom)

Figure 36 shows the depth profile of Cl for model 1 at 1971, 1975, 1985, 1995, 2005, 2015 and 2025. The depths of the fresh groundwater values are visible at a chloride concentration close to 0 mg L^{-1} and the depths of the salt groundwater values are visible at a chloride concentration close to 16600 mgl^{-1}. The gradient of the values between the fresh and saline water values (mixing zone gradient) do not change over the course of time. The infiltration depth of the transition between the fresh to saline water decreases over the course of time from -16.7 m between 1975-1985 to -3.3 m between 2015-2025.

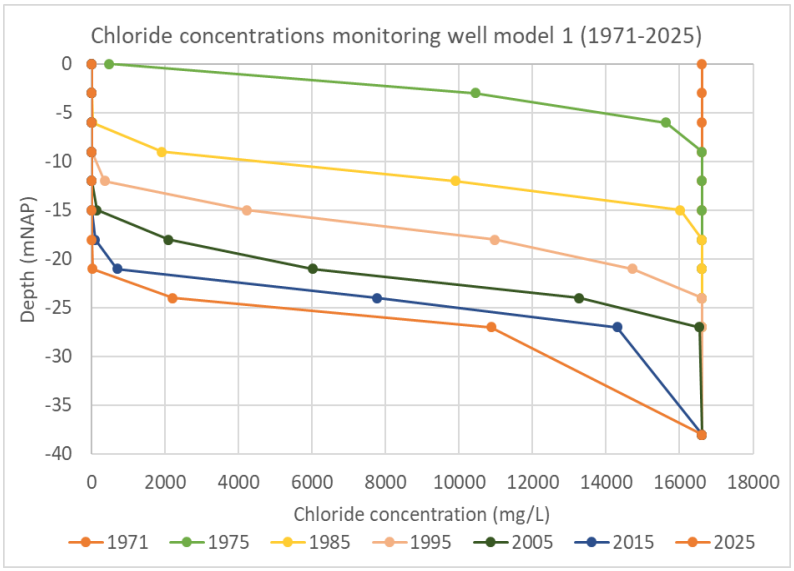

Figure 36, Chloride concentration against depth of model 1 for the years 1971-2025

Figure 37 shows the historical (green) and recent (brown) chloride concentrations along the depth of monitoring well B42F0081 and the chloride concentrations along the depth for the observation points of model 1 (red) for the years 1992, 1993, 1994, 1995 and 2019. The depth of the mixing zone for the historical values between 1992-1995 ranges between -5 and -15 m NAP and the depth of the mixing zone for model 1 for the same period ranges between -9 and -24 m NAP. The difference in depth between the fresh to saline water lines of the historical data and the model is 4.5 m. The depth of the mixing zone for the year 2019 is located between -8 to -20 m NAP and the depth of the mixing zone for model 1 in the year 2019 is located between -21 to -38 m NAP. The difference between mixing gradients of the recent data and the model is 7.5 m.

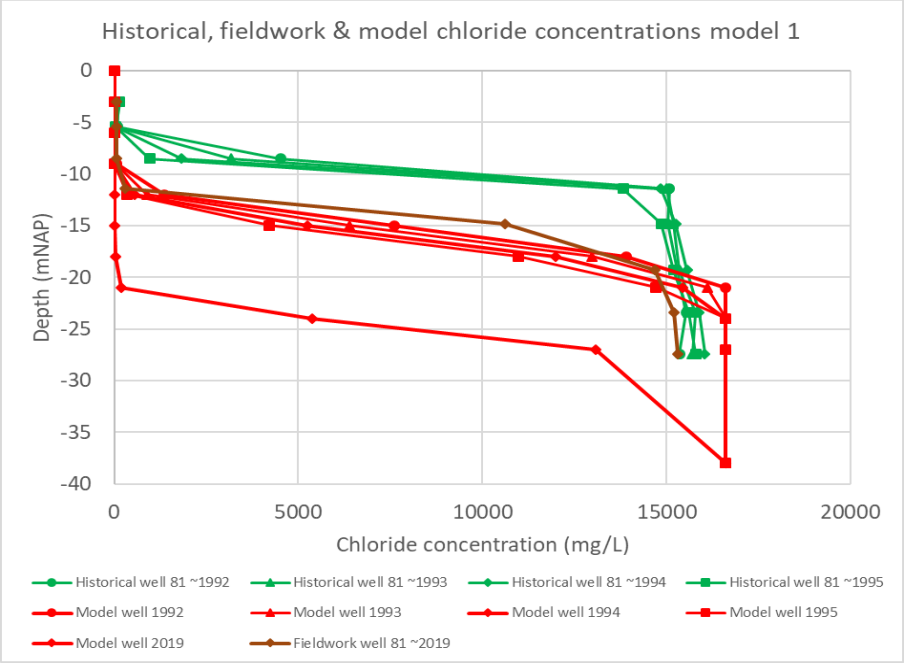

Figure 37, Chloride concentration against depth of model 1, historical data and field data

5.2.2. Model 2

Figure 38 shows the salinity of model 2 for the evolution of the fresh water lens of Veermansplaat for the years 1975, 1985, 1995, 2005 and 2019 for a non-tidal system with a K scaling of 0.033. In 2019, the average infiltration depth reaches a value of -11 m NAP at the centre of the fresh water lens with a thickness for the mixing zone ranging between 1 and 5 m. The increase of infiltration depth of fresh water does not change at the same rate along the entire island. The fresh water infiltration is absent 50 m land inward from the west and east border for years 1971-1975 and starts between the year 1975 and 1985. The fresh water infiltration depth of at these locations do not significantly increase toward the year 2005. The shape of the fresh water lens is angular between 1975 and 2005 and lens shaped in the year 2019. Starting in 2005 a west wards horizontal brackish lobe forms below the local sandy clay layers (figure 33). Model 2 shows the growth of an increased fresh water infiltration depth at the western border starting in 1975 and the growth of indentation of salt and brackish water at the middle of the island at the bottom of the fresh water lens starting in 1985. The growth of the increased fresh water infiltration depth at the western border increases slowly through the course of 48 years. The indentation by brackish and saline water in the middle of the island increases and decreases in area for brackish water over the years between 1985 and 2019.

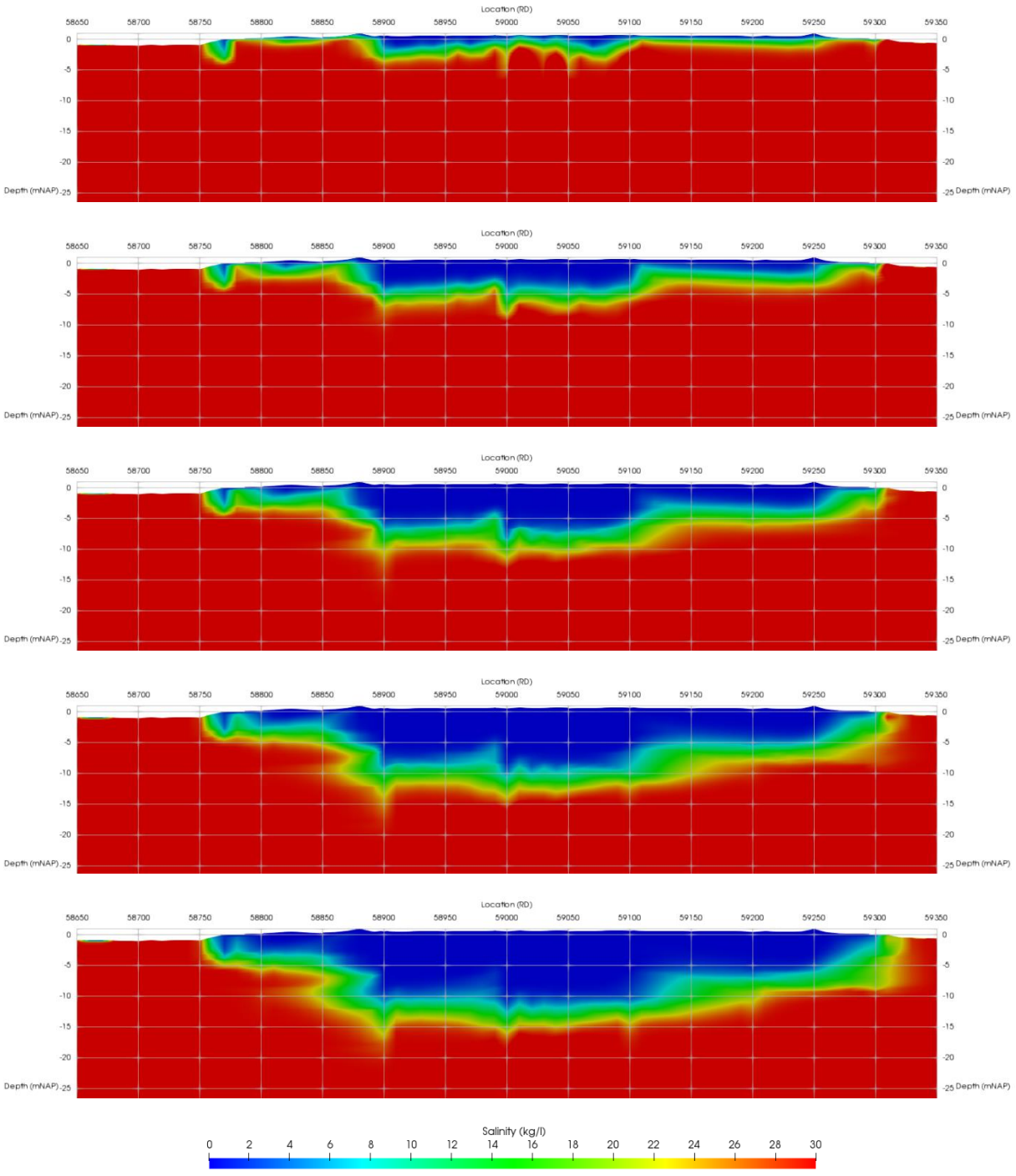

Figure 38, Salt concentration of groundwater of model 2 for the year 1975, 1985, 1995, 2005, 2019 (from top to bottom)

Figure 39 shows the results of model 2 for the evolution of the fresh water lens of Veermansplaat for the years 2019, 2021, 2023 and 2025 for a non-tidal system. Through the course of these 6 years the average fresh water infiltration depth increases from -11 m NAP to -12 m NAP with an unchanged mixing zone ranging between 1 and 5 m. In the western part of the fresh water lens the brackish water lobe further extends westward around the local sandy clay layers (figure 33). At the eastern border a small part of saline groundwater at the surface is encapsulated by brackish water. The saline groundwater part increases and decreases in size over the time span of 6 years.

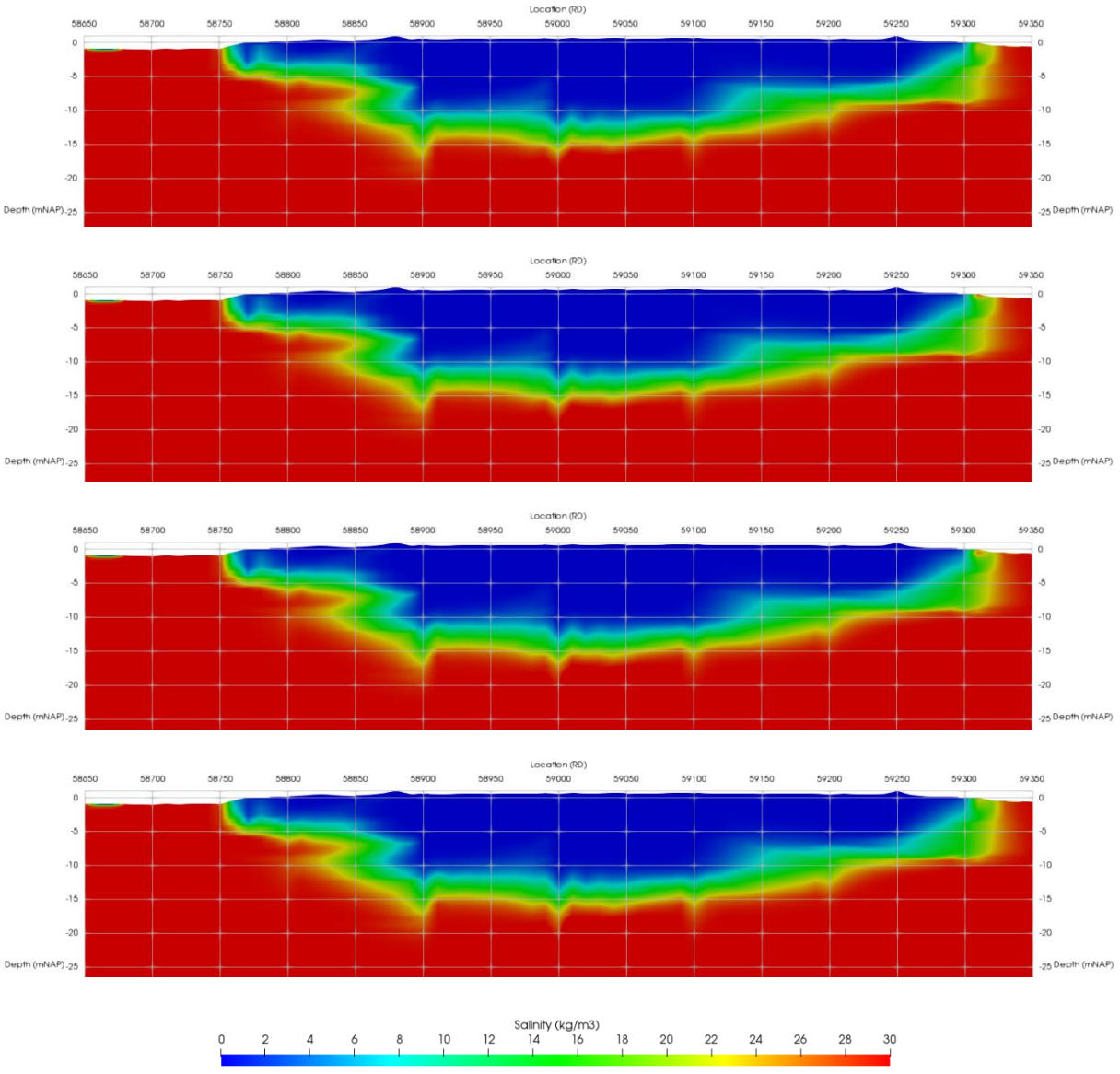

Figure 39, Salt concentration of groundwater of model 2 for the year 2019, 2021, 2023 and 2025 (from top to bottom)

Figure 40 shows the depth profile of Cl for model 2 at 1971, 1975, 1985, 1995, 2005, 2015 and 2025. The mixing zone gradients do not change over the course of the years. The change in the depths of the mixing gradients along the years decreases. The change in depths of the mixing gradient decreases from -4.1 m between 1985-1995 to -2.0 m between the years 2015-2025.

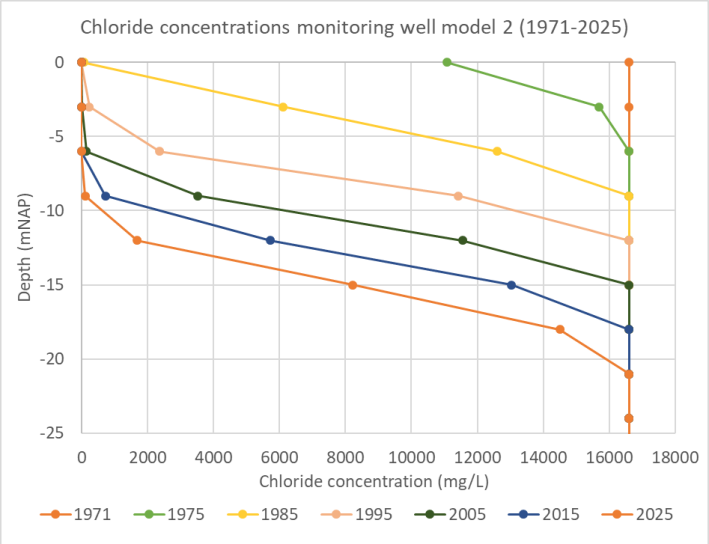

Figure 40, Chloride concentration against depth of model 2 for the years 1971-2025

Figure 41 shows the historical (green) and recent (brown) chloride concentrations along the depth of monitoring well B42F0081 and the chloride concentrations along the depth for the monitoring well of model 1 (red) for the years 1992, 1993, 1994, 1995 and 2019. The depth of the mixing zone for the historical values between 1992-1995 ranges between -5 to -15 m NAP and the depth of the mixing zone for model 1 for the same period ranges between -3 to -12 m NAP. The difference in depth between the fresh to saline water lines of the historical data and the model is 2.3 m. The depth of the mixing zone for the year 2019 is located between -8 to -20 m NAP and the depth of the mixing zone for model 1 in the year 2019 is located between -9 to -18 m NAP. The difference in depth between the mixing gradients of the recent data and the model is 0 m.

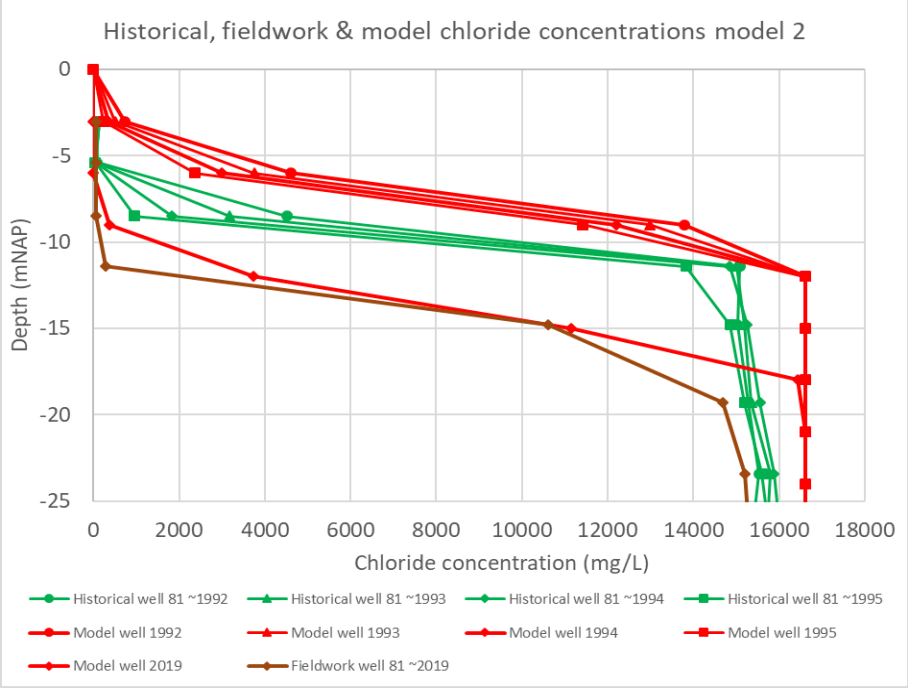

Figure 41, Chloride concentration against depth of model 1, historical data and field data

5.3. Fresh water lens in a tidal system for 2019-2023

This subchapter shows the results of the evolution of the fresh water lens of Veermansplaat from 2019 to 2023 in a tidal system starting in the year 2022. Model 3 uses a K scaling of 0.3.

5.3.1. Model 3

Figure 42 shows the salinity for the evolution of the fresh water lens of Veermansplaat for the years 2019, 2020, 2021, 2022 and 2023. The average fresh water infiltration depth increases from -27 to -28 m NAP with a mixing zone thickness ranging between 1 to 15 m. The two lobes at the eastern part of the fresh water lens increase in the course of time and are located around two local sandy clay layers (figure 33). At the east border of the island a small part of saline water decreases in size between 2019 and 2022 and increases during the period of tide between 2022 and 2023. Also, the mixing zone increases in size at the western lake between 2022 and 2023.

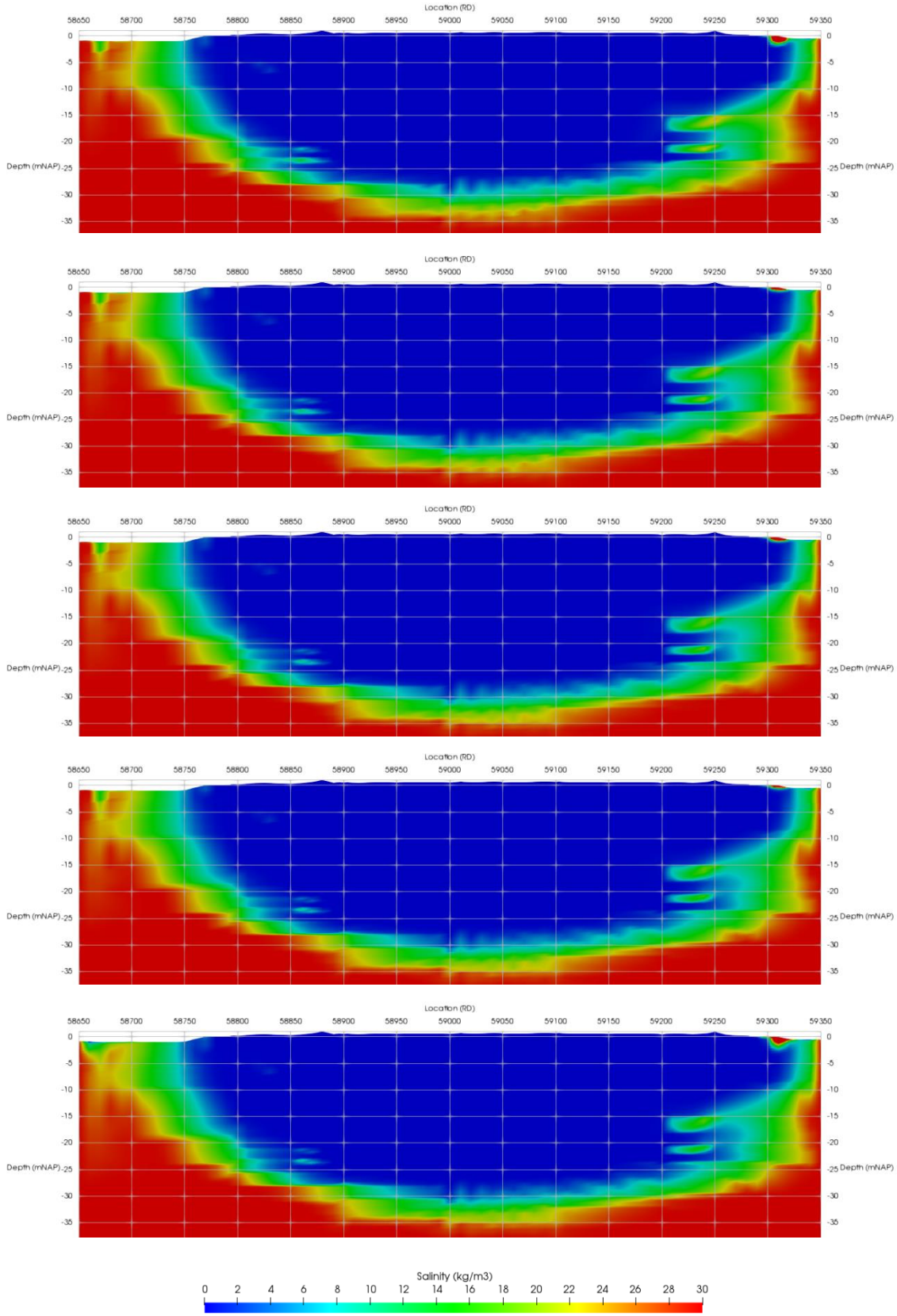

Figure 42, Salt concentration of groundwater of model 3 for the years 2016, 2019, 2021, 2022 and 2023 (from top to bottom)

Figure 43 shows the salinity of model 3 of the western and eastern border of Veermansplaat for the years 2021, 2022 and 2023. The change between in salinity between 2021 and 2022 shows the change for a non-tidal system and the change in salinity between 2022 and 2023 show the change for a tidal system. The salinity values between year 2021 and 2022 only show a significant decrease in salinity for the saline water part at the east border. The changes between 2022 and 2023 are more significant. As already shown in figure 42 the mixing zone increases at the western lake and the saline water part at the eastern border increases in size.

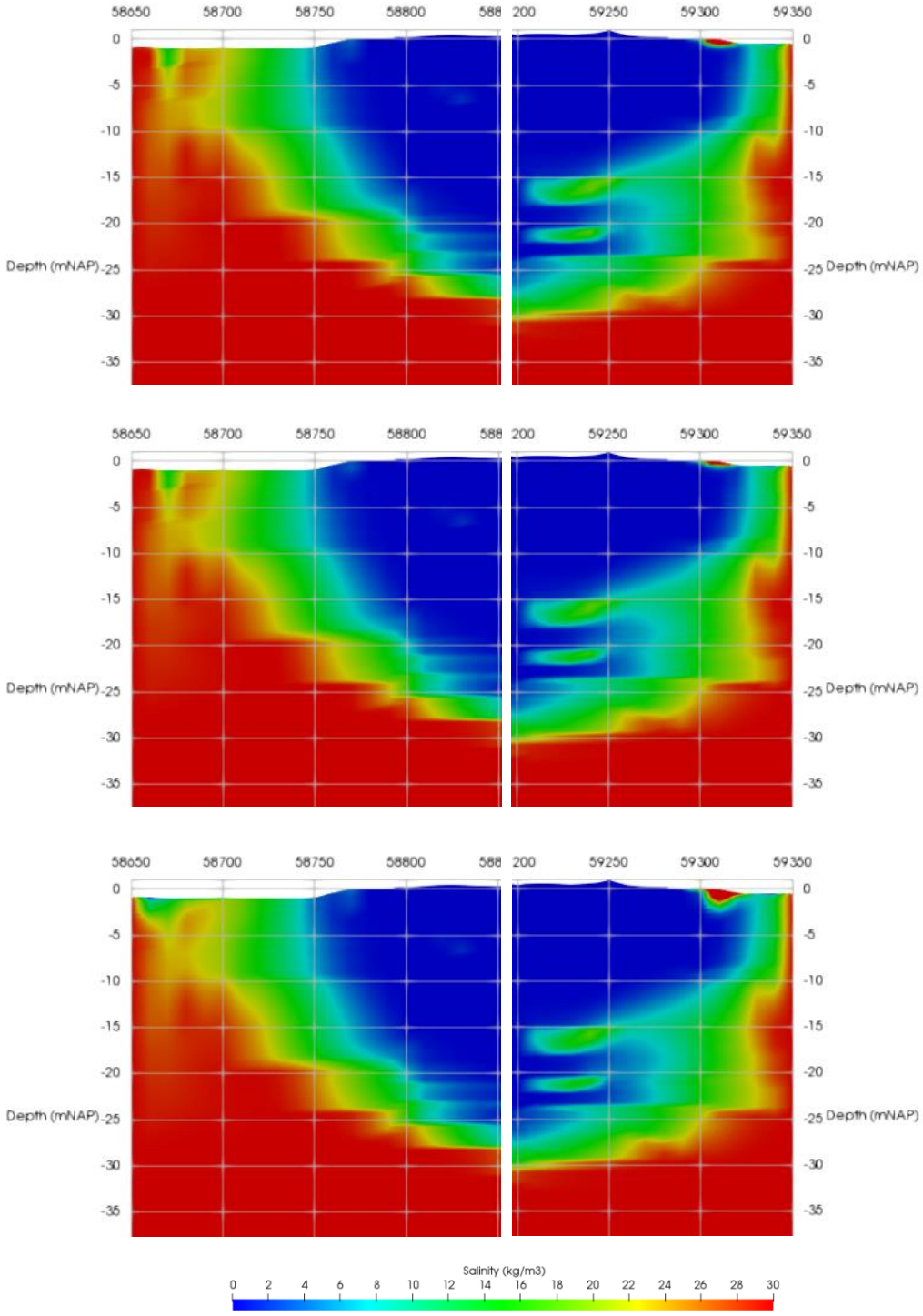

Figure 43, Salt concentration of groundwater of model 3 at the island border for the years 2021, 2022, 2023 (from top to bottom)

The effect of the tidal system on the fresh water lens of Veermansplaat is plotted for the observation point at -30 m NAP along the centre of model 3 (figure 44). Figure 44 shows the infiltration speed of the fresh water lens by plotting a trend line through the salinity values for the non-tidal system and the tidal system. This results in a desalinization rate of 7E-05 kg L^{-1} d^{-1} for a non-tidal system and 4E-05 kg L^{-1} d^{-1} for a tidal system. However, figure 44 can only give an indication of the change in desalinization at a single point in the model due to the limitation in data availability. More spatial data is needed to confirm the change in desalinization rate affected by the introduction of a restricted tide.

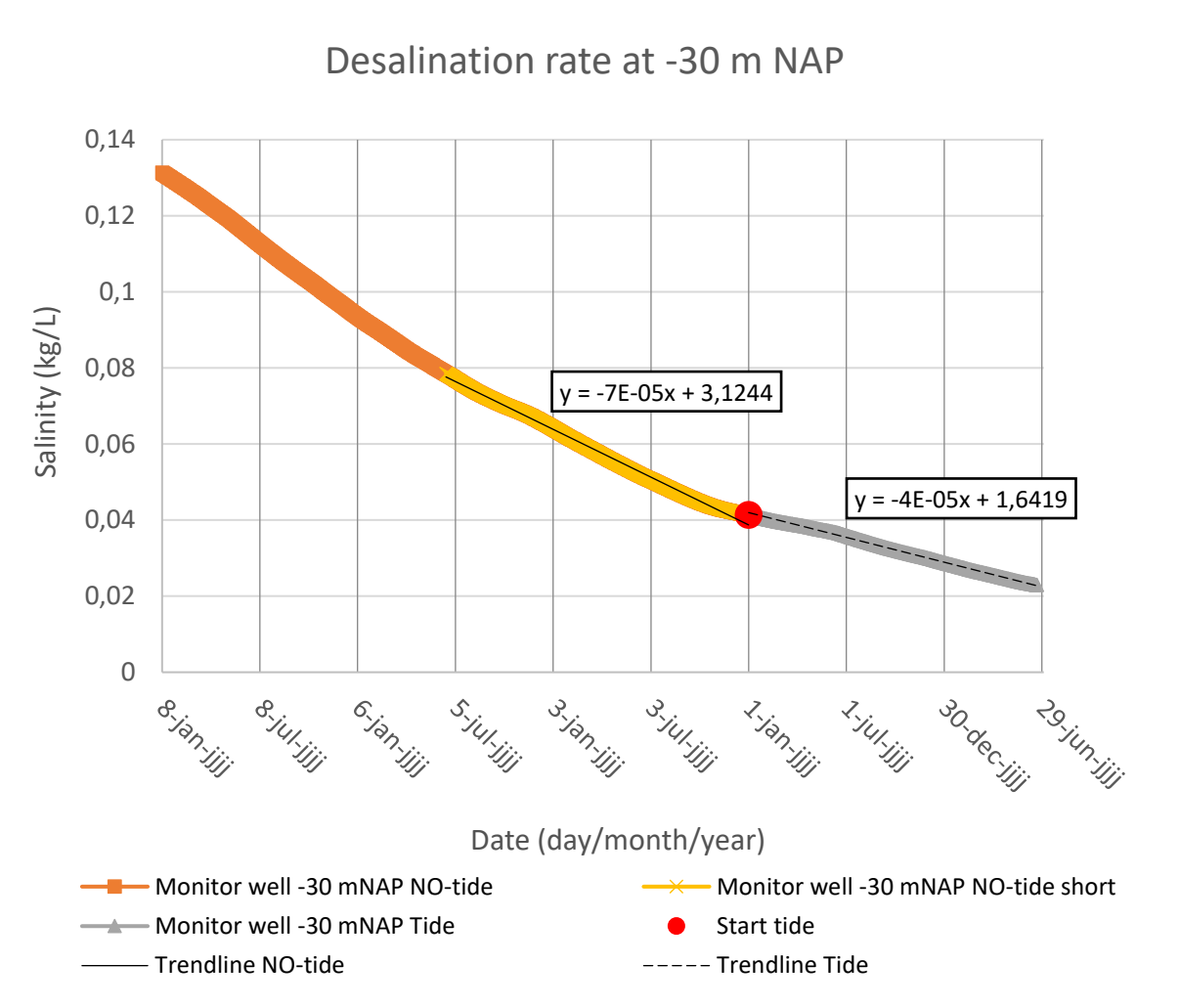

Figure 44, Salinity change over time at -30 m NAP for the transition to a tidal system

5. Discussion

This chapter will compare the gained knowledge of this research and will relate it to literature. The considerations made during the research will be explained. Finally, future actions for modelling a fresh water lens in a tidal system are discussed.

5.1. Relating results

The evolution of the fresh water lens of Veermansplaat in a non-tidal system evolves at a faster rate for model 1 compared to model 2 resulting in a difference of fresh water infiltration depth of 9 m. The only difference between the two models is scaling of the hydraulic conductivity, whereas the hydraulic conductivity values of model 1 are multiplied by 0.1 and model 2 by 0.033. The hydraulic conductivity reduction of 33% between model 1 and 2 therefore reduced the infiltration depth over the course of 54 years by 57%. However, according to research by Dose et al. (2014) and Ketabchi et al. (2014) infiltration depth should increase by reducing the hydraulic conductivity due to the mass balance of the groundwater. The decrease in fresh water infiltration depth by lowering the hydraulic conductivity for the models in this research therefore shows the undervaluing of the impact of mass balance. However, the relative hydraulic conductivity influences the evolution of the fresh water lens to a great extent. This is visible in all the models where preferential flow limits the growth of the fresh water lens at the presence of local sandy clay layers.

The values of the fresh water infiltration depth of model 1 and 2 compared to the recent and historical measurements (figure 37 & 41) show model 2 to be most corresponding to reality. Model 2 shows a fresh water infiltration depth difference of 2.3 m compared to the historical values for the years 1992-1995 and equals the fresh water infiltration depth in the year 2019. However, considering the undervaluation of the mass balance of groundwater by the models the shape and infiltration depth of the fresh water lens of models could differ from reality.

The shape and salinity distribution of the fresh water lens of Veermansplaat of model 3 shows no to little changes for the non-tidal period between the years 2016-2022. However, due to the introduction of a tidal system in 2022 the shape and salt distribution considerably change compared to the non-tidal situation. The biggest changes appear at the coastal areas of Veermansplaat. The mixing zone and salinity values increase at the east and west border. Hunt Jr. and Peterson 1980 and Wheatecraft and Buddemeier (1981) also show the increase of the mixing zone due to the introduction of a tidal system. The mixing zone and salinities at the centre of Veermansplaat are less effected by the introduction of the tidal system. The desalinization rate at -30 m NAP shows a small decrease after the introduction of the tidal system. However, the desalination rate also decreases 1 month prior to the introduction of the tidal system. Therefore, it is uncertain if the decrease of the desalinization rate is affected by the introduction of a tidal system or decreases naturally.

5.2. Considerations

This research has attempted to reconstruct the evolution of the fresh water lens of Veermansplaat between 1971 and 2019 and the future evolution for a non-tidal and tidal system. However, the models presented in this research come with some limitations. Because Hydrogeosphere is a physically based model, the accuracy for the representation of the reality by the models is heavily dependent on the quantity and detail of the input variables. The input data of this research therefore limits the representation of the reality. Firstly, the rainfall and evaporation values originate from different geographical locations. The rainfall values originate from Brouwershaven and the evaporation values originate from Vlissingen. Secondly, the hydraulic conductivity is derived from the lithological classes

of GeoTOP (TNO, 2019b) which are interpolated values between measurements resulting a large grid and uncertainties. Lastly, the exclusion of the influence of vegetation and organic soil formation results in the simplification of the surface evaporation and hydraulic conductivity values compared to the reality.

The models generated using Hydrogeosphere do come with some errors which should be taken into consideration. The fresh water infiltration depth of the models increases at several point along the bottom of the fresh water lens, visible in model 1 and 2 and probably present in model 3. This could be due to the large grid size and contrast of the hydraulic conductivity values and preferential flow. The increased values are positioned at the boundaries of the hydraulic conductivity grid (figure 33). Another error is the increased salinity located at the eastern island border of all the models. The salinity of this part reaches values of 80 kg m^{-3} which is a result of high numerical errors. These errors could be fixed by increasing the complexity of the model but were kept in the final results due to the setbacks of Hydrogeosphere and the limited time.

Hydrogeosphere is a very detailed and flexible program and can therefore be used for in depth scenario-based modelling researches. However, this complexity and flexibility also comes with multiple setbacks. During this research the use of Hydrogeosphere resulted in multiple problems and setbacks, which prolonged the research period and limited the research on implementing a climate scenario analysis, a 100-year model time duration and a total model coverage of the island. Firstly, the learning curve of Hydrogeosphere is slow, resulting in a very long learning process of the coding language and understanding of the physical model. Secondly, the runtime of the model increases drastically if density dependent transport of a solute is introduced, resulting in the change toward a 2D slice instead of a 3D model. Thirdly, the introduction of a tidal system resulted into the lowering of the time steps for the tidal system, resulting in runtimes up to weeks and very large data sets. Finally, the program for Hydrogeosphere is used on a virtual machine to enable flexible access. However, the virtual machine has 2 processor cores, has a limited storage space and randomly shuts down. This resulted in a slow calculation time and the termination of long runs.

5.3. Future actions

This research gives a detailed overview of the evolution of the fresh water lens of Veermansplaat from 1971 to 2019 and an indication of the effects of a tidal and non-tidal system on the fresh water lens of Veermansplaat for the near future. The model results for the scenario of a tidal and non-tidal system can be used by the RSV to get a better understanding of the hydrological processes in the subsurface. It is advised to conduct further research on the effect of a tidal system on the fresh water lens of Veermansplaat. It is recommended to increase the duration of the tidal system and to use another modelling program with a faster learning curve such as MOCDENS3D or FEFLOW (Oude-Essink, 2001; Pauw, De Louw & Oude-Essink, 2012; Lemieux et al., 2015).

6. Conclusion

The mitigation plan of the Rijksstructuurvisie Grevelingen en Volkerak-Zoommeer will introduce a restricted tide of 50 cm to lake Grevelingen. Lake Grevelingen will therefore be reintroduced to a tidal system since its enclosure from the sea in 1971. It is uncertain how this will affect the evolution of the fresh water lens below Veermansplaat. This research conducts a field and modelling investigation on the influence of a restricted tide on the evolution of the fresh water lens of Veermansplaat.

Since the reclamation of Veermansplaat in 1971 the fresh water lens has reached a depth of -13 m NAP for the year 2019. The fresh water lens does not resemble a perfect shaped lens. The northern and southern border of the island have low infiltration depth presumably due to salt spray and flooding and the infiltration depth shows a variation due to a variation of soil formation, vegetation and the retention of water by sand ridges. The surface infiltration rates at some areas at the border of the island are lower compared the inland values due to the presence of local clay and mud layers. The geochemistry of the groundwater shows the presence of desalinization along the depth of Veermansplaat. Rainfall and to a smaller extent the water level of lake Grevelingen have a direct effect on the groundwater levels at on Veermansplaat. The model for the fresh water lens of Veermansplaat in a non-tidal system also shows an irregular shaped fresh water lens with lower infiltration depths at the borders of the island. The non-tidal model simulates a further increase of the infiltration depth from -11 to -12 m NAP with a decreasing infiltration rate over time. The shape of the fresh water lens will extend to the coastal boundaries of Veermansplaat resulting in closer representation of a lens shape. The model for the fresh water lens of Veermansplaat in a tidal system shows an increase in size of the mixing zones at the island borders and a decrease in the infiltration rate of the fresh water lens within a single year resulting in the salinization of the island borders. Altogether, the evolution of the fresh water lens of Veermansplaat will be affected by the introduction of a restricted tide of 50 m.

It is recommended to the Rijksstructuurvisie Grevelingen en Volkerak-Zoommeer to take caution with the decision to introduce a restricted tide at lake Grevelingen. The difficulty of implementing a tidal system on the fresh water lens of Veermansplaat with Hydrogeosphere has resulted in limited data on the effect of a restricted tide on the fresh water lens of Veermansplaat. For future research it is recommended to use other modelling programs reducing the complexity but in return decreasing the runtime.

References

Aquanty inc. (2016). HGS User Manual. Waterloo, Ontario

Badon Ghyben, W. (1889). Nota in verband met de voorgenomen putboring nabij Amsterdam. *Tijdschrift Kon. Instit. Ingenieurs,* The Hague, 1888/1889, 209-223.

Blauw, T. S., Haas, H. A., & Adriaanse, L. A. (2004). Dynamiek terug in de delta. *De Levende Natuur*, *105*(5), 162-167.

Brunner, P., & Simmons, C. T. (2012). Hydrogeosphere: a fully integrated, physically based hydrological model. *Groundwater*, *50*(2), 170-176.

Dahlin, T. (1993). On the automation of 2D resistivity surveying for engineering and environmental applications, Ph.D. thesis, Dept. Eng. Geol., Lund Univ., Lund, Sweden.

De Kraker, K. (2012). Vegetatie van de Grevelingen: kartering meetsoorten 2009-2011. *Sandvicensis, Ecologisch adviesbureau*. 206

Di Prima, S., Castellini, M., Najm, M. R. A., Stewart, R. D., Angulo-Jaramillo, R., Winiarski, T., & Lassabatere, L. (2019). Experimental assessment of a new comprehensive model for single ring infiltration data. *Journal of Hydrology*, *573*, 937-951.

Dose, E. J., Stoeckl, L., Houben, G. J., Vacher, H. L., Vassolo, S., Dietrich, J., & Himmelsbach, T. (2014). Experiments and modeling of fresh water lenses in layered aquifers: steady state interface geometry. *Journal of hydrology*, *509*, 621-630.

Du Commun, J. (1828). On the causes of fresh water springs, fountains etc. *Am. J. Sci (1st ser.) 14*, 174-176.

Elrick, D. E., Parkin, G. W., Reynolds, W. D., & Fallow, D. J. (1995). Analysis of early-time and steady state single-ring infiltration under falling head conditions. *Water Resources Research*, *31*(8), 1883-1893.

Erler, A. R., Frey, S. K., Khader, O., d'Orgeville, M., Park, Y. J., Hwang, H. T., ... & Sudicky, E. A. (2019). Simulating Climate Change Impacts on Surface Water Resources Within a Lake-Affected Region Using Regional Climate Projections. *Water Resources Research*, *55*(1), 130-155.

Fetter Jr, C. W. (1972). Position of the saline water interface beneath oceanic islands. *Water Resources Research*, *8*(5), 1307-1315.

Gat, J. R., & Matsui, E. (1991). Atmospheric water balance in the Amazon Basin: an isotopic evapotranspiration model. *Journal of Geophysical Research: Atmospheres*, *96*(D7), 13179-13188.

Gerritsen, H. (2005). What happened in 1953? The Big Flood in the Netherlands in retrospect. *Philosophical Transactions of the Royal Society of London A: Mathematical, Physical and Engineering Sciences*, *363,* 1831: 1271-1291.

Herzberg, B. (1901). Die Wasserversorgung einiger Nordseebader. J. Gasbeleuchtung & Wasserversorgung, *44*, 815-819 & 842-844.

Holding, S., & Allen, D. M. (2015). Wave overwash impact on small islands: Generalised observations of fresh water lens response and recovery for multiple hydrogeological settings. *Journal of Hydrology*, *529*, 1324-1335.

Hunt Jr, C. D., & Peterson, F. L. (1980). Groundwater resources of Kwajalein Island, Marshall Islands. *Technical Report*, *126*.

KELLER AG für Druckmesstechnik (2014). Logger 5.1 Manual.

Ketabchi, H., Mahmoodzadeh, D., Ataie-Ashtiani, B., Werner, A. D., & Simmons, C. T. (2014). Sea-level rise impact on fresh groundwater lenses in two-layer small islands. *Hydrological Processes*, *28*(24), 5938-5953.

KNMI (2019a). Dagwaarden neerslag stations, 736 Brouwershaven. Retrieved May 14, 2019, from https://www.knmi.nl/nederland-nu/klimatologie/monv/reeksen

KNMI (2019b). Daggegevens van het weer in Nederland, 310 Vlissingen. Retrieved May 30, 2019, from https://www.knmi.nl/nederland-nu/klimatologie/daggegevens

Lemieux, J. M., Hassaoui, J., Molson, J., Therrien, R., Therrien, P., Chouteau, M., & Ouellet, M. (2015). Simulating the impact of climate change on the groundwater resources of the Magdalen Islands, Québec, Canada. *Journal of Hydrology: Regional Studies*, *3*, 400-423.

Loke, M. H. (2001). Electrical imaging surveys for environmental and engineering studies. A practical guide to 2D and 3D surveys.

Okpoli, C. C. (2013). Sensitivity and resolution capacity of electrode configurations. *International Journal of Geophysics*, *2013*.

Oude-Essink, G. H. (2001). Salt water intrusion in a three-dimensional groundwater system in the Netherlands: a numerical study. *Transport in porous media*, *43*(1), 137-158.

Pauw, P. S. (2015). Field and model investigations of fresh water lenses in coastal aquifers. *Wageningen University*.

Pauw, P., De Louw, P. G., & Oude-Essink, G. H. (2012). Groundwater salinisation in the Wadden Sea area of the Netherlands: quantifying the effects of climate change, sea-level rise and anthropogenic interferences. *Netherlands Journal of Geosciences*, *91*(3), 373-383.

Rijkswaterstaat (2019). Rijkswaterstaat Waterinfo, waterhoogten Bommenende 1. Retrieved May 30, 2019, from https://waterinfo.rws.nl/#!/kaart/Waterhoogten/Waterhoogte___20Oppervlaktewater___20t.o.v.___20Normaal___20Amsterdams___20Peil___20in___20cm/

Saefuddin, R., Saito, H., & Šimůnek, J. (2019). Experimental and numerical evaluation of a ring-shaped emitter for subsurface irrigation. *Agricultural water management*, *211*, 111-122.

SIKB (2007). Het nemen van grondwatermonsters. *24*. SIKB

Slager, H., & Visser, J. (1990). *Abiotische kenmerken van de drooggevallen gebieden in de Grevelingen*. Rijkswaterstaat, Directie Flevoland.

Slim, P. A., & van Zonneveld, G. (2004). Afsluiten van zeearmen in de Delta. *Zee in zicht, 67*, 199-200

Stewart, R. D., & Abou Najm, M. R. (2018). A Comprehensive Model for Single Ring Infiltration II: Estimating Field-Saturated Hydraulic Conductivity. *Soil Science Society of America Journal*.

Stuyfzand, P. J. (1993). Hydrochemistry and hydrology of the coastal dune area of the Western Netherlands. *Ph.D. thesis, Free Univ., Amsterdam, Netherlands,* 366

Stuyfzand, P. J., Oskam, B., & Van Loon, D. (2014). Ontwikkeling van zoet-zoutgradiënten met en zonder dynamisch kustbeheer. *KWR*

Sulzbacher, H., Wiederhold, H., Siemon, B., Grinat, M., Igel, J., Burschil, T., ... & Hinsby, K. (2012). Numerical modelling of climate change impacts on fresh water lenses on the North Sea Island of Borkum. *Hydrology & Earth System Sciences Discussions*, *9*(3).

Surface height. (2019). In *Ecohydrogeochemistry of Former Tidal Wetlands*. Retrieved from https://solisservices.sharepoint.com/sites/EcohydrogeochemistryTFW

Tangelder, M., Wijsman, J., Janssen, J., Nolte, A., Walles, B., & Ysebaert, T. (2018). Scenariostudie natuurperspectief Grevelingenmeer. *Wageningen Marine Research,* No. C021/18

Therrien, R. (1992). Three-dimensional analysis of variably saturated flow and solute transport in discretely-fractured porous media. *Ph.D. thesis, University of Waterloo, Waterloo, Ont.*

TNO (2017). GeoTOP. Retrieved February 14, 2017, from https://www.dinoloket.nl/ondergrondmodellen

TNO (2019a). REGIS II v2.2. Retrieved June 25, 2019, from https://www.dinoloket.nl/ondergrondmodellen

TNO (2019b). GeoTOP v1.3. Retrieved June 25, 2019, from https://www.dinoloket.nl/ondergrondmodellen

Van de Haterd, R. J. W., Lengkeek, W., Bouma, S., & Collombon, M. T. (2010). Herintroductie getij in de Grevelingen en effecten op natuur in intergetijdengebieden. *Culemborg, Bureau Waardenburg*, *75*.

Van den Hengel, D. (2007). Slachtoffers bij overstromingen: analyse van een slachtoffermodel aan de hand van de Watersnoodramp van 1953 en overstromingssimulaties. *Technische Universiteit Delft*

Van Haperen, A.M.M. (2009). Een wereld van verschil. Landschap en plantengroei van de duinen op de Zeeuwse en Zuid-Hollandse Eilanden. *Proefschrift Wageningen Universiteit*

Vandenbohede, A., & Lebbe, L. (2012). Groundwater chemistry patterns in the phreatic aquifer of the central Belgian coastal plain. *Applied Geochemistry*, *27*(1), 22-36.

Viessman, W. & Lewis, G.L., (1996). Introduction to Hydrology, 4th Edition*, Harper Collins College Publisher, New York*

Wheatcraft, S. W., & Buddemeier, R. W. (1981). Atoll island hydrology. *Groundwater*, *19*(3), 311-320.

White, I., & Falkland, T. (2010). Management of fresh water lenses on small Pacific islands. *Hydrogeology Journal*, *18*(1), 227-246.

Zhang, R. (1997). Determination of soil sorptivity and hydraulic conductivity from the disk infiltrometer. *Soil Science Society of America Journal*, *61*(4), 1024-1030.

Appendices

Appendix 1 – Infiltration test locations

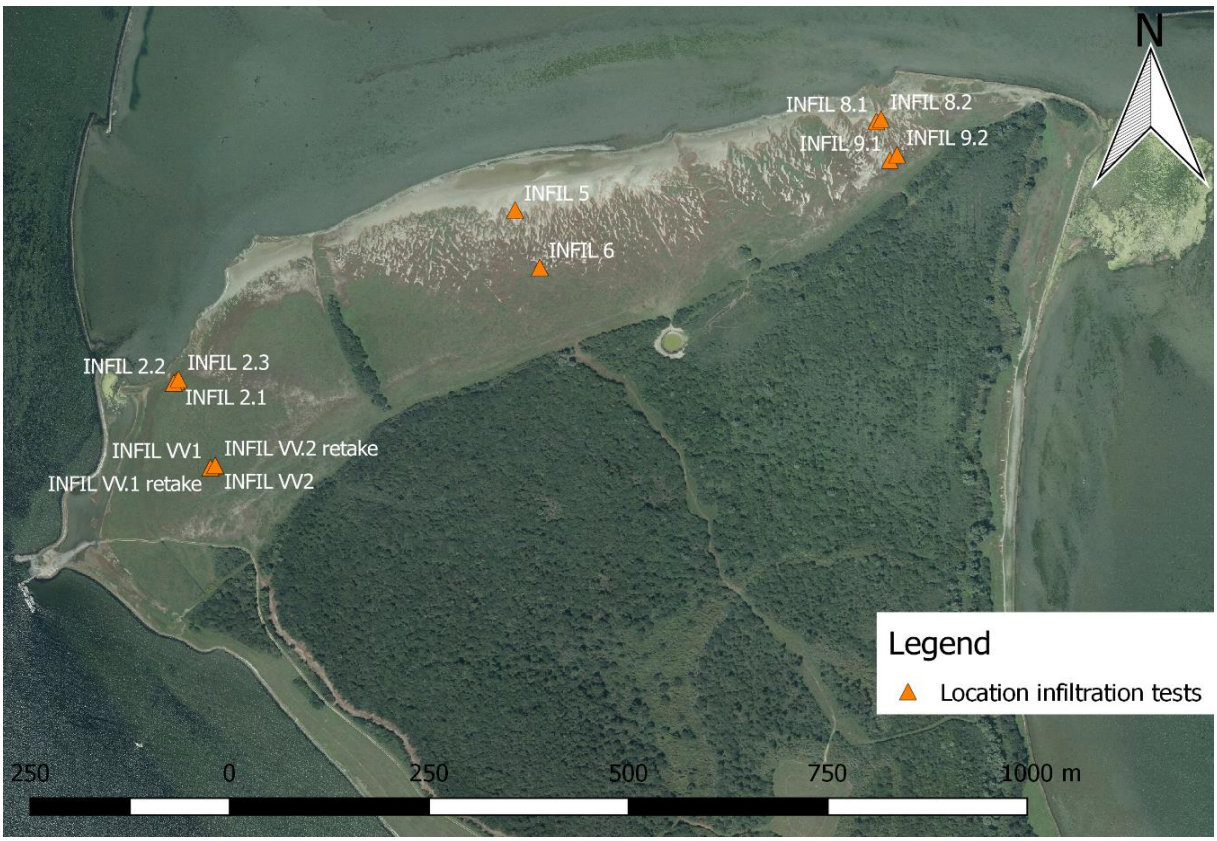

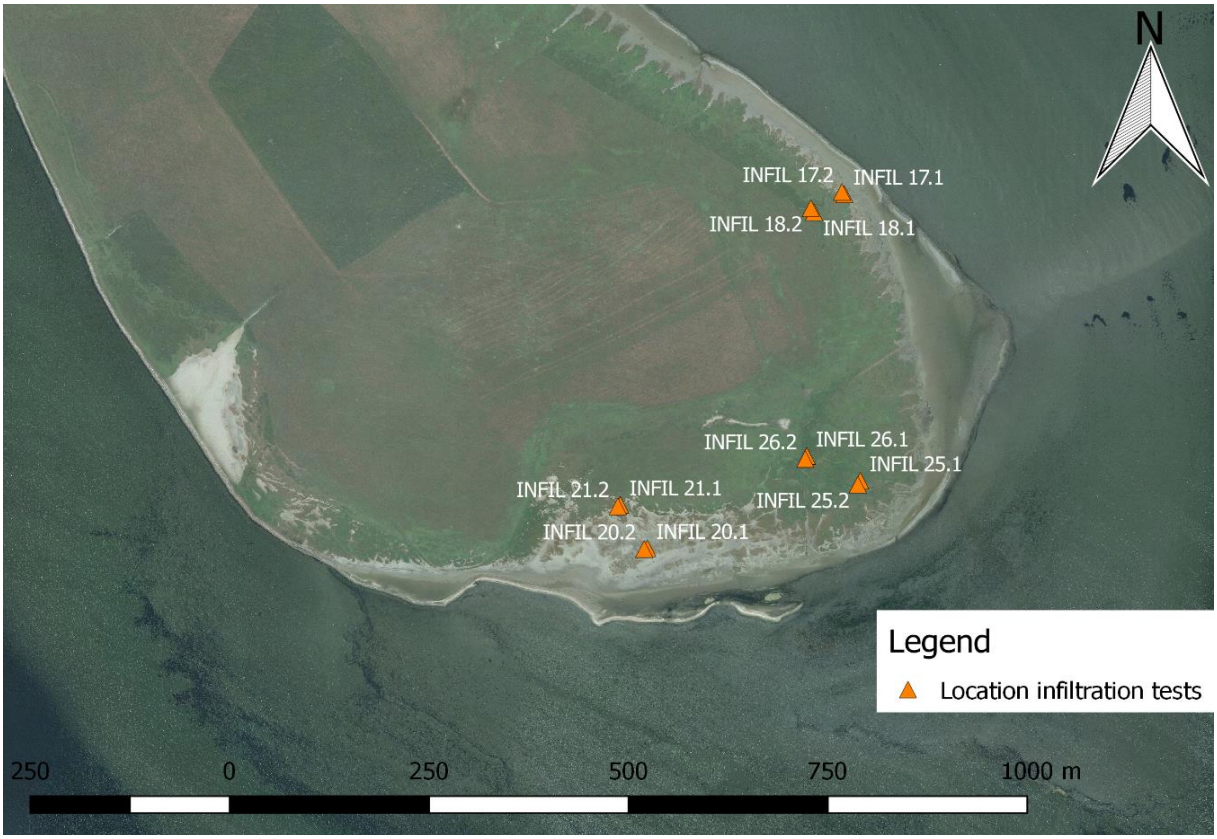

Appendix 2 – Graphs cumulative infiltration per infiltration test

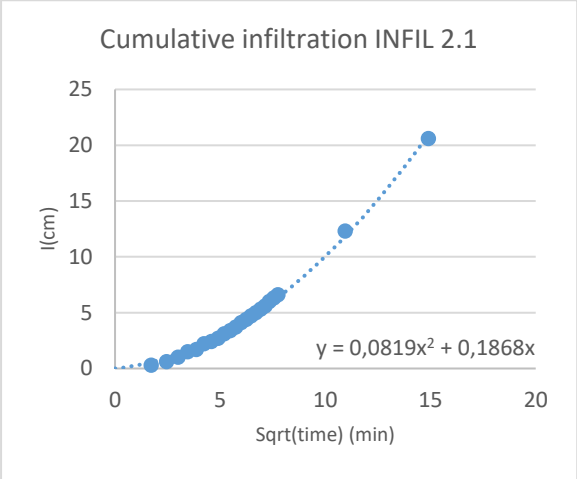

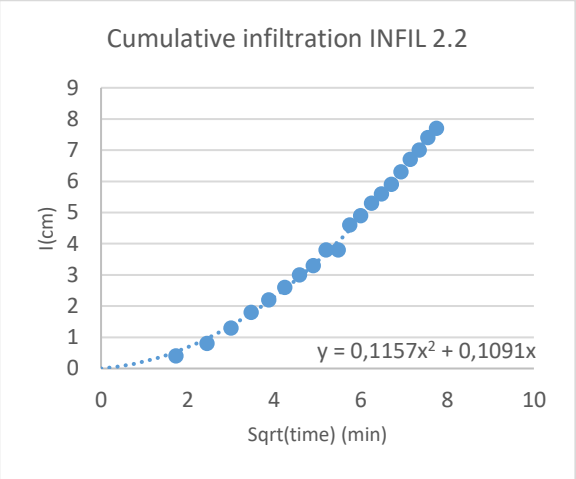

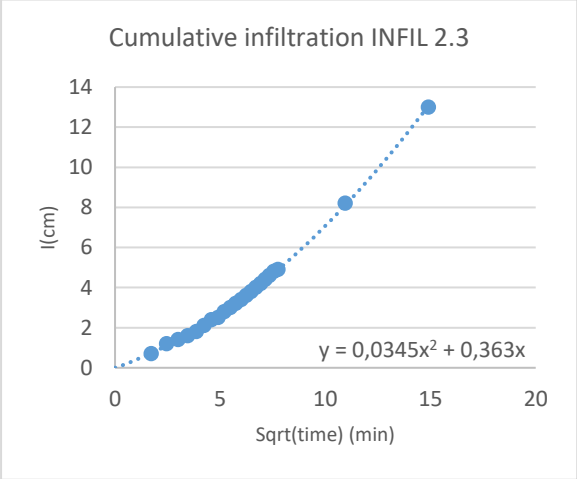

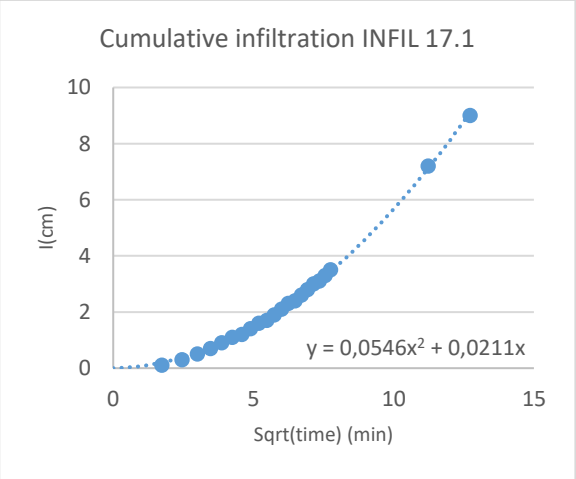

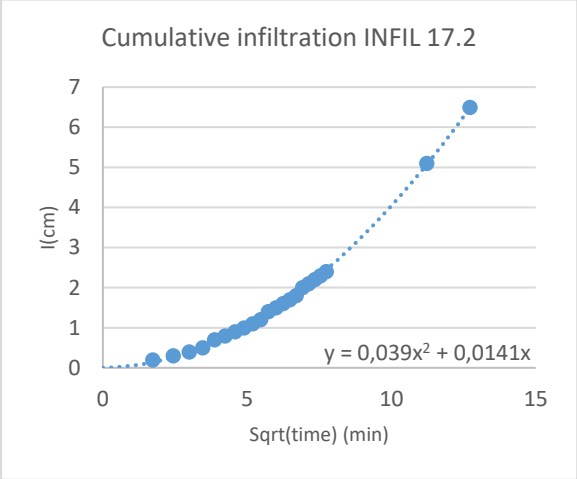

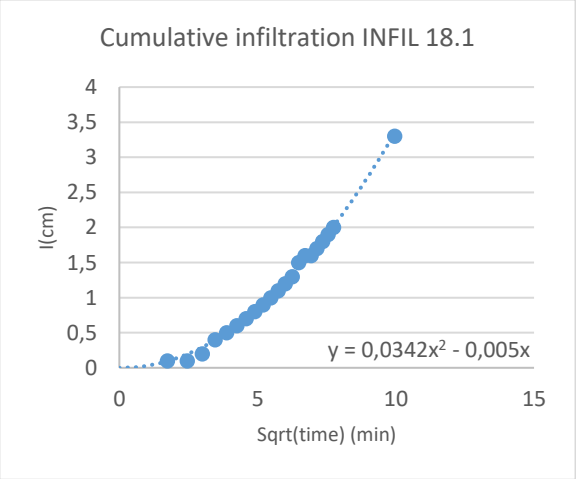

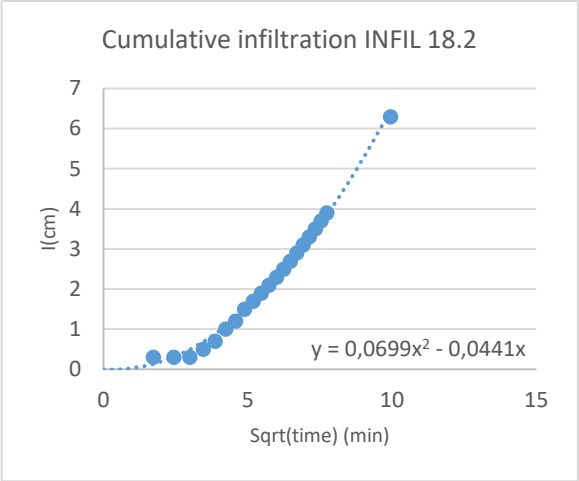
Cumulative infiltration INFIL 18.2
I(cm)
Sqrt(time) (min)
y = 0,0699x² - 0,0441x

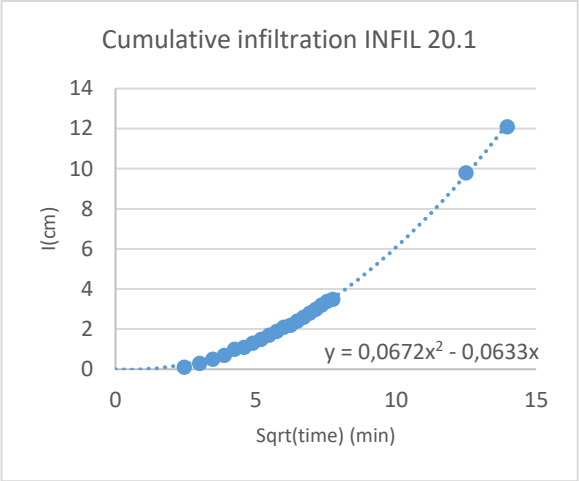
Cumulative infiltration INFIL 20.1
I(cm)
Sqrt(time) (min)
y = 0,0672x² - 0,0633x

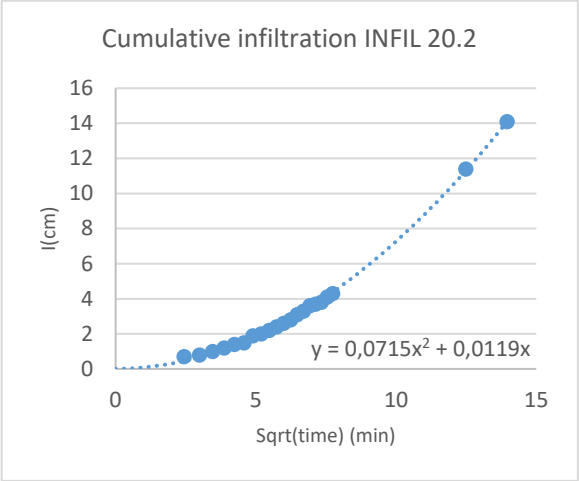
Cumulative infiltration INFIL 20.2
I(cm)
Sqrt(time) (min)
y = 0,0715x² + 0,0119x

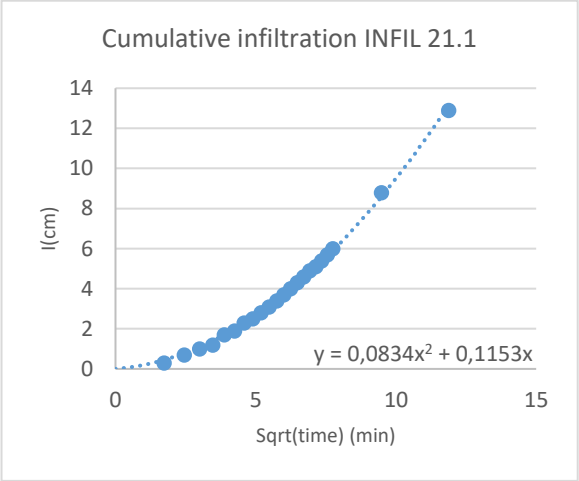
Cumulative infiltration INFIL 21.1
I(cm)
Sqrt(time) (min)
y = 0,0834x² + 0,1153x

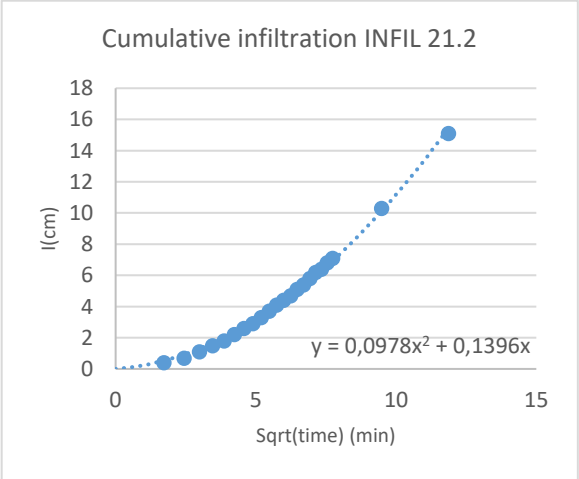
Cumulative infiltration INFIL 21.2
I(cm)
Sqrt(time) (min)
y = 0,0978x² + 0,1396x

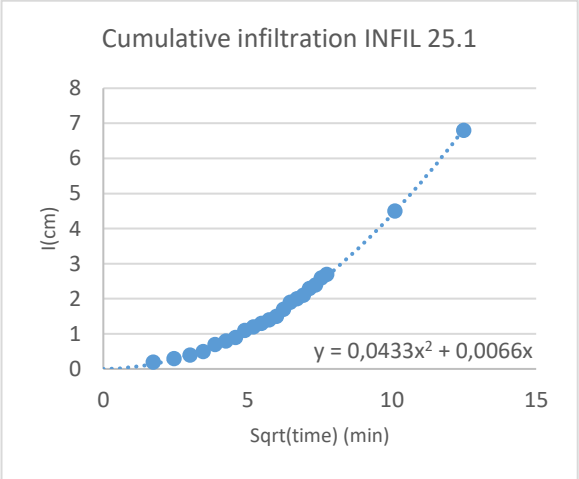
Cumulative infiltration INFIL 25.1
I(cm)
Sqrt(time) (min)
y = 0,0433x² + 0,0066x

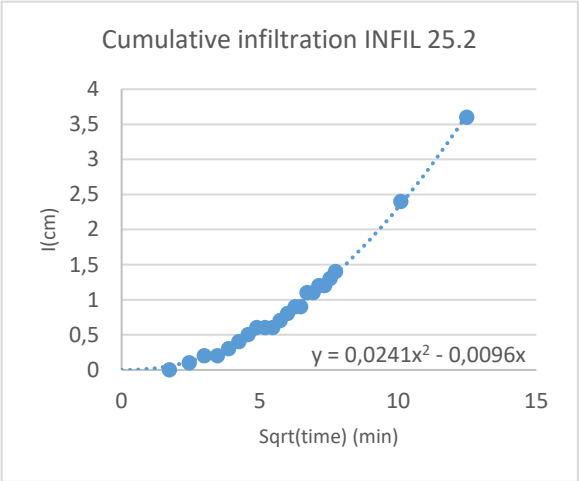
Cumulative infiltration INFIL 25.2
I(cm)
Sqrt(time) (min)
y = 0,0241x² - 0,0096x

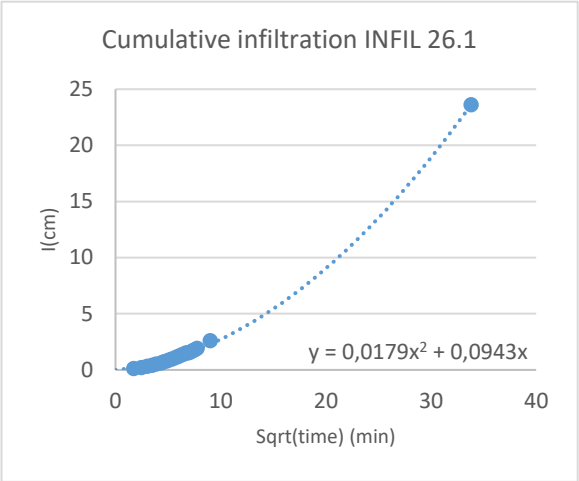
Cumulative infiltration INFIL 26.1
I(cm)
Sqrt(time) (min)
y = 0,0179x² + 0,0943x

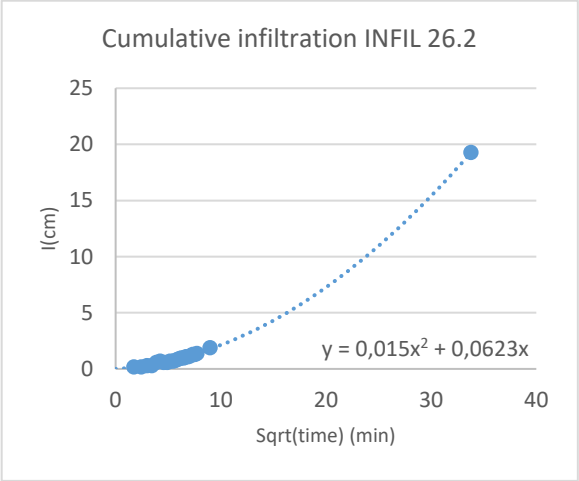
Cumulative infiltration INFIL 26.2
I(cm)
Sqrt(time) (min)
y = 0,015x² + 0,0623x

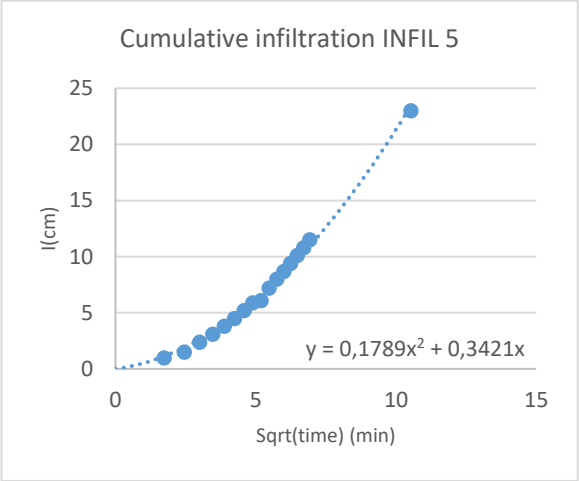
Cumulative infiltration INFIL 5
I(cm)
Sqrt(time) (min)
y = 0,1789x² + 0,3421x

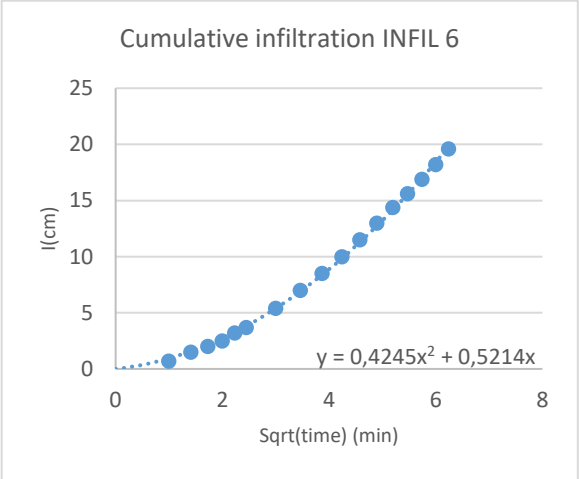
Cumulative infiltration INFIL 6
I(cm)
Sqrt(time) (min)
y = 0,4245x² + 0,5214x

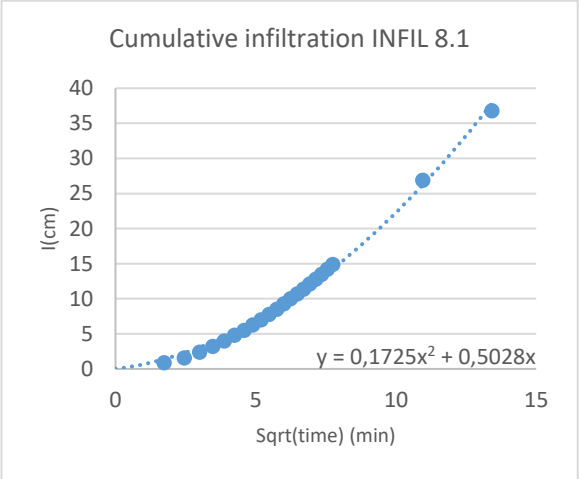
Cumulative infiltration INFIL 8.1
I(cm)
Sqrt(time) (min)
y = 0,1725x² + 0,5028x

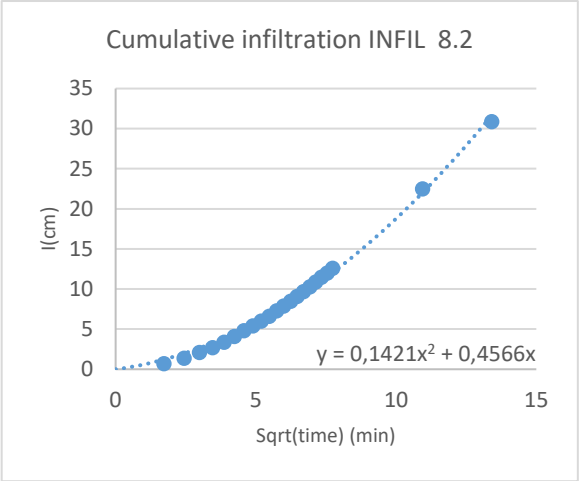
Cumulative infiltration INFIL 8.2
I(cm)
Sqrt(time) (min)
y = 0,1421x² + 0,4566x

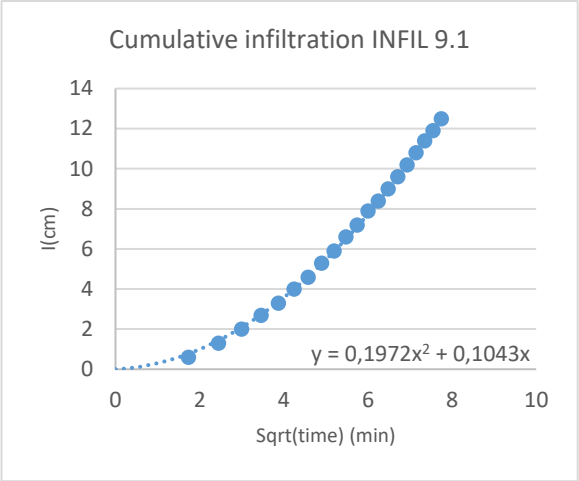
Cumulative infiltration INFIL 9.1
I(cm)
Sqrt(time) (min)
y = 0,1972x² + 0,1043x

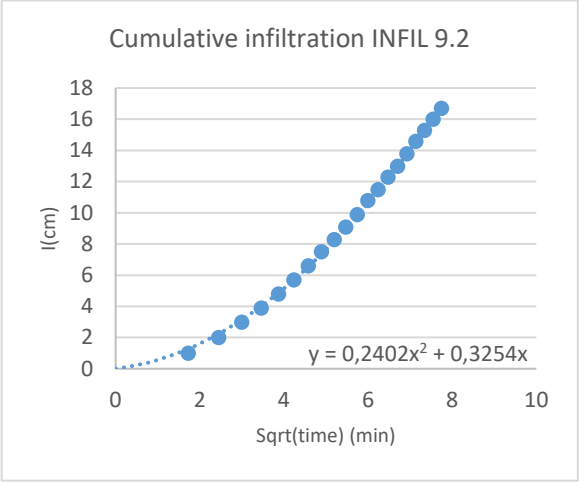
Cumulative infiltration INFIL 9.2
I(cm)
Sqrt(time) (min)
y = 0,2402x² + 0,3254x

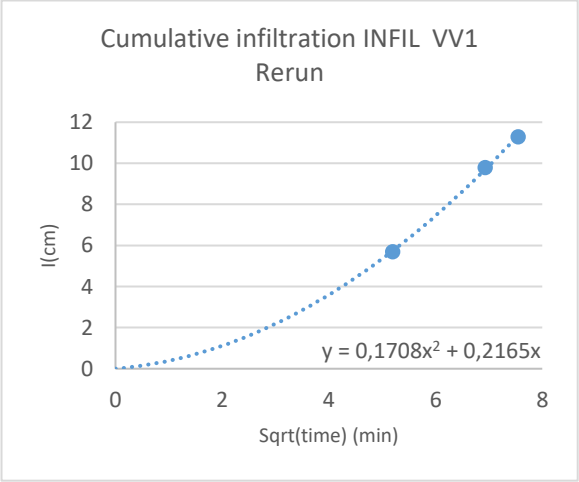
Cumulative infiltration INFIL VV1 Rerun
I(cm)
Sqrt(time) (min)
y = 0,1708x² + 0,2165x

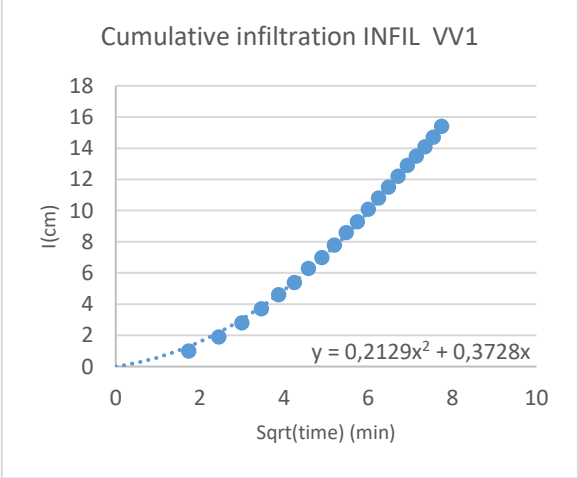
Cumulative infiltration INFIL VV1
I(cm)
Sqrt(time) (min)
y = 0,2129x² + 0,3728x

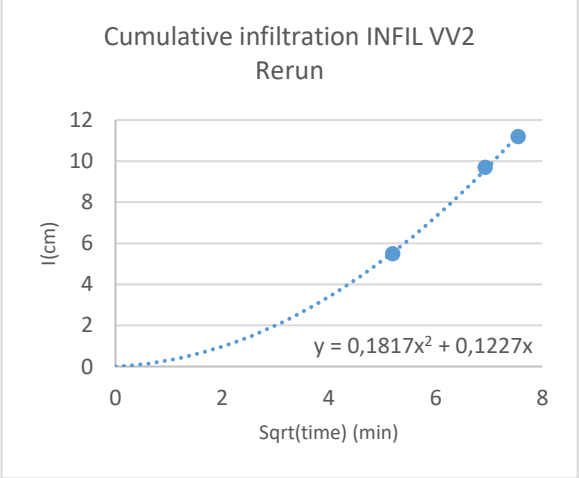
Cumulative infiltration INFIL VV2 Rerun
I(cm)
Sqrt(time) (min)
y = 0,1817x² + 0,1227x

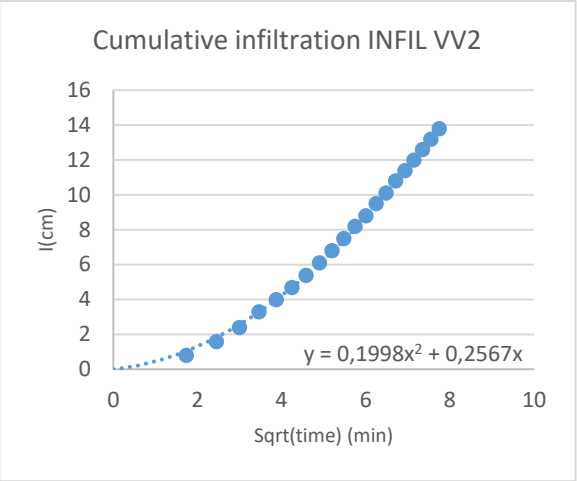
Cumulative infiltration INFIL VV2
16
14
12
10
8
6
4
2
0
I(cm)
0
2
4
6
8
10
Sqrt(time) (min)
y = 0,1998x² + 0,2567x

Appendix 3 - Chemical composition groundwater per groundwater sample

Nr	Well / Surface water	Sample codes			Ground Surface	Location				Sampling	Infiltration			Electrical Conductivity Field (25oC)	Calculated
		Well / Name	Tube	Code		X	Y	Z			Z_{infil}	Z/Z_{infil}	Z_{infil}/Z		
					m NAP			m BGS	m NAP	Date	m BGS	Time	Flushes	µS/cm (25oC)	µS/cm (25oC)
1	Deep Well	B42F0072	I	72-I	1.05	58582	418960	2.05	1.00	March 8, 2019	20.0	0.10	9.76	888	848
2		B42F0072	II	72-II				4.05	3.00	March 8, 2019		0.20	4.94	791	694
3		B42F0072	III	72-III				7.05	6.00	March 8, 2019		0.35	2.84	959	885
4		B42F0072	IV	72-IV				9.95	8.90	March 8, 2019		0.50	2.01	1,220	1,217
5		B42F0072	V	72-V				14.05	13.00	March 8, 2019		0.70	1.42	1,828	1,722
6		B42F0072	VI	72-VI				18.15	17.10	March 8, 2019		0.91	1.10	10,260	9,803
7		B42F0072	VII	72-VII				23.15	22.10	March 8, 2019		1.16	0.86	41,500	42,587
8		B42F0072	VIII	72-VIII				26.15	25.10	March 8, 2019		1.31	0.76	41,700	42,527
9		B42F0072	IX	72-IX				29.85	28.80	March 8, 2019		1.49	0.67	42,200	43,230
10		B42F0073	I	73-I	0.35	59660	416574	2.95	2.60	March 4, 2019	11.0	0.27	3.73	1,506	1,368
11		B42F0073	II	73-II				5.95	5.60	March 4, 2019		0.54	1.85	1,447	1,335
12		B42F0073	III	73-III				9.15	8.80	March 4, 2019		0.83	1.20	3,440	3,575
13		B42F0073	IV	73-IV				12.45	12.10	March 4, 2019		1.13	0.88	39,300	40,280
14		B42F0073	V	73-V				16.65	16.30	March 4, 2019		1.51	0.66	42,800	43,321
15		B42F0073	VI	73-VI				20.05	19.70	March 4, 2019		1.82	0.55	43,900	45,132
16		B42F0073	VII	73-VII				25.05	24.70	March 4, 2019		2.28	0.44	44,100	44,180
17		B42F0073	VIII	73-VIII				29.75	29.40	March 4, 2019		2.70	0.37	44,200	45,265
18		B42F0077	I	77-I	0.55	58381	419295	3.05	2.43	February 28, 2019	14.3	0.21	4.69	1,424	1,376
19		B42F0077	II	77-II				5.95	5.33	February 28, 2019		0.42	2.40	1,933	1,852
20		B42F0077	III	77-III				9.15	8.53	February 28, 2019		0.64	1.56	1,843	1,842
21		B42F0077	IV	77-IV				12.15	11.53	February 28, 2019		0.85	1.18	4,170	4,265
22		B42F0077	V	77-V				16.15	15.53	February 28, 2019		1.13	0.89	39,400	40,380
23		B42F0077	VI	77-VI				19.95	19.33	February 28, 2019		1.40	0.72	42,800	43,828
24		B42F0077	VII	77-VII				24.95	24.33	February 28, 2019		1.74	0.57	43,900	44,535
25		B42F0077	VIII	77-VIII				29.55	28.93	February 28, 2019		2.07	0.48	44,000	45,149
26		B42F0078	I	78-I	0.65	58760	419045	1.95	1.36	March 7, 2019	16.5	0.12	8.46	1,204	1,074
27		B42F0078	II	78-II				3.85	3.26	March 7, 2019		0.23	4.29	1,375	1,255
28		B42F0078	III	78-III				6.95	6.36	March 7, 2019		0.42	2.37	916	838
29		B42F0078	IV	78-IV				9.95	9.36	March 7, 2019		0.60	1.66	2,084	1,977
30		B42F0078	V	78-V				13.85	13.26	March 7, 2019		0.84	1.19	2,500	2,437
31		B42F0078	VI	78-VI				17.95	17.36	March 7, 2019		1.09	0.92	32,500	32,878
32		B42F0078	VII	78-VII				21.95	21.36	March 8, 2019		1.33	0.75	41,600	42,481
33		B42F0078	VIII	78-VIII				25.85	25.26	March 8, 2019		1.57	0.64	42,800	43,377
34		B42F0078	IX	78-IX				29.25	28.66	March 8, 2019		1.77	0.56	43,200	43,269
35		B42F0079	I	79-I	0.65	58409	418861	2.05	1.40	March 11, 2019	16.4	0.13	8.00	1,260	1,126
36		B42F0079	II	79-II				4.05	3.40	March 11, 2019		0.25	4.05	1,155	1,062
37		B42F0079	III	79-III				7.05	6.40	March 11, 2019		0.43	2.33	988	916
38		B42F0079	IV	79-IV				9.95	9.30	March 11, 2019		0.61	1.65	1,010	944
39		B42F0079	V	79-V				14.05	13.40	March 11, 2019		0.86	1.17	1,177	1,103
40		B42F0079	VI	79-VI				18.05	17.40	March 11, 2019		1.10	0.91	36,700	36,874
41		B42F0079	VII	79-VII				22.05	21.40	March 11, 2019		1.34	0.74	42,000	42,468
42		B42F0079	VIII	79-VIII				26.05	25.40	March 11, 2019		1.59	0.63	42,400	42,375
43		B42F0079	IX	79-IX				29.15	28.50	March 11, 2019		1.78	0.56	42,400	42,979
44		B42F0080	I	80-I	0.70	58791	418606	2.10	1.45	March 11, 2019	15.6	0.13	7.43	1,564	1,462
45		B42F0080	II	80-II				4.10	3.45	March 11, 2019		0.26	3.80	1,952	1,885
46		B42F0080	III	80-III				7.00	6.35	March 11, 2019		0.45	2.23	1,320	1,300
47		B42F0080	IV	80-IV				10.00	9.35	March 11, 2019		0.64	1.56	2,700	2,728
48		B42F0080	V	80-V				14.10	13.45	March 11, 2019		0.90	1.11	10,470	9,996
49		B42F0080	VI	80-VI				18.10	17.45	March 11, 2019		1.16	0.86	39,900	40,261
50		B42F0080	VII	80-VII				22.10	21.45	March 11, 2019		1.42	0.71	43,100	43,242
51		B42F0080	VIII	80-VIII				26.10	25.45	March 11, 2019		1.67	0.60	44,000	44,545
52		B42F0080	IX	80-IX				29.20	28.55	March 11, 2019		1.87	0.53	44,000	44,193
53		B42F0081	I	81-I	0.60	59109	417790	3.70	3.01	March 6, 2019	14.3	0.26	3.86	1,031	952
54		B42F0081	II	81-II				6.10	5.41	March 6, 2019		0.43	2.34	863	840
55		B42F0081	III	81-III				9.20	8.51	March 6, 2019		0.64	1.55	1,080	1,059
56		B42F0081	IV	81-IV				12.10	11.41	March 6, 2019		0.85	1.18	2,143	2,097
57		B42F0081	V	81-V				15.50	14.81	March 6, 2019		1.08	0.92	31,600	32,068
58		B42F0081	VI	81-VI				20.00	19.31	March 6, 2019		1.40	0.72	41,800	42,289
59		B42F0081	VII	81-VII				24.10	23.41	March 6, 2019		1.69	0.59	42,700	43,183
60		B42F0081	VIII	81-VIII				28.10	27.41	March 6, 2019		1.97	0.51	43,300	43,734
61		B42F0082	I	82-I	0.30	59463	416920	3.00	2.63	March 5, 2019	11.5	0.26	3.83	1,168	1,076
62		B42F0082	II	82-II				5.10	4.73	March 5, 2019		0.44	2.25	1,268	1,174
63		B42F0082	III	82-III				9.20	8.83	March 5, 2019		0.80	1.25	2,730	3,099
64		B42F0082	IV	82-IV				12.10	11.73	March 5, 2019		1.05	0.95	27,300	27,754
65		B42F0082	V	82-V				16.20	15.83	March 5, 2019		1.41	0.71	43,900	44,561
66		B42F0082	VI	82-VI				20.10	19.73	March 5, 2019		1.75	0.57	44,100	44,396
67		B42F0082	VII	82-VII				24.20	23.83	March 5, 2019		2.10	0.48	44,200	44,825
68		B42F0082	VIII	82-VIII				28.30	27.93	March 5, 2019		2.46	0.41	44,400	44,386
69		B42F0082	IX	82-IX				31.80	31.43	March 5, 2019		2.77	0.36	44,000	44,256
70		B42F0083	I	83-I	0.30	59758	416403	3.00	2.65	March 1, 2019	11.3	0.27	3.77	1,140	1,058
71		B42F0083	II	83-II				5.90	5.55	March 1, 2019		0.52	1.92	1,249	1,205
72		B42F0083	III	83-III				9.10	8.75	March 1, 2019		0.81	1.24	2,114	2,053
73		B42F0083	IV	83-IV				12.10	11.75	March 1, 2019		1.07	0.93	29,100	29,825
74		B42F0083	V	83-V				15.90	15.55	March 1, 2019		1.41	0.71	42,300	42,386
75		B42F0083	VI	83-VI				19.90	19.55	March 1, 2019		1.76	0.57	43,400	43,517
76		B42F0083	VII	83-VII				25.00	24.65	March 1, 2019		2.21	0.45	43,900	43,663
77		B42F0083	VIII	83-VIII				29.70	29.35	March 1, 2019		2.63	0.38	44,300	44,985
78	Shallow well	PB-1		PB-1	1.09	57999	419144	3.95	2.86	March 11, 2019				1,307	1,217
79	Surface water	Grevelingen-North		Grev-N	-	58277	419682	-	-	March 11, 2019				45,100	45,895
80		Grevelingen-East		Grev-E	-	59543	417318	-	-	March 8, 2019				44,600	44,950
81		Grevelingen-South		Grev-S	-	59931	416102	-	-	March 4, 2019				44,900	45,868
82		Grevelingen-West		Grev-W	-	58631	418166	-	-	March 8, 2019				44,700	45,480
83		Hollestelle-North		HS-N	-	58502	419452	-	-	March 11, 2019				574	543
84		Hollestelle-Middle		HS-M	-	58793	418238	-	-	March 8, 2019				360	412
85		Hollestelle-South		HS-S	-	59293	417272	-	-	March 8, 2019				669	566

Difference	O2	Tempe-rature	pH		Alkalinity					DOC	IC				
	Field	Field	Field	Lab	Field	Lab	CO_2 Calculated	HCO_3^- Calculated	CO_3^{2-} Calculated		F^-	Cl^-	NO_2^-	Br^-	NO_3^-
%	mg/l	°C	-	-	meq/l	meq/l	mg/l	mg/l	mg/l	mgC/l	mg/l	mg/l	mg/l	mg/l	mg/l
-5	0.61	9.0	7.22	7.05		9.5	0.0	0.0	0.0	21.83	0.414	34	<0.007	0.217	0.145
-12	0.73	9.3	7.73	7.68		6.6	0.0	0.0	0.0	11.27	0.564	27	0.00756	0.148	0.158
-8	0.45	9.5	8.19	8.04		8.5	0.0	0.0	0.0	10.16	0.547	39	0.0277	0.153	0.181
0	0.43	9.5	8.40	7.87		10.5	0.0	0.0	0.0	11.23	0.924	77	0.00711	0.154	0.125
-6	0.25	9.7	8.93	8.65		14.0	0.0	0.0	0.0	36.85	4.67	109	<0.007	0.428	0.121
-4	0.48	9.4	8.31	8.05		18.3	0.0	0.0	0.0	38.30	2.08	2607	<0.07	9.53	1.08
3	0.41	10.0	7.89	7.43		4.7	0.0	0.0	0.0	4.22	0.99	14888	<0.4	53.1	<4
2	0.52	10.0	7.85	7.32		4.2	0.0	0.0	0.0	2.86	0.92	14759	<0.4	52.7	<4
2	0.67	9.9	7.54	7.22		4.4	0.0	0.0	0.0	3.03	0.885	15131	<0.4	53.9	<4
-9	0.85	9.2	7.72	7.85		13.0	Molaliteit ->	0.0	0.0	9.69	0.61	105	<0.007	0.313	<0.08
-8	0.34	10.0	8.60	8.37		12.0	CO2	HCO3	CO3	8.06	1.34	76	0.00908	0.241	<0.08
4	0.36	10.4	8.81	8.55		14.3	mg/l	mg/l	mg/l	27.38	2.56	626	<0.007	2.28	<0.08
2	0.77	9.2	7.69	7.48		5.2	99.0	553.5	0.4	4.06	0.813	13843	<0.4	49.1	<4
1	0.59	10.2	7.59	7.43		5.0	16.1	379.9	1.1	3.60	0.777	15106	<0.4	53.7	<4
3	0.50	9.7	7.51	7.41		4.5	8.9	487.3	3.4	3.30	0.813	15914	<0.4	56.7	<4
0	0.40	9.7	7.48	7.36		5.6	16.6	618.0	3.0	3.32	0.734	15470	<0.4	55	<4
2	0.68	9.4	7.66	7.58		6.9	3.4	767.6	23.5	6.93	0.682	15986	<0.4	57	<4
-3	0.69	10.7	8.82	8.30	9.9	10.1	15.6	1,012.9	10.8	11.56	0.839	125	<0.007	0.256	<0.08
-4	0.57	10.5	8.19	8.17	8.6	8.3	11.6	223.9	0.9	13.36	0.134	169	<0.007	0.311	<0.08
0	0.07	10.5	8.86	8.64	17.8	17.3	13.3	200.1	0.6	52.91	3.98	75	0.0319	0.422	<0.08
2	0.17	10.2	8.54	8.38	26.2	26.2	17.8	214.0	0.5	71.88	1.81	629	<0.007	2.53	<0.08
2	0.48	10.6	7.81	7.63	6.3	5.9	20.6	742.2	3.6	4.91	0.784	13919	0.524	49.4	< 4
2	0.40	10.3	7.70	7.64	6.7	5.9	5.8	682.6	10.6	4.28	0.795	15348	<0.4	54.7	<4
1	0.39	10.3	7.73	7.47		4.4	4.1	780.6	21.3	3.46	0.736	15619	<0.4	20.8	<4
3	0.48	10.4	7.61	7.47		4.2	11.8	254.6	1.1	3.75	0.709	16036	<0.4	56.6	<4
-11	0.62	8.6	6.93	7.12		12.0	12.2	237.5	0.9	28.71	0.342	45	<0.007	0.224	<0.08
-9	0.63	9.8	8.11	7.91		13.2	11.2	210.0	0.8	7.41	0.265	59	0.0208	0.190	<0,08
-9	0.36	9.7	8.64	8.20		7.9	15.9	264.1	0.9	14.04	0.823	44	0.0126	0.14	<0.08
-5	0.41	10.0	8.51	8.22		16.5	11.5	319.7	1.8	48.62	1.58	144	<0.007	0.655	<0.08
-3	0.37	10.4	8.75	8.35		18.5	5.8	579.8	7.7	53.86	3.11	239	0.0385	0.983	0.197
1	0.69	10.4	7.69	7.59		8.8	6.1	464.2	4.9	5.87	0.785	11090	<0.4	39.3	<4
2	0.91	10.1	7.61	7.39		4.8	4.2	943.8	28.6	4.09	0.676	14914	<0.4	53.1	<4
1	1.00	9.9	7.80	7.49		5.5	11.2	1,455.5	28.0	3.77	0.854	15313	<0.4	54.6	<4
0	0.65	10.2	7.52	7.23		4.5	9.3	282.6	1.7	4.11	0.814	15268	<0.4	54.5	<4
-11	0.48	8.7	7.70	7.85		9.5	8.7	273.9	1.7	12.46	0.713	92	<0.007	0.238	<0.08
-8	0.80	9.4	8.36	8.18		9.0	9.6	206.0	0.9	10.91	0.824	79	0.00964	0.217	<0.08
-7	0.57	10.1	8.29	8.16		6.6	9.1	195.9	0.8	5.77	0.169	83	0.0122	0.117	<0,08
-7	0.41	9.9	8.30	8.05		6.8	104.1	693.3	0.6	7.16	0.108	85	0.0364	0.147	<0.08
-6	0.52	9.7	9.16	8.87		9.5	18.6	762.8	4.1	21.32	1.95	74	0.0136	0.185	<0.08
0	0.62	10.3	7.74	7.41		6.9	5.9	460.5	4.5	3.96	0.885	12500	<0.4	40.9	<4
1	0.61	9.9	7.56	7.42		3.8	10.8	920.3	10.7	2.82	0.835	14966	<0.4	53.3	<4
0	0.77	9.9	7.67	7.59		5.1	8.6	1,001.7	16.3	3.82	0.77	14754	<0.4	52.6	<4
1	0.61	9.9	7.58	7.47		3.9	16.6	441.2	2.3	3.08	0.847	15071	<0.4	53.6	<4
-7	0.74	7.6	8.00	7.87		11.8	12.9	227.8	0.8	6.37	0.799	111	<0.007	0.4	<0.08
-3	0.45	8.7	8.95	8.65		13.8	11.5	257.1	1.1	16.59	1.46	181	0.0214	0.708	<0,08
-2	0.45	9.3	9.12	8.88		10.7	17.5	215.2	0.5	25.83	3.11	47	0.0207	0.0915	<0.08
1	0.34	9.0	8.70	8.50		14.7	15.4	547.4	2.6	85.75	4.37	419	0.0157	1.62	<0.08
-5	0.34	9.1	8.21	7.96		18.2	6.8	514.4	5.1	17.47	0.733	2670	<0.07	9.75	<0.8
1	0.50	9.1	7.66	7.60		4.7	5.3	379.2	3.5	3.91	0.77	13892	<0.4	48.9	<4
0	0.60	9.0	7.67	7.61		6.3	7.1	396.2	2.8	4.81	0.839	15015	<0.4	53.4	<4
1	0.47	9.5	7.74	7.62		6.5	1.4	507.9	24.1	4.29	0.837	15670	<0.4	55.8	<4
0	1.33	9.3	7.62	7.50		5.0	19.1	342.6	1.2	3.85	0.824	15498	<0.4	54.8	<4
-8	0.59	9.3	8.17	8.08		9.1	9.5	180.1	0.7	10.26	0.506	60	0.0219	0.184	<0.08
-3	0.58	10.0	8.59	8.32		7.2	8.5	239.0	1.3	5.08	0.301	53	<0.007	0.151	0.199
-2	0.62	9.8	9.25	9.00		9.5	8.7	184.3	0.8	18.57	2.07	51	0.0316	0.161	0.082
-2	0.70	9.9	8.99	8.67		11.9	18.0	678.7	3.4	24.67	4.99	294	<0.007	1.09	<0.08
1	0.81	9.7	7.81	7.54		5.9	3.3	756.8	23.4	8.12	0.975	10608	<0.4	37.5	<4
1	0.99	10.1	7.82	7.28		3.8	1.5	562.3	28.1	2.89	0.862	14687	<0.4	52.1	<4
1	0.47	10.0	7.83	7.53		4.1	4.8	793.3	18.4	3.80	0.868	15210	<0.4	54.2	<4
1	0.48	10.2	7.76	7.53		4.4	19.0	1,005.9	8.8	4.15	0.842	15304	<0.4	54.5	<4
-8	0.57	9.5	7.72	7.68		12.1	7.9	224.4	1.2	8.53	0.861	34	<0.007	0.148	<0.08
-7	0.42	10.0	8.19	7.98		12.7	10.1	297.9	1.7	0.02	0.709	46	<0.007	0.178	<0.08
14	0.43	10.3	8.64	8.33		15.9	10.1	305.3	1.8	34.93	2.9	413	<0.007	1.56	<0.08
2	0.52	10.0	7.75	7.68		8.6	10.3	235.7	1.1	6.56	0.847	8873	0.488	27	<4
2	0.42	10.8	7.60	7.45		6.8	8.7	523.6	4.0	5.20	0.768	15825	<0.4	56.6	<4
1	0.44	10.7	7.56	7.49		6.3	4.0	412.9	5.4	3.60	0.732	15606	<0.4	55.8	<4
1	0.54	9.9	7.42	7.38		6.6	1.0	491.4	31.3	3.86	0.726	15880	<0.4	57.2	<4
0	0.57	10.1	7.42	7.36		6.6	2.7	647.7	21.2	5.55	0.764	15551	<0.4	55.5	<4
1	0.55	10.0	7.21	7.18		4.7	12.7	300.5	1.4	4.20	0.453	15569	<0.4	54.7	<4
-7	1.08	9.4	8.29	8.17		11.7	13.1	179.3	0.5	7.56	0.614	40	<0.007	0.124	<0.08
-3	0.28	10.7	8.43	8.22		12.6	7.9	192.7	0.9	7.67	0.889	46	<0.007	0.153	<0.08
-3	0.18	10.6	8.94	8.63		15.8	8.4	207.2	1.0	48.50	4.77	177	<0.007	0.676	<0.08
2	0.29	10.7	7.95	7.87		8.9	28.9	698.4	2.2	8.18	0.836	9799	<0.4	34.2	<4
0	0.51	10.7	7.84	7.74		5.3	15.1	728.8	4.7	3.68	0.84	14707	<0.4	51.9	<4
0	0.40	10.5	8.04	7.52		3.8	8.0	898.8	14.5	3.57	0.805	15346	<0.4	53.9	<4
-1	0.31	10.7	7.73	7.44		4.5	14.0	443.5	2.7	3.33	0.764	15318	<0.4	53.9	<4
2	0.33	10.8	7.63	7.54		6.9	15.8	324.3	1.3	5.45	0.779	16013	<0.4	56.4	<4
-7	1.66	9.3	7.35	7.68		10.5	13.4	301.2	1.3	19.56	0.924	93	<0.007	0.266	<0.08
2	12.38	5.0	8.15	7.23		2.3	18.2	317.2	1.1	2.08	1.16	16363	<0.4	57.3	<4
1	13.14	5.1	8.36	8.05		2.4	18.8	312.5	1.0	2.18	1.12	15782	<0.4	55.5	<4
2	13.42	5.2	8.59	8.25		2.4	20.6	226.9	0.5	2.71	1.12	16290	<0.4	57.5	<4
2	13.26	4.8	8.81	8.32		2.4	8.9	662.3	6.5	2.49	1.14	16049	<0.4	56.5	<4
-5	13.57	5.4	8.79	7.84		2.9	8.5	711.8	7.8	15.54	0.15	52	0.0143	0.0456	<0.08
14	12.20	5.0	8.54	8.20		4.0	4.0	866.3	25.9	8.83	0.144	34	0.0265	0.0627	<0.08
-15	12.52	5.1	8.62	7.75		2.1	8.9	444.1	4.2	15.87	0.334	70	0.047	0.331	0.4

		AA3					Photometric		ICP (mg/kg)						
PO_4^{3-}	SO_4^{2-}	NOX	NO_3^-	NO_2^-	NH_4^+ Frozen	NH_4^+ Acid	PO_4^{3-}	S^{2-}	Al	As 188.979	As 193.696	B	Ba 233.527	Ba 455.403	Be
mg/l	mg/l	mg/l	mg/l	mg/l	mg/l	mg/l	mg/l	µgS/l	mg/kg	mg/kg	mg/kg	mg/kg	mg/kg	mg/kg	mg/kg
<0.4	32	0.030	0.004	0.026	0.180	0.263	0.227	2.05	0.000	0.010	0.026	0.038	0.010	0.008	0.000
<0.4	23	0.013	0.003	0.010	0.318	2.032	0.416	3.44	0.002	0.001	0.015	0.163	0.010	0.009	0.000
0.799	26	0.030	0.010	0.020	0.857	0.916	1.027	8.87	0.005	0.006	0.011	0.352	0.008	0.008	0.000
1.91	71	0.000	0.000	0.000	2.911	2.926	2.094	24.80	0.002	0.006	0.005	0.870	0.012	0.014	0.000
17.3	58	0.107	0.085	0.022	0.756	2.290	18.732	22.15	0.116	0.001	0.007	3.627	0.009	0.009	0.000
12.4	337	0.186	0.092	0.094	0.739	1.369	11.469	11.00	0.039			4.374	0.039		
<20	2053	0.091	0.003	0.088	2.894	3.106	2.624	1.34	0.332			3.455	0.045		
<20	2049	0.066	0.003	0.063	2.500	3.832	2.749	3.44	0.319			3.488	0.038		
<20	2128	0.011	0.001	0.010	1.491	2.745	4.210	0.78	0.307			3.351	0.050		
<0.4	18	0.009	0.012	0.000	0.793	0.983	0.605	0.00	0.006	0.025	0.008	0.594	0.005	0.004	0.000
2.3	60	0.010	0.013	0.000	0.669	0.932	2.559	5.11	0.001	0.007	0.002	1.492	0.003	0.001	0.000
6.5	142	0.062	0.047	0.015	0.670	0.913	7.326	20.85	0.012			3.254	0.000		
<20	2108	0.000	0.003	0.000	2.729	4.743	1.977	0.00	0.375			3.577	0.028		
<20	2060	0.022	0.000	0.022	2.998	4.902	7.168	0.00	0.348			3.438	0.025		
<20	2170	0.068	0.009	0.058	3.265	4.793	10.576	0.11	0.395			3.440	0.036		
<20	2052	0.070	0.006	0.064	3.506	4.961	12.912	0.13	0.275			3.396	0.037		
<20	2083	0.197	0.003	0.194	5.215	7.536	14.957	6.35	0.347			3.407	0.052		
3.13	86	0.038	0.013	0.025	1.956	2.594	4.065	92.67	0.009	0.019	0.006	0.851	0.005	0.004	0.000
0.519	351	0.037	0.000	0.037	4.067	2.028	0.657	4.18	0.019	0.002	0.011	0.648	0.012	0.015	0.000
22.6	2	0.154	0.113	0.041	0.902	2.175	26.262	14.39	0.187	0.018	0.009	4.055	0.014	0.013	0.000
22.4	1	0.110	0.056	0.053	0.883	5.620	24.111	4.17	0.006			5.125	0.007		
<20	2089	0.186	0.003	0.183	2.425	5.276	4.886	0.21	0.282			3.630	0.043		
<20	2031	0.141	0.001	0.140	3.413	5.308	4.747	0.11	0.320			3.505	0.037		
<20	2139	0.360	0.005	0.356	3.933	4.721	6.124	0.89	0.364			3.567	0.055		
<20	2220	0.153	0.001	0.152	3.308	3.585	8.253	1.79	0.308			3.442	0.062		
<0.4	0	0.060	0.013	0.047	0.065	0.132	0.519	1.54	0.000	0.008	0.019	0.160	0.020	0.020	0.000
1.30	3	0.050	0.007	0.043	6.422	3.586	1.526	9.44	0.004	0.034	0.005	0.975	0.090	0.083	0.000
6.83	17	0.059	0.008	0.051	1.785	2.228	7.619	57.22	0.031	0.002	0.004	1.064	0.013	0.010	0.000
62.7	0	0.123	0.054	0.069	1.247	1.948	66.379	37.01	0.104	0.039	0.030	2.886	0.028	0.029	0.000
>67.9	20	0.229	0.120	0.109	0.657	1.191	104.360	24.49	0.182	0.011	0.030	4.184	0.016	0.015	0.000
25.4	1721	0.099	0.003	0.096	3.545	3.852	14.511	0.83	0.148			3.463	0.033		
<20	2020	0.082	0.001	0.081		8.435	14.476	0.00	0.372			3.387	0.038		
<20	2039	0.095	0.002	0.092	5.912	4.510	11.633	0.73	0.336			3.406	0.062		
<20	2098	0.000	0.003	0.000	3.940	2.805	10.019	0.00	0.317			3.439	0.061		
<0.4	45	0.000	0.017	0.000	0.860	0.993	0.674	0.90	0.003	0.003	0.007	0.442	0.006	0.005	0.000
1.58	41	0.045	0.012	0.033	1.299	1.577	1.741	37.92	0.000	-0.005	0.001	0.645	0.007	0.006	0.000
0.496	43	0.093	0.003	0.089	2.831	2.921	0.580	1.34	0.003	0.001	0.002	0.544	0.016	0.015	0.000
0.512	29	0.166	0.014	0.151	4.245	4.551	0.597	0.20	0.003	0.005	0.001	0.505	0.061	0.063	0.000
8.67	15	0.080	0.031	0.049	0.743	0.779	9.334	9.43	0.069	0.006	0.015	1.669	0.003	0.002	0.000
<20	1963	0.000	0.000	0.000	2.790	3.704	2.944	1.54	0.369			3.448	0.024		
<20	2089	0.024	0.001	0.024	2.442	2.619	3.020	0.10	0.324			3.391	0.035		
<20	2015	0.036	0.001	0.035	2.133	5.289	5.608	0.98	0.296			3.445	0.043		
<20	2120	0.054	0.000	0.053	1.641	3.898	4.919	0.74	0.362			3.377	0.061		
3.04	96	0.100	0.004	0.097	0.685	1.046	3.695	60.56	0.001	0.015	0.001	0.992	0.016	0.016	0.000
14.8	42	0.054	0.014	0.040	1.776	1.843	16.047	598.10	0.072	0.028	0.009	2.298	0.006	0.006	0.000
14.1	69	0.094	0.065	0.029	0.634	1.811	14.842	9.62	0.140	0.002	0.011	2.524	0.006	0.005	0.000
35.8	0	0.444	0.269	0.175	0.749	1.278	37.880	2.96	0.082			4.376	0.011		
32.3	294	0.117	0.026	0.091	2.507	2.695	33.362	0.44	0.024			4.128	0.002		
<20	2145	0.100	0.003	0.097	4.824	2.274	7.209	0.21	0.277			3.632	0.020		
<20	2030	0.085	0.002	0.084	6.324	5.729	5.290	0.10	0.319			3.610	0.036		
<20	2041	0.045	0.005	0.040	5.615	5.838	4.085	0.00	0.385			3.569	0.051		
<20	2105	0.119	0.003	0.116	3.933	3.868	5.874	0.25	0.277			3.541	0.054		
0.764	0	0.039	0.009	0.029	2.874	3.325	0.984	9.22	0.011	0.002	0.002	0.738	0.006	0.005	0.000
1	7	0.050	0.006	0.044	2.379	2.531	1.062	7.04	0.008	0.006	0.010	0.753	0.002	0.002	0.000
8.03	15	0.023	0.013	0.010	0.538	0.653	8.336	27.48	0.069	0.001	0.013	1.716	0.006	0.006	0.000
15.5	41	0.076	0.051	0.024	0.431	1.702	16.821	22.29	0.078	0.014	0.015	3.317	0.013	0.012	0.000
<20	1922	0.081	0.001	0.080	2.108	4.502	2.742	0.85	0.167			3.601	0.022		
<20	2058	0.080	0.002	0.078	1.908	4.070	3.361	0.00	0.354			3.398	0.044		
<20	2114	0.043	0.001	0.042	2.678	4.145	3.987	2.45	0.319			3.462	0.045		
<20	2109	0.075	0.001	0.074	2.973	4.100	4.898	12.83	0.371			3.574	0.029		
<0.4	0	0.062	0.003	0.059	0.313	0.385	0.864	1.04	0.009	0.002	0.002	0.466	0.004	0.004	0.000
0.561	8	0.000	0.000	0.000	1.081	1.465	0.700	8.56	0.007	0.015	0.001	0.845	0.004	0.003	0.000
15.4	156	0.172	0.065	0.106	0.830	1.751	16.976	59.68	0.002			4.053	0.003		
<20	1596	0.209	0.008	0.201	4.072	3.971	4.911	1.39	0.171			3.798	0.019		
<20	2044	0.088	0.003	0.085		9.608	6.783	2.23	0.342			3.509	0.032		
<20	2064	0.115	0.002	0.113		8.081	5.777	0.82	0.299			3.447	0.040		
<20	2049	0.035	0.019	0.016		6.827	5.149	1.15	0.363			3.436	0.038		
<20	2003	0.000	0.007	0.000		9.893	8.800	2.59	0.289			3.452	0.046		
<20	2132	0.005	0.004	0.002	2.831	0.076	4.766	1.04	0.300			3.453	0.064		
0.566	0	0.057	0.001	0.056	0.690	0.842	0.735	7.77	0.010	0.000	0.010	0.425	0.003	0.002	0.000
1.36	0	0.013	0.015	0.000	1.830	2.252	1.784	12.78	0.003	0.006	0.004	1.054	0.004	0.004	0.000
12.5	3	0.209	0.108	0.101	0.445	0.707	15.031	33.98	0.346	0.017	0.012	3.761	0.009	0.006	0.000
<20	1587	0.043	0.010	0.033	3.978	4.290	3.775	31.42	0.173			3.654	0.016		
<20	1997	0.067	0.000	0.067	2.255	0.109	37.796	3.96	0.305			3.538	0.029		
<20	2132	0.093	0.001	0.092	1.605	0.042	3.751	1.61	0.363			3.535	0.042		
<20	2086	0.077	0.002	0.075	2.142	0.047	9.969	1.03	0.359			3.439	0.045		
<20	2054	0.078	0.007	0.071	3.351	4.390	13.330	1.99	0.391			3.385	0.052		
<0.4	49	0.011	0.007	0.004	0.742	1.148	0.597	1.89	0.006	0.001	0.003	0.358	0.003	0.004	0.000
<20	2336	0.621	0.041	0.580	0.045	0.243	0.050	0.63	0.303			3.660	0.020		
<20	2260	0.372	0.030	0.342	0.003	0.324	0.050	0.97	0.261			3.551	0.018		
<20	2327	0.123	0.018	0.104	0.000	0.049	0.050	1.32	0.347			3.575	0.003		
<20	2296	0.126	0.011	0.115	0.000	0.011	0.050	0.03	0.296			3.575	0.009		
<0.4	66	0.069	0.025	0.044	0.000	0.069	0.050	1.00	0.004	0.003	0.013	0.056	0.005	0.005	0.000
<0.4	15	0.085	0.008	0.076	0.017	0.078	0.050	0.31	0.016	0.003	0.002	0.055	0.005	0.006	0.000
6.04	25	0.305	0.021	0.285	0.227	0.355	8.480	0.49	0.020	0.030	0.025	0.113	0.007	0.007	0.000

Ca	Cd	Co	Cr	Cu	Fe	K	Li	Mg	Mn	Mo	Na	Ni	P	Pb	S	Sb
mg/kg	mg/kg	mg/kg	mg/kg	mg/kg	mg/kg	mg/kg	mg/kg	mg/kg	mg/kg	mg/kg	mg/kg	mg/kg	mg/kg	mg/kg	mg/kg	mg/kg
133.706	0.001	0.000	0.004	0.000	8.176	0.282	0.034	7.674	0.710	0.004	18.485	0.000	0.071	0.005	10.536	0.002
89.153	0.000	0.002	0.002	0.000	2.573	21.499	0.043	20.847	0.200	0.003	14.002	0.001	0.063	0.008	7.406	0.001
38.604	0.000	0.001	0.000	0.001	0.275	68.514	0.065	50.868	0.086	0.000	32.583	0.000	0.324	0.006	8.563	0.003
19.309	0.000	0.002	0.001	0.002	0.077	67.434	0.063	42.710	0.050	0.001	128.447	0.001	0.652	0.010	24.918	0.001
3.533	0.000	0.003	0.013	0.005	0.916	20.118	0.038	5.787	0.024	0.000	401.221	0.006	6.171	0.003	22.346	0.008
36.971					2.475	71.771	0.031	117.879	0.065	0.001	1984.609		4.003		117.344	
316.856					3.568	230.536	0.001	1032.761	0.385	0.007	8600.830		0.072		626.408	
327.236					3.569	236.346	0.012	1058.466	0.684	0.033	8666.383		0.087		631.328	
330.165					2.267	238.068	0.004	1063.883	1.076	0.008	8728.291		0.653		650.747	
83.908	0.001	0.001	0.000	0.002	1.440	75.067	0.100	74.017	0.050	0.004	50.132	0.001	0.199	0.003	5.927	0.001
8.620	0.001	0.001	0.003	0.002	0.171	47.299	0.060	36.175	0.010	0.002	212.399	0.000	0.759	0.005	20.545	0.007
6.954					0.479	26.063	0.001	21.785	0.007	0.001	804.506		2.239		49.870	
296.090					0.742	222.699	0.003	980.783	0.351	0.008	8164.685		0.160		656.381	
323.652					2.747	240.044	0.017	1065.180	0.829	0.008	8832.555		1.498		646.415	
338.029					3.630	256.647	0.026	1103.957	1.146	0.022	9150.385		2.668		683.700	
335.347					4.855	252.991	0.066	1085.861	1.335	0.013	8999.771		3.353		656.037	
351.524					0.610	246.522	0.010	1116.051	1.522	0.004	9152.406		3.951		652.655	
16.749	0.000	0.001	0.005	0.001	0.048	36.238	0.060	12.048	0.032	0.004	237.131	0.002	1.222	0.010	30.855	0.001
42.848	0.000	0.003	0.001	0.001	0.182	115.190	0.099	88.398	0.093	0.002	159.402	0.002	0.145	0.013	121.832	0.005
4.210	0.000	0.003	0.013	0.003	1.089	20.400	0.054	7.160	0.062	0.002	468.246	0.004	8.311	0.007	2.708	0.015
8.473					1.507	28.346	0.002	25.825	0.044	0.000	1026.130		7.528		4.096	
289.790					2.885	231.621	0.026	970.109	0.622	0.024	8154.345		1.058		666.458	
330.952					2.753	253.681	0.052	1075.051	0.760	0.014	8898.568		0.897		658.137	
344.393					5.004	253.446	0.082	1103.416	1.002	0.009	9070.802		1.487		713.003	
352.135					1.790	252.569	0.059	1105.063	1.514	0.028	9010.763		2.148		718.808	
179.563	0.001	0.001	0.001	0.001	5.901	9.117	0.049	16.717	1.189	0.002	24.443	0.002	0.153	0.007	0.780	0.004
31.130	0.001	0.001	0.004	0.001	0.297	92.182	0.080	66.464	0.282	0.006	84.369	0.000	0.462	0.017	1.348	0.004
6.842	0.000	0.001	0.002	0.001	0.078	27.573	0.028	14.187	0.052	0.000	138.093	0.002	2.148	0.014	6.188	0.002
6.597	0.000	0.002	0.024	0.005	0.816	25.865	0.067	12.393	0.152	0.000	472.508	0.008	20.987	0.001	3.587	0.007
4.930	0.000	0.002	0.019	0.013	2.152	22.555	0.045	7.987	0.063	0.005	573.549	0.009	31.783	0.002	11.128	0.000
218.363					0.605	196.485	0.054	693.359	0.887	0.005	6472.585		4.278		558.344	
320.586					2.871	235.923	0.005	1020.357	1.270	0.014	8496.614		4.015		658.283	
330.372					5.629	241.401	0.037	1054.852	1.541	0.009	8645.909		3.034		655.411	
331.181					2.180	250.465	0.006	1059.910	1.304	0.002	8599.715		2.600		679.217	
78.332	0.001	0.001	0.000	0.002	1.863	42.463	0.042	47.578	0.084	0.001	60.753	0.002	0.141	0.004	15.144	0.002
36.894	0.000	0.002	-0.001	0.001	0.045	48.668	0.043	40.688	0.059	0.003	99.896	0.000	0.506	-0.019	14.105	-0.010
27.832	0.001	0.002	0.001	0.002	0.110	74.099	0.088	43.007	0.083	0.003	46.208	0.001	0.127	0.007	14.225	0.004
26.634	0.000	0.001	0.002	0.002	0.039	89.040	0.067	39.368	0.169	0.002	51.719	0.001	0.162	0.013	9.830	0.002
2.138	0.001	0.001	0.007	0.003	0.435	14.497	0.043	2.940	0.016	0.004	243.501	0.000	2.906	0.010	6.431	0.005
270.912					1.144	211.203	0.004	896.855	0.776	0.016	7385.371		0.512		629.025	
316.430					2.869	245.999	0.011	1030.070	1.144	0.007	8414.283		0.653		674.135	
328.371					2.218	239.320	0.050	1039.251	0.926	0.001	8575.431		1.426		672.339	
333.434					1.803	241.093	0.037	1052.753	1.444	0.023	8622.870		0.831		696.535	
62.169	0.000	0.000	0.002	0.001	0.067	51.439	0.066	52.195	0.054	0.004	152.005	0.000	1.082	0.015	33.357	0.002
3.709	0.000	0.002	0.009	0.003	0.046	23.026	0.034	6.818	0.019	0.000	429.200	0.000	5.204	0.009	19.292	0.001
2.557	0.000	0.002	0.009	0.004	0.591	15.057	0.041	3.090	0.031	0.005	308.880	0.003	5.010	0.012	26.336	0.003
7.445					4.677	18.446	0.003	14.012	0.067	0.002	640.135		11.685		3.877	
28.917					0.430	76.298	0.024	101.884	0.047	0.001	2075.800		10.332		102.584	
295.265					1.684	228.386	0.004	967.272	0.258	0.007	8104.615		1.843		711.909	
326.839					0.846	250.241	0.005	1066.752	0.386	0.001	8856.448		0.950		681.089	
334.203					2.110	250.833	0.004	1104.452	0.859	0.015	9021.701		0.665		671.707	
334.334					1.537	259.259	0.045	1084.654	0.975	0.016	8967.430		1.254		701.189	
34.252	0.001	0.002	0.000	0.000	0.192	61.568	0.012	49.067	0.055	0.000	56.063	0.001	0.264	0.010	0.310	0.004
12.366	0.000	0.002	0.001	0.000	0.040	66.620	0.038	31.151	0.021	0.003	87.269	0.001	0.336	0.011	2.604	0.003
1.783	0.000	0.002	0.004	0.004	0.578	12.291	0.032	2.261	0.015	0.003	245.376	0.000	2.689	0.009	5.958	0.002
3.220	0.000	0.002	0.007	0.003	0.861	22.730	0.034	5.967	0.030	0.006	463.008	0.002	5.429	0.004	15.198	0.002
217.630					1.735	200.393	0.052	709.952	0.132	0.003	6393.344		0.510		652.583	
328.377					6.765	238.642	0.063	1055.478	0.536	0.008	8575.528		0.464		686.607	
329.864					5.650	240.327	0.007	1059.951	0.597	0.017	8610.221		0.796		697.813	
341.156					2.818	246.460	0.073	1087.479	0.986	0.020	8860.863		0.974		701.490	
73.344	0.000	0.001	0.001	0.001	1.263	63.053	0.095	68.580	0.025	0.001	21.399	0.000	0.208	0.010	0.409	0.007
22.939	0.000	0.003	0.002	0.001	0.303	88.741	0.066	92.767	0.031	0.004	38.133	0.000	0.248	0.015	3.117	0.003
5.523					0.541	22.068	0.003	13.675	0.020	0.001	730.348		5.089		57.071	
164.186					0.184	166.064	0.034	551.043	0.338	0.004	5681.169		1.097		536.147	
300.000					2.564	259.609	0.008	1082.151	0.838	0.002	8884.909		1.502		671.437	
335.350					2.638	259.717	0.013	1093.274	0.810	0.028	8972.571		1.191		696.958	
336.898					1.723	256.277	0.065	1090.339	0.793	0.019	8987.189		1.445		685.659	
348.150					3.363	248.701	0.012	1115.824	0.972	0.000	9017.010		2.533		687.183	
362.081					5.743	253.591	0.049	1087.621	0.620	0.017	8915.792		1.032		735.039	
20.678	0.000	0.002	0.001	0.001	0.239	85.498	0.088	87.075	0.029	0.004	23.600	0.001	0.201	0.009	0.313	0.004
18.643	0.000	0.001	0.002	0.001	0.446	93.364	0.094	65.793	0.028	0.006	102.741	0.000	0.580	0.008	0.371	0.004
4.248	0.000	0.002	0.011	0.008	0.894	23.792	0.082	8.208	0.018	0.007	504.357	0.005	4.958	0.011	4.167	0.007
195.520					0.392	184.580	0.049	624.804	0.256	0.001	5946.060		0.883		553.789	
329.044					2.476	247.012	0.005	1049.694	0.567	0.004	8639.346		0.639		697.570	
337.020					5.587	252.941	0.062	1066.081	0.734	0.010	8681.809		0.701		734.108	
335.475					6.201	251.485	0.073	1073.151	1.156	0.009	8821.564		2.438		720.020	
352.914					2.611	249.924	0.010	1105.696	1.793	0.015	8937.620		3.636		690.360	
107.809	0.000	0.001	0.002	0.000	1.405	40.114	0.082	48.776	0.132	0.006	55.223	0.001	0.104	0.007	16.946	0.004
351.909					0.026	285.828	0.052	1121.341	0.014	0.003	9129.219		0.204		815.682	
347.671					0.004	274.398	0.066	1118.091	0.015	0.004	9133.565		0.220		793.309	
348.143					0.009	265.801	0.048	1123.812	0.009	0.003	9220.377		0.181		798.065	
350.087					0.006	272.007	0.036	1134.759	0.010	0.030	9198.134		0.221		795.295	
63.221	0.001	0.000	0.001	0.003	0.024	7.187	0.036	7.364	0.018	0.003	25.879	0.004	0.020	0.012	22.932	0.006
35.119	0.000	0.004	0.002	0.002	0.019	4.948	0.059	5.894	0.001	0.013	20.318	0.001	0.002	0.010	5.164	0.001
50.845	0.000	0.001	0.002	0.002	0.031	28.078	0.049	14.842	0.010	0.008	39.264	0.000	2.783	0.014	8.812	0.004

							ICP (mg/l)								
Si	Sr	Ti	V	Y	Zn	Zr	Al	As 188.979	As 193.696	B	Ba 233.527	Ba 455.403	Be	Ca	Cd	Co
mg/kg	mg/kg	mg/kg	mg/kg	mg/kg	mg/kg	mg/kg	mg/l	mg/l	mg/l	mg/l	mg/l	mg/l	mg/l	mg/l	mg/l	mg/l
5.500	0.643	0.002	0.003	0.000	0.181	0.001	0.000	0.010	0.026	0.038	0.010	0.008	0.000	133.431	0.001	0.000
18.675	0.715	0.001	0.002	0.000	0.005	0.001	0.002	0.001	0.015	0.163	0.010	0.009	0.000	88.949	0.000	0.002
18.103	0.498	0.001	0.000	0.000	0.004	0.000	0.005	0.006	0.011	0.351	0.008	0.007	0.000	38.522	0.000	0.001
16.004	0.320	0.001	0.003	0.000	0.001	0.000	0.002	0.006	0.005	0.868	0.012	0.013	0.000	19.274	0.000	0.002
14.040	0.058	0.148	0.077	0.004	0.025	0.023	0.116	0.001	0.007	3.622	0.009	0.009	0.000	3.528	0.000	0.003
17.463	0.564		0.064				0.039			4.389	0.039			37.097		
14.308	4.251		0.003				0.341			3.543	0.047			324.936		
14.605	4.231		0.011				0.327			3.577	0.039			335.581		
16.152	4.201		0.006				0.315			3.438	0.051			338.750		
20.431	1.076	0.001	0.001	0.000	0.208	0.000	0.006	0.025	0.008	0.593	0.005	0.004	0.000	83.767	0.001	0.001
7.509	0.154	0.003	0.006	0.000	0.001	0.000	0.001	0.007	0.002	1.489	0.003	0.001	0.000	8.604	0.001	0.001
14.223	0.081		0.041				0.012			3.252	0.000			6.951		
17.020	3.982		0.004				0.384			3.662	0.029			303.166		
16.538	4.359		0.005				0.357			3.528	0.026			332.099		
14.560	4.861		0.007				0.406			3.535	0.037			347.324		
14.989	4.695		0.011				0.282			3.487	0.038			344.334		
17.388	4.793		0.006				0.356			3.501	0.053			361.261		
15.065	0.169	0.009	0.006	0.000	0.002	0.002	0.009	0.019	0.006	0.850	0.005	0.004	0.000	16.719	0.000	0.001
20.248	0.874	0.001	0.001	0.000	0.002	0.000	0.019	0.002	0.011	0.647	0.012	0.015	0.000	42.785	0.000	0.003
16.626	0.076	0.162	0.112	0.005	0.005	0.025	0.186	0.018	0.009	4.050	0.014	0.013	0.000	4.205	0.000	0.003
20.508	0.095		0.092				0.006			5.127	0.007			8.477		
17.097	4.047		0.003				0.289			3.718	0.044			296.745		
17.028	4.556		0.003				0.329			3.598	0.038			339.689		
15.643	4.699		0.007				0.374			3.663	0.057			353.691		
15.598	5.034		0.005				0.316			3.537	0.063			361.819		
15.463	0.938	0.003	0.002	0.000	0.006	0.001	0.000	0.008	0.019	0.160	0.020	0.020	0.000	179.237	0.001	0.001
21.297	0.484	0.000	0.001	0.000	0.001	0.001	0.004	0.034	0.005	0.974	0.090	0.083	0.000	31.076	0.001	0.001
16.291	0.099	0.009	0.005	0.000	0.001	0.001	0.031	0.002	0.004	1.062	0.013	0.010	0.000	6.828	0.000	0.001
18.757	0.120	Overrang	0.063	0.003	0.004	0.030	0.104	0.039	0.030	2.882	0.028	0.029	0.000	6.589	0.000	0.002
15.289	0.114	Overrang	0.096	0.004	0.015	0.056	0.181	0.011	0.030	4.180	0.016	0.015	0.000	4.925	0.000	0.002
17.567	3.061		0.003				0.150			3.527	0.034			222.425		
14.752	4.466		0.012				0.381			3.473	0.039			328.729		
12.954	4.397		0.002				0.345			3.495	0.064			338.995		
15.537	4.362		0.005				0.325			3.529	0.062			339.825		
22.030	0.765	0.001	0.001	0.000	0.012	0.002	0.003	0.003	0.007	0.441	0.006	0.005	0.000	78.181	0.001	0.001
17.397	0.463	0.000	0.001	0.000	0.002	0.001	0.000		0.001	0.644	0.007	0.006	0.000	36.820	0.000	0.002
16.139	0.417	0.000	0.001	0.000	0.006	0.000	0.003	0.001	0.002	0.543	0.015	0.015	0.000	27.771	0.001	0.002
18.841	0.398	0.000	0.001	0.000	0.003	0.000	0.003	0.005	0.001	0.504	0.061	0.063	0.000	26.577	0.000	0.001
12.119	0.039	0.070	0.029	0.001	0.005	0.011	0.069	0.006	0.015	1.665	0.003	0.002	0.000	2.134	0.001	0.001
15.052	3.449		0.006				0.377			3.522	0.024			276.737		
15.130	4.635		0.003				0.332			3.477	0.036			324.467		
18.134	4.722		0.006				0.303			3.532	0.044			336.712		
16.045	4.495		0.003				0.372			3.464	0.062			342.070		
22.487	0.698	0.004	0.004	0.000	0.001	0.002	0.001	0.015	0.001	0.990	0.016	0.016	0.000	62.068	0.000	0.000
15.009	0.064	0.068	0.033	0.001	0.019	0.010	0.072	0.027	0.009	2.294	0.006	0.006	0.000	3.704	0.000	0.002
10.586	0.040	0.100	0.052	0.003	0.038	0.015	0.140	0.002	0.011	2.520	0.006	0.005	0.000	2.552	0.000	0.002
13.547	0.107		0.092				0.082			4.372	0.011			7.438		
14.152	0.387		0.020				0.024			4.142	0.002			29.018		
14.572	4.173		0.006				0.284			3.719	0.020			302.322		
16.805	4.412		0.006				0.327			3.704	0.037			335.370		
17.331			0.006				0.395			3.666	0.053			343.259		
17.196	4.703		0.005				0.284			3.636	0.055			343.294		
17.987	0.437	0.000	0.001	0.000	0.001	0.000	0.011	0.002	0.002	0.737	0.006	0.005	0.000	34.180	0.001	0.002
10.285	0.224	0.000	0.002	0.000	0.004	0.000	0.008	0.006	0.010	0.751	0.002	0.002	0.000	12.338	0.000	0.002
8.878	0.028	0.056	0.032	0.001	0.019	0.012	0.069	0.001	0.013	1.713	0.006	0.006	0.000	1.779	0.000	0.002
9.339	0.064	0.074	0.092	0.002	0.006	0.019	0.078	0.014	0.015	3.313	0.013	0.012	0.000	3.216	0.000	0.002
13.919	3.137		0.004				0.170			3.666	0.023			221.569		
11.402	4.431		0.002				0.363			3.484	0.045			336.685		
13.631	4.376		0.003				0.327			3.552	0.046			338.440		
17.458	4.512		0.004				0.381			3.668	0.030			350.163		
23.062	0.927	0.001	0.001	0.000	0.139	0.001	0.009	0.002	0.002	0.465	0.004	0.004	0.000	73.207	0.000	0.001
8.756	0.423	0.000	0.001	0.000	0.002	0.001	0.007	0.015	0.001	0.843	0.004	0.003	0.000	22.896	0.000	0.003
20.935	0.064		0.067				0.002			4.051	0.003			5.519		
20.669	2.202		0.005				0.173			3.856	0.019			166.665		
17.971	4.675		0.006				0.351			3.604	0.033			308.100		
17.597	4.925		0.001				0.307			3.540	0.041			344.404		
17.217	4.670		0.002				0.373			3.529	0.039			346.062		
18.713	4.531		0.002				0.296			3.545	0.047			357.550		
19.357	5.005		0.001				0.308			3.546	0.066			371.821		
13.383	0.382	0.000	0.001	0.000	0.006	0.001	0.010	0.000	0.010	0.424	0.003	0.002	0.000	20.637	0.000	0.002
10.846	0.364	0.001	0.002	0.000	0.002	0.002	0.003	0.006	0.004	1.052	0.004	0.004	0.000	18.608	0.000	0.001
13.999	0.074	0.121	0.090	0.003	0.084	0.025	0.345	0.017	0.012	3.757	0.009	0.006	0.000	4.243	0.000	0.002
21.136	2.722		0.002				0.176			3.714	0.017			198.746		
16.447	4.475		0.010				0.313			3.628	0.029			337.402		
11.045	4.703		0.004				0.372			3.627	0.043			345.850		
13.248	4.670		0.003				0.368			3.530	0.046			344.298		
17.018	4.719		0.002				0.402			3.478	0.053			362.584		
31.748	1.149	0.001	0.002	0.000	0.002	0.001	0.006	0.001	0.003	0.357	0.003	0.004	0.000	107.615	0.000	0.001
0.219	5.606		0.001				0.312			3.763	0.021			361.763		
0.228	5.141		0.002				0.268			3.648	0.019			357.163		
0.185	4.951		0.002				0.357			3.675	0.003			357.891		
0.136	4.825		0.003				0.304			3.673	0.009			359.750		
1.130	0.427	0.001	0.001	0.000	0.002	0.000	0.004	0.003	0.012	0.056	0.005	0.005	0.000	63.061	0.001	0.000
0.077	0.257	0.000	0.001	0.000	0.003	0.001	0.016	0.003	0.002	0.055	0.005	0.006	0.000	35.028	0.000	0.004
2.645	0.586	0.000	0.004	0.000	0.004	0.001	0.020	0.030	0.025	0.113	0.007	0.007	0.000	50.714	0.000	0.001

Cr	Cu	Fe	K	Li	Mg	Mn	Mo	Na	Ni	P	Pb	S	Sb	Si	Sr	Ti
mg/l	mg/l	mg/l	mg/l	mg/l	mg/l	mg/l	mg/l	mg/l	mg/l	mg/l	mg/l	mg/l	mg/l	mg/l	mg/l	mg/l
0.004	0.000	8.159	0.281	0.034	7.658	0.709	0.004	18.447	0.000	0.071	0.005	10.514	0.002	5.488	0.641	0.002
0.002	0.000	2.567	21.450	0.043	20.799	0.200	0.003	13.970	0.001	0.063	0.008	7.389	0.001	18.633	0.713	0.001
0.000	0.001	0.274	68.369	0.065	50.761	0.086	0.000	32.514	0.000	0.323	0.006	8.545	0.003	18.064	0.497	0.001
0.001	0.002	0.077	67.310	0.063	42.632	0.050	0.001	128.210	0.001	0.651	0.010	24.872	0.001	15.974	0.319	0.001
0.013	0.005	0.914	20.088	0.038	5.778	0.024	0.000	400.627	0.006	6.162	0.003	22.313	0.008	14.020	0.058	0.148
		2.483	72.015	0.031	118.280	0.066	0.001	1991.356		4.017		117.743		17.522	0.566	
		3.659	236.415	0.001	1059.096	0.395	0.007	8820.151		0.074		642.382		14.673	4.360	
		3.660	242.373	0.012	1085.457	0.702	0.034	8887.375		0.089		647.427		14.977	4.339	
		2.326	244.257	0.004	1091.544	1.104	0.008	8955.227		0.670		667.667		16.572	4.310	
0.000	0.002	1.438	74.941	0.100	73.893	0.050	0.004	50.048	0.001	0.199	0.003	5.917	0.001	20.396	1.074	0.001
0.003	0.001	0.171	47.216	0.060	36.111	0.010	0.002	212.023	0.000	0.757	0.005	20.509	0.007	7.495	0.154	0.003
		0.478	26.052	0.001	21.775	0.007	0.001	804.152		2.238		49.848		14.216	0.081	
		0.759	228.021	0.003	1004.224	0.360	0.008	8359.821		0.164		672.069		17.426	4.077	
		2.819	246.309	0.017	1092.981	0.850	0.008	9063.084		1.537		663.287		16.970	4.473	
		3.730	263.705	0.027	1134.316	1.178	0.022	9402.021		2.741		702.502		14.960	4.995	
		4.986	259.771	0.068	1114.962	1.370	0.013	9240.965		3.443		673.619		15.390	4.821	
		0.627	253.351	0.010	1146.965	1.564	0.005	9405.927		4.060		670.734		17.870	4.926	
0.005	0.001	0.048	36.173	0.059	12.027	0.032	0.004	236.709	0.002	1.220	0.010	30.800	0.001	15.038	0.169	0.009
0.001	0.001	0.182	115.021	0.099	88.268	0.093	0.002	159.167	0.002	0.144	0.013	121.653	0.005	20.218	0.872	0.001
0.012	0.003	1.088	20.373	0.054	7.150	0.062	0.002	467.638	0.004	8.300	0.007	2.704	0.015	16.604	0.076	0.162
		1.507	28.357	0.002	25.835	0.044	0.000	1026.541		7.531		4.097		20.517	0.095	
		2.954	237.180	0.027	993.392	0.637	0.025	8350.049		1.083		682.453		17.508	4.144	
		2.826	260.378	0.053	1103.432	0.780	0.015	9133.490		0.920		675.512		17.478	4.677	
		5.139	260.289	0.084	1133.208	1.029	0.010	9315.714		1.528		732.254		16.066	4.826	
		1.839	259.515	0.060	1135.452	1.556	0.029	9258.559		2.207		738.575		16.027	5.173	
0.001	0.001	5.891	9.100	0.049	16.687	1.186	0.002	24.398	0.002	0.153	0.007	0.779	0.004	15.435	0.936	0.003
0.004	0.001	0.297	92.022	0.080	66.348	0.281	0.006	84.222	0.000	0.461	0.017	1.345	0.004	21.260	0.483	0.000
0.002	0.001	0.077	27.513	0.028	14.156	0.051	0.000	137.793	0.002	2.143	0.014	6.174	0.002	16.256	0.099	0.009
0.024	0.005	0.815	25.834	0.067	12.378	0.152	0.000	471.936	0.008	20.962	0.001	3.583	0.007	18.734	0.119	Overrang
0.019	0.013	2.150	22.536	0.045	7.980	0.063	0.005	573.044	0.009	31.755	0.002	11.118	0.000	15.276	0.113	Overrang
		0.616	200.140	0.055	706.255	0.904	0.005	6592.975		4.358		568.729		17.894	3.118	
		2.944	241.915	0.005	1046.274	1.303	0.015	8712.428		4.117		675.003		15.127	4.580	
		5.776	247.702	0.038	1082.384	1.581	0.009	8871.567		3.113		672.517		13.292	4.511	
		2.237	257.002	0.006	1087.574	1.338	0.002	8824.168		2.668		696.944		15.942	4.476	
0.000	0.002	1.859	42.381	0.042	47.486	0.084	0.001	60.635	0.002	0.141	0.004	15.115	0.002	21.987	0.764	0.001
	0.001	0.045	48.570	0.043	40.606	0.059	0.003	99.695		0.505		14.076		17.362	0.462	0.000
0.001	0.002	0.110	73.938	0.088	42.913	0.083	0.003	46.107	0.001	0.126	0.007	14.194	0.004	16.104	0.416	0.000
0.002	0.002	0.039	88.849	0.066	39.283	0.168	0.002	51.607	0.001	0.162	0.013	9.808	0.002	18.801	0.397	0.000
0.007	0.003	0.434	14.467	0.043	2.934	0.016	0.004	243.012	0.000	2.900	0.010	6.418	0.005	12.095	0.039	0.070
		1.169	215.744	0.004	916.138	0.792	0.016	7544.156		0.523		642.549		15.376	3.523	
		2.942	252.247	0.011	1056.234	1.173	0.007	8628.006		0.670		691.258		15.514	4.753	
		2.274	245.398	0.052	1065.648	0.949	0.001	8793.247		1.462		689.417		18.594	4.842	
		1.850	247.337	0.037	1080.020	1.481	0.024	8846.202		0.852		714.575		16.460	4.611	
0.002	0.001	0.067	51.355	0.066	52.110	0.054	0.004	151.757	0.000	1.080	0.015	33.303	0.002	22.451	0.697	0.004
0.009	0.003	0.045	22.994	0.034	6.808	0.019	0.000	428.599	0.000	5.197	0.009	19.265	0.001	14.988	0.064	0.068
0.009	0.004	0.590	15.030	0.041	3.084	0.031	0.005	308.309	0.003	5.001	0.012	26.288	0.003	10.566	0.040	0.100
		4.672	18.429	0.003	13.999	0.067	0.002	639.546		11.674		3.874		13.535	0.107	
		0.431	76.565	0.024	102.241	0.047	0.001	2083.066		10.368		102.944		14.201	0.389	
		1.724	233.844	0.004	990.390	0.264	0.007	8298.315		1.887		728.924		14.920	4.272	
		0.868	256.772	0.005	1094.595	0.396	0.001	9087.602		0.975		698.865		17.244	4.528	
		2.167	257.631	0.004	1134.382	0.883	0.015	9266.189		0.684		689.910		17.801		
		1.578	266.208	0.046	1113.722	1.001	0.017	9207.758		1.287		719.980		17.657	4.829	
0.000	0.000	0.192	61.440	0.012	48.965	0.055	0.000	55.946	0.001	0.263	0.010	0.309	0.004	17.950	0.436	0.000
0.001	0.000	0.040	66.471	0.038	31.082	0.020	0.003	87.075	0.001	0.335	0.011	2.598	0.003	10.262	0.224	0.000
0.004	0.004	0.577	12.266	0.032	2.256	0.015	0.003	244.871	0.000	2.684	0.009	5.946	0.002	8.859	0.028	0.056
0.007	0.003	0.859	22.699	0.034	5.958	0.030	0.006	462.365	0.002	5.422	0.004	15.177	0.002	9.326	0.064	0.074
		1.767	204.020	0.053	722.802	0.135	0.003	6509.063		0.519		664.395		14.171	3.194	
		6.936	244.680	0.064	1082.182	0.549	0.008	8792.489		0.476		703.978		11.691	4.543	
		5.797	246.576	0.007	1087.510	0.612	0.017	8834.087		0.817		715.956		13.986	4.490	
		2.892	252.966	0.075	1116.189	1.012	0.020	9094.790		1.000		720.009		17.918	4.631	
0.001	0.001	1.260	62.935	0.095	68.451	0.025	0.001	21.359	0.000	0.208	0.010	0.408	0.007	23.019	0.926	0.001
0.002	0.001	0.302	88.576	0.066	92.595	0.031	0.004	38.062	0.000	0.248	0.015	3.111	0.003	8.740	0.422	0.000
		0.541	22.056	0.003	13.667	0.020	0.001	729.924		5.086		57.038		20.923	0.064	
		0.187	168.572	0.035	559.364	0.343	0.004	5766.954		1.113		544.242		20.981	2.236	
		2.633	266.618	0.008	1111.369	0.860	0.002	9124.801		1.542		689.566		18.456	4.801	
		2.709	266.730	0.013	1122.792	0.832	0.029	9214.831		1.223		715.776		18.072	5.058	
		1.770	263.248	0.067	1119.997	0.815	0.020	9231.640		1.484		704.309		17.685	4.797	
		3.454	255.416	0.012	1145.951	0.998	0.000	9260.470		2.601		705.736		19.219	4.654	
		5.897	260.413	0.050	1116.878	0.636	0.017	9155.627		1.060		754.812		19.877	5.140	
0.001	0.001	0.238	85.332	0.088	86.905	0.029	0.004	23.554	0.001	0.200	0.009	0.313	0.004	13.357	0.381	0.000
0.002	0.001	0.446	93.192	0.093	65.672	0.028	0.006	102.552	0.000	0.578	0.008	0.370	0.004	10.826	0.363	0.001
0.011	0.008	0.893	23.762	0.081	8.198	0.018	0.007	503.727	0.005	4.952	0.011	4.162	0.007	13.982	0.074	0.121
		0.398	187.625	0.050	635.113	0.260	0.001	6044.170		0.897		562.927		21.485	2.767	
		2.539	253.286	0.005	1076.357	0.581	0.004	8858.785		0.655		715.289		16.865	4.589	
		5.733	259.569	0.063	1094.012	0.753	0.010	8909.272		0.719		753.341		11.334	4.826	
		6.364	258.099	0.075	1101.375	1.187	0.009	9053.571		2.502		738.956		13.597	4.792	
		2.682	256.772	0.011	1135.992	1.843	0.016	9182.511		3.735		709.276		17.485	4.849	
0.002	0.000	1.403	40.042	0.081	48.688	0.132	0.006	55.123	0.001	0.103	0.007	16.916	0.004	31.691	1.147	0.001
		0.027	293.831	0.054	1152.738	0.014	0.003	9384.837		0.210		838.521		0.225	5.763	
		0.004	281.889	0.068	1148.615	0.015	0.004	9382.911		0.226		814.966		0.234	5.282	
		0.009	273.244	0.050	1155.278	0.009	0.003	9478.547		0.186		820.411		0.190	5.089	
		0.006	279.515	0.037	1166.079	0.010	0.030	9452.002		0.227		817.245		0.140	4.959	
0.001	0.003	0.024	7.169	0.036	7.345	0.018	0.003	25.813	0.004	0.020	0.012	22.874	0.006	1.127	0.426	0.001
0.002	0.002	0.019	4.936	0.059	5.879	0.001	0.012	20.266	0.001	0.002	0.010	5.150	0.001	0.077	0.257	0.000
0.002	0.002	0.031	28.006	0.048	14.804	0.010	0.008	39.163	0.000	2.776	0.014	8.789	0.004	2.638	0.584	0.000

				Stable Isotopes			Ion Balance				Watertype	Total Dissolved Solids	Density Calculated with Phreeqc		Ratios
V	Y	Zn	Zr	$\delta^{18}O$	$\delta^{2}H$		ΣC HGS	ΣA HGS	(ΣC-ΣA) / (ΣC+ΣA) *	(ΣC-ΣA) / (ΣC+ΣA) *			kg/l (25oC)	kg/l (T_{Field})	K/Na
mg/l	mg/l	mg/l	mg/l		Mean	SD	meq/l	meq/l	meq/l %	meq/l %		mg/l			meq/l
0.003	0.000	0.181	0.001	-6.84	-44.3	0.3	8.4	11.1	-13.6	-14.3	F4CaHCO3	275	0.9979	1.0007	0.0090
0.002	0.000	0.005	0.001	-7.45	-48.0	0.0	7.5	7.8	-1.9	-2.0	g3CaHCO3+	240	0.9977	1.0004	0.9027
0.000	0.000	0.004	0.000	-6.48	-41.7	1.2	9.3	10.2	-4.2	-4.5	F4MgHCO3+	297	0.9979	1.0006	1.2363
0.003	0.000	0.001	0.000	-6.28	-40.1	0.9	11.9	14.3	-8.8	-9.3	F4NaHCO3+	467	0.9982	1.0009	0.3087
0.077	0.004	0.025	0.023	-6.21	-42.5	0.8	18.8	18.5	0.6	0.1	F4NaHCO3+	707	0.9985	1.0012	0.0295
0.064				-5.24	-35.7	1.4	100.2	99.1	0.6	0.5	b5NaCl+	5,373	1.0034	1.0061	0.0213
0.003				-2.13	-14.8	0.6	494.7	467.7	2.8	2.7	S3NaCl	28,116	1.0255	1.0283	0.0158
0.011				-2.06	-14.2	1.0	500.4	464.3	3.7	3.7	S3NaCl	28,098	1.0255	1.0282	0.0160
0.006				-1.99	-13.4	2.2	504.1	474.7	3.0	2.9	S3NaCl	28,650	1.0260	1.0288	0.0160
0.001	0.000	0.208	0.000	-5.20	-32.5	0.8	14.5	16.4	-6.1	-6.5	F4MgHCO3+	#VALUE!	0.9983	1.0011	0.8804
0.006	0.000	0.001	0.000	-5.57	-35.1	1.4	13.9	15.5	-5.3	-5.6	F4NaHCO3+	#VALUE!	0.9982	1.0009	0.1309
0.041				-5.39	-34.9	1.1	37.9	35.0	3.9	3.9	B4NaCl+	#VALUE!	0.9996	1.0022	0.0190
0.004				-2.33	-15.9	1.3	468.5	438.4	3.3	3.3	S3NaCl	27,259	1.0239	1.0268	0.0160
0.005				-1.75	-11.8	1.1	508.7	473.9	3.5	3.5	S3NaCl	29,062	1.0261	1.0288	0.0160
0.008				-1.57	-10.9	1.6	528.2	498.3	2.9	2.8	S3NaCl	30,542	1.0275	1.0303	0.0165
0.012				-1.51	-10.0	1.4	519.3	485.6	3.4	3.3	S3NaCl	29,904	1.0268	1.0295	0.0165
0.006				-1.57	-10.5	1.2	529.9	501.6	2.7	2.6	S3NaCl	30,823	1.0277	1.0305	0.0158
0.006	0.000	0.002	0.002	-6.07	-38.7	1.0	13.2	15.4	-7.8	-8.1	F4NaHCO3+	1,620	0.9982	1.0008	0.0898
0.001	0.000	0.002	0.000	-5.91	-36.5	0.1	19.4	20.3	-2.4	-2.6	f4NaMix+	1,322	0.9985	1.0012	0.4249
0.112	0.005	0.005	0.025	-6.18	-40.3	1.0	21.8	19.7	5.2	4.7	F5NaHCO3+	909	0.9987	1.0013	0.0256
0.092				-5.74	-37.8	0.3	48.3	44.1	4.6	4.4	B5NaHCO3+	2,096	1.0004	1.0031	0.0162
0.003				-2.32	-15.0	0.1	467.3	441.5	2.8	2.8	S3NaCl	27,430	1.0240	1.0267	0.0167
0.003				-1.68	-11.4	1.2	513.5	479.7	3.4	3.3	S3NaCl	29,692	1.0264	1.0292	0.0168
0.007				-1.80	-12.4	0.5	524.6	489.0	3.5	3.5	S3NaCl	30,429	1.0270	1.0297	0.0164
0.005				-1.59	-10.9	0.7	522.7	501.8	2.0	1.9	S3NaCl	30,382	1.0275	1.0302	0.0165
0.002	0.000	0.006	0.001	-6.60	-42.7	1.1	11.9	13.3	-5.5	-5.7	F4CaHCO3+	581	0.9982	1.0010	0.2193
0.001	0.000	0.001	0.000	-5.94	-38.4	0.9	13.3	14.9	-5.9	-6.2	F4MgHCO3+	596	0.9983	1.0009	0.6424
0.005	0.000	0.001	0.001	-6.96	-44.8	0.0	8.3	9.6	-7.1	-7.6	F3NaHCO3+	580	0.9978	1.0005	0.1174
0.063	0.003	0.004	0.030	-6.97	-45.9	0.1	22.7	20.7	4.5	3.1	F5NaHCO3+	1,162	0.9988	1.0015	0.0322
0.096	0.004	0.015	0.056	-6.21	-41.0	0.4	26.5	25.9	1.2	-0.7	f5NaHCO3+	1,690	0.9991	1.0018	0.0231
0.004				-2.95	-19.7	0.5	362.1	357.8	0.6	0.4	S4NaCl+	21,672	1.0186	1.0213	0.0178
0.012				-1.92	-14.6	0.7	489.6	467.3	2.3	2.2	S3NaCl	29,029	1.0254	1.0282	0.0163
0.002				-1.80	-13.2	0.3	500.2	479.6	2.1	2.0	S3NaCl	30,169	1.0261	1.0289	0.0164
0.005				-1.76	-13.2	0.5	498.5	479.8	1.9	1.8	S3NaCl	28,969	1.0261	1.0288	0.0171
0.001	0.000	0.012	0.002	-6.31	-39.6	0.8	11.7	13.1	-5.8	-6.1	F4MgHCO3+	706	0.9981	1.0008	0.4109
0.001	0.000	0.002	0.001	-6.27	-38.9	1.1	10.9	12.1	-5.6	-6.0	F4NaHCO3+	612	0.9980	1.0007	0.2864
0.001	0.000	0.006	0.000	-6.53	-41.2	1.1	9.0	9.9	-4.7	-4.9	F3MgHCO3+	564	0.9978	1.0005	0.9428
0.001	0.000	0.003	0.000	-6.46	-40.2	0.5	9.3	9.9	-2.6	-2.8	F3KHCO3+	1,162	0.9979	1.0005	1.0122
0.029	0.001	0.005	0.011	-6.75	-44.4	1.2	11.4	12.0	-2.9	-3.4	F4NaHCO3+	1,195	0.9980	1.0007	0.0350
0.006				-2.86	-18.8	0.7	423.9	400.4	2.9	2.8	S3NaCl	24,608	1.0215	1.0242	0.0168
0.003				-2.14	-14.4	1.2	486.6	470.4	1.7	1.5	S2NaCl	29,041	1.0254	1.0282	0.0172
0.006				-1.99	-12.1	2.0	494.9	464.5	3.2	3.1	S3NaCl	29,027	1.0254	1.0281	0.0164
0.003				-1.98	-12.2	1.4	498.7	474.0	2.5	2.4	S2NaCl	28,977	1.0259	1.0286	0.0164
0.004	0.000	0.001	0.002	-6.12	-38.8	0.8	15.4	16.9	-4.8	-5.2	F4NaHCO3+	838	0.9984	1.0012	0.1990
0.032	0.001	0.019	0.010	-6.02	-38.2	0.2	20.1	19.9	0.6	0.1	f4NaHCO3+	1,035	0.9986	1.0014	0.0315
0.052	0.003	0.038	0.015	-6.46	-41.4	0.8	14.3	13.6	2.4	1.9	F4NaHCO3+	771	0.9982	1.0009	0.0287
0.092				-6.66	-43.5	0.4	30.1	26.7	5.8	5.2	B4NaHCO3+	1,835	0.9991	1.0018	0.0169
0.020				-5.20	-33.5	0.2	102.6	99.7	1.4	1.3	b5NaCl+	5,978	1.0035	1.0063	0.0216
0.006				-2.28	-14.1	0.7	464.8	441.5	2.6	2.5	S3NaCl	27,069	1.0239	1.0267	0.0166
0.007				-1.79	-10.1	0.0	510.2	471.7	3.9	3.9	S3NaCl	29,023	1.0261	1.0289	0.0166
0.007				-1.69	-10.0	0.6	521.9	491.9	3.0	2.9	S3NaCl	30,032	1.0271	1.0298	0.0163
0.005				-1.62	-10.1	1.3	517.6	486.1	3.1	3.1	S3NaCl	29,718	1.0268	1.0296	0.0170
0.001	0.000	0.001	0.000	-6.35	-38.6	1.2	9.9	10.8	-4.3	-4.6	F4MgHCO3+	487	0.9979	1.0006	0.6457
0.002	0.000	0.004	0.000	-5.80	-36.2	1.7	8.8	8.9	-0.3	-0.4	F3NaHCO3+	529	0.9978	1.0004	0.4488
0.032	0.001	0.019	0.012	-5.58	-35.3	3.2	11.3	11.4	-0.4	-0.8	F4NaHCO3+	571	0.9979	1.0006	0.0295
0.092	0.002	0.006	0.019	-5.97	-38.7	2.0	21.5	21.3	0.4	0.0	f4NaHCO3+	1,613	0.9986	1.0013	0.0289
0.005				-3.14	-20.5	1.4	359.7	345.0	2.1	2.0	S3NaCl+	21,714	1.0181	1.0208	0.0184
0.002				-1.93	-13.7	1.1	496.3	461.3	3.7	3.6	S2NaCl	28,589	1.0253	1.0280	0.0164
0.003				-1.83	-11.4	2.1	498.8	476.9	2.2	2.1	S3NaCl	29,460	1.0260	1.0287	0.0164
0.004				-1.71	-11.4	0.9	513.1	480.0	3.3	3.3	S3NaCl	30,082	1.0264	1.0291	0.0164
0.001	0.000	0.139	0.001	-5.31	-31.5	2.1	11.9	13.1	-4.8	-5.1	F4MgHCO3+	532	0.9981	1.0008	1.7324
0.001	0.000	0.002	0.001	-5.45	-33.8	1.5	12.8	14.2	-5.3	-5.6	F4MgHCO3+	623	0.9981	1.0008	1.3682
0.067				-5.19	-33.5	0.8	33.8	30.9	4.5	4.2	B4NaHCO3+	1,804	0.9994	1.0021	0.0178
0.005				-3.14	-21.5	1.5	310.1	292.1	3.0	3.0	b4NaCl+	17,995	1.0151	1.0178	0.0172
0.006				-1.63	-10.9	0.3	512.3	495.0	1.7	1.6	S3NaCl	30,018	1.0270	1.0297	0.0172
0.001				-1.55	-12.1	0.2	519.0	489.4	2.9	2.9	S3NaCl	29,863	1.0270	1.0296	0.0170
0.002				-1.54	-11.8	0.9	519.7	496.4	2.3	2.2	S3NaCl	30,223	1.0272	1.0300	0.0168
0.003				-1.48	-11.7	1.0	523.5	488.3	3.5	3.4	S3NaCl	30,067	1.0270	1.0297	0.0162
0.001				-1.50	-11.3	1.8	516.9	489.2	2.8	2.7	S3NaCl	29,777	1.0269	1.0296	0.0167
0.001	0.000	0.006	0.001	-5.61	-35.8	1.0	11.4	12.9	-5.9	-6.3	F4MgHCO3+	475	0.99805	1.0008	2.1301
0.002	0.000	0.002	0.002	-5.57	-34.0	0.4	13.3	13.9	-2.2	-2.3	F4NaHCO3+	555	0.99816	1.0008	0.5343
0.090	0.003	0.084	0.025	-5.46	-34.3	1.2	23.5	21.1	5.3	5.1	f4NaHCO3+	1,036	0.99875	1.0014	0.0277
0.002				-3.19	-20.3	1.2	330.6	318.4	1.9	1.8	b4NaCl+	19,825	1.0165	1.0191	0.0183
0.010				-1.80	-10.5	0.8	498.5	461.5	3.9	3.8	S3NaCl	28,817	1.0254	1.0281	0.0168
0.004				-1.60	-9.9	1.5	503.1	479.8	2.4	2.3	S2NaCl	29,851	1.0262	1.0289	0.0171
0.003				-1.51	-9.4	1.1	509.9	479.6	3.1	3.0	S3NaCl	29,461	1.0263	1.029	0.0168
0.002				-1.46	-9.7	1.0	519.5	501.0	1.8	1.7	S3NaCl	30,171	1.0274	1.0301	0.0164
0.002	0.000	0.002	0.001	-6.40	-39.3	0.1	12.9	14.2	-4.8	-5.0	F4CaHCO3+	785	0.9982	1.0009	0.4271
0.001				-1.10	-7.8	1.4	530.3	513.6	1.6	1.4	S2NaCl	31,152	1.028	1.031	0.0184
0.002				-1.23	-8.6	1.5	529.1	495.2	3.3	3.2	S2NaCl	30,442	1.0273	1.0303	0.0177
0.002				-1.29	-7.4	0.5	533.8	510.6	2.2	2.1	S2NaCl	31,035	1.028	1.031	0.0169
0.003				-1.23	-8.1	0.9	533.7	501.6	3.1	3.0	S2NaCl	31,180	1.0276	1.0307	0.0174
0.001	0.000	0.002	0.000	-4.09	-32.3	0.7	5.1	5.7	-6.3	-6.6	F2CaHCO3	1,004	0.99746	1.0004	0.1633
0.001	0.000	0.003	0.001	-5.27	-37.2	0.9	3.2	5.3	-24.1	-24.9	F3CaHCO3	1,039	0.99741	1.0003	0.1432
0.004	0.000	0.004	0.001	-3.99	-28.6	1.0	6.2	4.7	14.2	13.9	F2CaMix	738	0.99743	1.0004	0.4204

			Parts							Changes					
Mg/Na	Ca/Na	Ca/Cl	Na / ΣC	K / ΣC	Mg / ΣC	Ca / ΣC	Cl / ΣA	SO4 / ΣA	HCO3 + CO3 / ΣA	d Na	d K	d Mg	d Ca	d Cl	d SO4
meq/l	meq/l	meq/l	meq/l %	meq/l %	meq/l %	meq/l %	meq/l %	meq/l %	meq/l %	meq/l	meq/l	meq/l	meq/l	meq/l	meq/l
0.7851	8.2980	7.0116	9.91	0.09	7.78	82.22	58.93	41.07	0.00	0.00	0.00	0.00	0.00	0.00	0.00
2.8158	7.3045	5.7815	8.32	7.51	23.42	60.75	61.88	38.12	0.00	0.00	0.00	0.00	0.00	0.00	0.00
2.9526	1.3592	1.7394	15.27	18.88	45.10	20.75	67.04	32.96	0.00	0.00	0.00	0.00	0.00	0.00	0.00
0.6289	0.1725	0.4411	47.39	14.63	29.81	8.17	59.46	40.54	0.00	0.00	0.00	0.00	0.00	0.00	0.00
0.0273	0.0101	0.0574	93.73	2.76	2.56	0.95	71.89	28.11	0.00	0.00	0.00	0.00	0.00	0.00	0.00
0.1123	0.0214	0.0252	86.58	1.84	9.73	1.85	91.28	8.72	0.00	0.00	0.00	0.00	0.00	0.00	0.00
0.2271	0.0423	0.0386	77.81	1.23	17.68	3.29	90.76	9.24	0.00	0.00	0.00	0.00	0.00	0.00	0.00
0.2310	0.0433	0.0402	77.49	1.24	17.91	3.36	90.71	9.29	0.00	0.00	0.00	0.00	0.00	0.00	0.00
0.2305	0.0434	0.0396	77.52	1.24	17.87	3.36	90.60	9.40	0.00	0.00	0.00	0.00	0.00	0.00	0.00
2.7923	1.9201	1.4110	15.17	13.35	42.36	29.12	88.88	11.12	0.00	0.00	0.00	0.00	0.00	0.00	0.00
0.3221	0.0466	0.2003	66.68	8.73	21.48	3.10	N/A	N/A	N/A	N/A	N/A	N/A	N/A	N/A	N/A
0.0512	0.0099	0.0196	92.58	1.76	4.74	0.92	N/A	N/A	N/A	N/A	N/A	N/A	N/A	N/A	N/A
0.2272	0.0416	0.0387	77.83	1.25	17.69	3.24	88.05	9.90	2.05	-0.06	-0.01	0.43	6.62	0.00	0.57
0.2281	0.0420	0.0389	77.75	1.24	17.74	3.27	89.66	9.03	1.32	-0.09	0.54	1.55	4.41	0.00	0.40
0.2282	0.0424	0.0386	77.69	1.28	17.73	3.29	89.39	9.00	1.61	0.41	1.73	3.95	1.88	0.00	0.44
0.2282	0.0427	0.0394	77.67	1.28	17.73	3.32	89.18	8.73	2.09	3.60	1.69	3.05	0.87	0.00	1.28
0.2306	0.0441	0.0400	77.48	1.23	17.87	3.41	88.82	8.55	2.63	14.64	0.47	-0.17	0.05	0.00	0.90
0.0961	0.0810	0.2375	78.93	7.09	7.59	6.40	15.78	8.01	76.21	21.16	0.76	-5.45	-1.08	0.00	-0.49
1.0488	0.3084	0.4489	35.94	15.27	37.71	11.08	30.17	46.38	23.45	9.76	-0.12	0.40	-0.55	0.00	-0.17
0.0289	0.0103	0.0991	93.91	2.41	2.72	0.97	38.86	0.60	60.54	15.93	0.09	3.33	0.13	0.00	0.12
0.0476	0.0095	0.0238	93.17	1.51	4.44	0.88	83.39	0.05	16.56	9.55	-0.02	1.66	-0.13	0.00	0.70
0.2250	0.0408	0.0377	77.97	1.30	17.55	3.18	87.56	9.70	2.74	-0.46	1.87	5.47	4.06	0.00	0.07
0.2285	0.0427	0.0392	77.64	1.30	17.74	3.31	88.94	8.69	2.37	7.31	1.18	2.53	0.34	0.00	1.03
0.2301	0.0436	0.0401	77.51	1.27	17.84	3.38	88.36	8.93	2.71	19.25	0.41	-1.86	-0.36	0.00	1.15
0.2319	0.0448	0.0399	77.32	1.27	17.94	3.47	89.97	9.19	0.84	16.00	0.10	1.98	-0.46	0.00	3.99
1.2935	8.4277	6.9971	9.14	2.00	11.83	77.03	24.57	0.04	75.39	14.48	-0.20	1.40	-0.21	0.00	-0.32
1.4899	0.4233	0.9387	28.12	18.07	41.91	11.90	31.86	1.25	66.88	8.90	-0.11	0.06	-0.34	0.00	-0.34
0.1943	0.0568	0.2727	73.07	8.58	14.20	4.15	20.94	6.01	73.04	13.06	-0.02	1.07	0.00	0.00	-1.54
0.0496	0.0160	0.0808	91.09	2.93	4.52	1.46	43.41	0.07	56.52	7.26	-0.40	0.68	0.27	0.00	-2.36
0.0263	0.0099	0.0364	94.40	2.18	2.49	0.93	39.90	2.42	57.68	7.17	0.87	0.26	0.70	0.00	1.43
0.2026	0.0387	0.0355	79.42	1.42	16.09	3.07	87.77	10.05	2.18	2.68	2.87	6.27	1.95	0.00	6.83
0.2271	0.0433	0.0390	77.71	1.27	17.65	3.36	87.79	8.78	3.43	18.45	0.49	0.15	0.13	0.00	-0.18
0.2307	0.0438	0.0392	77.46	1.27	17.88	3.40	86.53	8.51	4.97	28.84	0.45	-1.56	-0.28	0.00	-1.79
0.2331	0.0442	0.0394	77.25	1.32	18.01	3.41	89.90	9.12	0.98	13.30	0.07	0.16	-0.65	0.00	3.67
1.4811	1.4792	1.5042	22.87	9.40	33.89	33.84	32.12	11.59	56.30	5.42	0.22	0.29	-0.43	0.00	-2.66
0.7703	0.4237	0.8242	40.31	11.55	31.06	17.08	34.34	13.21	52.45	6.43	0.10	1.15	-0.04	0.00	-1.19
1.7602	0.6910	0.5903	22.75	21.46	40.07	15.72	36.26	13.72	50.03	-6.72	-0.09	-1.13	-0.11	0.00	-0.74
1.4396	0.5908	0.5556	24.73	25.04	35.62	14.61	16.60	4.24	79.16	-0.10	0.21	1.11	8.89	0.00	-0.13
0.0228	0.0101	0.0510	93.64	3.28	2.14	0.94	13.88	2.09	84.03	2.17	2.33	5.11	1.48	0.00	-0.11
0.2297	0.0421	0.0392	77.60	1.30	17.83	3.27	87.89	10.19	1.92	4.86	0.69	0.90	0.29	0.00	0.23
0.2315	0.0431	0.0384	77.40	1.33	17.93	3.34	87.75	9.04	3.21	16.85	0.60	0.17	0.17	0.00	-0.42
0.2292	0.0439	0.0404	77.54	1.27	17.78	3.41	87.60	8.83	3.57	18.82	0.48	-0.75	-0.03	0.00	-0.29
0.2309	0.0444	0.0402	77.41	1.27	17.88	3.43	89.21	9.26	1.53	3.62	0.46	-7.28	-1.46	0.00	3.35
0.6494	0.4692	0.9854	43.14	8.58	28.03	20.24	35.33	22.41	42.26	-6.46	-0.36	-2.10	-0.08	0.00	-0.12
0.0300	0.0099	0.0362	93.33	2.94	2.80	0.93	49.84	8.61	41.55	-9.85	-0.39	-1.49	-0.01	0.00	-0.85
0.0189	0.0095	0.0955	94.60	2.71	1.79	0.90	21.09	22.82	56.09	-10.75	-0.13	-0.79	0.08	0.00	0.50
0.0414	0.0133	0.0314	93.31	1.58	3.86	1.25	56.61	0.04	43.35	0.26	1.04	3.36	3.80	0.00	0.68
0.0928	0.0160	0.0192	88.46	1.91	8.21	1.41	83.66	6.79	9.55	2.29	1.21	2.87	1.75	0.00	0.63
0.2257	0.0418	0.0385	77.87	1.29	17.58	3.25	88.49	10.08	1.43	-0.15	1.85	3.04	1.29	0.00	0.65
0.2278	0.0423	0.0395	77.71	1.29	17.71	3.29	89.66	8.95	1.39	0.06	2.24	2.73	1.23	0.00	0.37
0.2315	0.0425	0.0388	77.49	1.27	17.95	3.29	89.54	8.61	1.85	8.66	0.34	-0.20	0.02	0.00	0.10
0.2288	0.0428	0.0392	77.60	1.32	17.76	3.32	89.83	9.01	1.16	5.11	0.03	1.47	-0.01	0.00	5.52
1.6552	0.7009	1.0158	24.99	16.13	41.37	17.51	36.04	0.13	63.84	-11.57	0.12	-2.91	-0.90	0.00	0.55
0.6751	0.1626	0.4135	43.73	19.63	29.53	7.11	26.65	2.46	70.89	1.10	0.04	-0.86	-0.04	0.00	-0.38
0.0174	0.0083	0.0614	94.77	2.79	1.65	0.79	30.14	6.35	63.50	-4.78	-0.05	-1.57	-0.14	0.00	0.89
0.0244	0.0080	0.0194	94.23	2.72	2.30	0.75	40.70	4.14	55.16	3.72	1.27	3.62	2.97	0.00	1.67
0.2100	0.0391	0.0370	78.89	1.45	16.57	3.08	84.90	11.35	3.74	13.97	0.51	-0.52	-0.02	0.00	0.36
0.2328	0.0439	0.0406	77.33	1.27	18.01	3.40	88.66	9.17	2.17	12.19	0.36	-0.03	0.07	0.00	1.31
0.2328	0.0439	0.0394	77.32	1.27	18.01	3.40	88.16	9.04	2.80	16.98	0.29	-1.36	-0.11	0.00	-1.20
0.2321	0.0442	0.0405	77.36	1.27	17.96	3.42	87.67	8.92	3.41	21.59	0.83	-7.61	-1.60	0.00	-1.55
6.0609	3.9319	3.7965	7.86	13.61	47.64	30.90	20.55	0.02	79.43	5.60	0.04	-0.51	-1.47	0.00	5.04
4.6009	0.6901	0.8853	13.05	17.86	60.08	9.01	20.16	2.66	77.18	11.21	0.14	1.44	-1.16	0.00	-0.55
0.0354	0.0087	0.0237	94.17	1.67	3.34	0.82	58.35	16.27	25.38	2.22	-0.11	0.84	-1.55	0.00	-2.20
0.1834	0.0332	0.0332	81.05	1.39	14.87	2.69	87.08	11.56	1.36	4.08	0.18	0.16	-1.34	0.00	-0.36
0.2303	0.0387	0.0344	77.74	1.34	17.91	3.01	89.70	8.55	1.75	0.91	1.55	3.68	1.63	0.00	-0.16
0.2304	0.0429	0.0390	77.50	1.32	17.86	3.32	89.81	8.77	1.42	2.44	1.68	2.25	0.55	0.00	-0.01
0.2294	0.0430	0.0386	77.56	1.30	17.80	3.34	89.64	8.54	1.82	9.34	0.29	-0.12	0.03	0.00	0.16
0.2340	0.0443	0.0407	77.24	1.25	18.08	3.42	89.22	8.48	2.30	12.59	0.45	-1.25	-0.19	0.00	0.01
0.2307	0.0466	0.0423	77.27	1.29	17.83	3.60	89.89	9.09	1.02	11.78	0.68	-3.14	-1.59	0.00	9.76
6.9781	1.0052	0.9168	9.00	19.16	62.80	9.04	27.51	0.10	72.39	16.11	0.23	3.31	0.21	0.00	3.61
1.2111	0.2082	0.7112	33.85	18.09	41.01	7.05	29.02	0.11	70.88	4.88	0.07	0.70	-0.30	0.00	3.39
0.0308	0.0097	0.0423	93.62	2.60	2.88	0.90	58.91	0.74	40.36	13.87	0.19	2.51	0.18	0.00	3.03
0.1987	0.0377	0.0359	79.70	1.45	15.84	3.01	86.11	10.30	3.59	0.08	1.60	5.43	3.61	0.00	-0.09
0.2298	0.0437	0.0406	77.50	1.30	17.81	3.39	88.54	8.87	2.58	0.51	2.25	7.35	1.09	0.00	0.05
0.2322	0.0445	0.0399	77.28	1.32	17.95	3.44	87.90	9.01	3.09	21.45	0.39	-1.29	-0.19	0.00	2.15
0.2301	0.0436	0.0398	77.49	1.30	17.83	3.38	89.48	8.99	1.52	29.54	0.67	-5.77	-1.71	0.00	9.53
0.2340	0.0453	0.0401	77.17	1.27	18.06	3.50	90.37	8.56	1.07	2.18	0.33	-0.93	-2.51	0.00	0.29
1.6704	2.2396	2.0426	18.73	8.00	31.30	41.96	30.48	11.78	57.75	N/A	N/A	N/A	N/A	N/A	N/A
0.2323	0.0442	0.0391	77.22	1.42	17.94	3.41	89.55	9.44	1.02	N/A	N/A	N/A	N/A	N/A	N/A
0.2315	0.0437	0.0400	77.34	1.37	17.91	3.38	89.50	9.46	1.04	N/A	N/A	N/A	N/A	N/A	N/A
0.2305	0.0433	0.0389	77.47	1.31	17.86	3.36	89.80	9.47	0.73	N/A	N/A	N/A	N/A	N/A	N/A
0.2333	0.0437	0.0397	77.25	1.34	18.03	3.37	88.49	9.34	2.16	N/A	N/A	N/A	N/A	N/A	N/A
0.5381	2.8026	2.1562	22.20	3.63	11.95	62.22	9.88	9.34	80.78	N/A	N/A	N/A	N/A	N/A	N/A
0.5486	1.9828	1.8085	27.21	3.90	14.93	53.96	5.91	1.93	92.16	N/A	N/A	N/A	N/A	N/A	N/A
0.7149	1.4856	1.2878	27.62	11.61	19.75	41.03	19.83	5.32	74.85	N/A	N/A	N/A	N/A	N/A	N/A

				Saturation Index at T_{Field}								
d (HCO3 + CO3)	d PO4	d DOC	Total	Carbon Dioxide	Calcite	Dolomite	Fehydroxy-phosphate	Gypsum	Pyrite	Rhodo-chrosite	Siderite	Vivianite
meq/l	meq/l	meq/l	meq/l	CO2(g)	CaCO3	CaMg(CO3)2		CaSO4·2 H2O	FeS2	MnCO3	FeCO3	Fe3(PO4) 2:8H2O
0.00	0.00	0.00	0.00	-1.41	0.2	-0.8	-1.1	-1.9	7.8	0.2	1.0	-0.2
0.00	0.00	0.00	0.00	-2.19	0.5	0.5	-0.2	-2.1	7.9	0.1	1.0	0.6
0.00	0.00	0.00	0.00	-2.45	0.6	1.4	-1.6	-2.5	7.4	0.0	0.4	-1.1
0.00	0.00	0.00	0.00	-2.18	0.2	0.8	-3.2	-2.4	7.8	-0.3	-0.2	-2.5
0.00	0.00	0.00	0.00	-2.86	0.2	0.8	1.9	-3.3	7.9	-0.3	1.4	3.4
0.00	0.00	0.00	0.00	-2.19	0.6	1.8	1.2	-1.9	8.4	-0.1	1.4	2.7
0.00	0.00	0.00	0.00	-2.28	0.1	0.8	-0.5	-0.7	7.1	-0.5	0.3	-0.2
0.00	0.00	0.00	0.00	-2.22	-0.1	0.5	-0.9	-0.7	7.8	-0.4	0.1	-0.4
0.00	0.00	0.00	0.00	-2.10	-0.2	0.4	-1.3	-0.7	6.4	-0.3	-0.2	-0.9
0.00	N/A	N/A	N/A	-2.08	0.9	1.8	18.1	-2.4	-1000.0	-0.3	0.7	-1.3
N/A	N/A	N/A	N/A	-2.63	0.4	1.5	-0.9	-2.8	6.5	-0.7	0.5	-0.7
N/A	N/A	N/A	N/A	-2.77	0.4	1.4	0.7	-2.7	7.7	-0.8	1.0	1.4
9.07	0.01	1.82	-2.66	-2.28	0.1	0.9	15.7	-0.7	-1000.0	-0.5	-0.4	-2.5
6.26	0.01	0.94	-0.26	-2.26	0.1	0.9	17.6	-0.7	-1000.0	-0.2	0.1	0.2
8.09	0.03	0.84	-0.59	-2.30	0.0	0.7	0.3	-0.7	5.2	-0.1	0.2	0.9
10.20	0.06	0.93	-2.33	-2.15	0.1	0.8	0.6	-0.7	5.4	0.0	0.4	1.4
13.33	0.59	3.06	0.18	-2.28	0.4	1.4	-1.7	-0.7	7.5	0.3	-0.3	-0.8
16.44	0.32	3.14	-0.88	-2.63	0.5	1.0	-2.3	-2.4	8.2	-0.3	-0.1	-1.8
0.69	-0.16	0.06	9.14	-2.61	0.6	1.7	-1.5	-1.5	6.7	0.1	0.3	-2.1
0.32	-0.15	-0.05	19.19	-2.76	0.4	1.1	1.7	-4.8	7.1	0.2	1.5	3.7
0.47	-0.11	-0.04	10.01	-2.34	0.5	1.7	1.1	-5.2	6.3	0.0	1.5	3.2
12.26	0.02	0.81	-1.40	-2.38	0.3	1.4	0.5	-0.7	5.5	0.0	0.5	0.5
11.53	0.08	0.67	-1.27	-2.40	0.4	1.4	0.4	-0.7	5.0	0.1	0.4	0.3
13.38	0.22	2.27	2.70	-2.36	0.1	0.9	0.4	-0.7	6.9	-0.1	0.4	1.0
1.41	-0.16	0.07	12.38	-2.38	0.1	0.8	-0.6	-0.7	6.9	0.0	-0.1	-0.1
0.41	-0.09	-0.04	15.46	-1.39	0.4	-0.1	-1.9	-4.3	6.8	0.6	1.0	0.1
-0.23	0.00	-0.08	9.08	-2.13	0.5	1.5	-2.2	-3.6	7.2	0.5	0.4	-1.2
0.77	0.09	-0.07	14.80	-2.63	0.0	0.4	-1.8	-3.3	8.1	-0.1	0.0	-0.5
1.59	0.14	0.22	8.44	-2.36	0.2	0.7	0.5	-5.3	8.0	0.4	1.0	3.6
9.73	0.13	0.96	-2.29	-2.46	0.1	0.6	2.6	-3.7	8.3	0.1	1.5	5.2
7.73	0.02	1.11	-0.80	-2.14	0.4	1.4	-1.0	-0.9	5.9	0.3	-0.1	-0.5
16.41	0.83	4.40	2.17	-2.24	0.0	0.7	17.8	-0.7	-1000.0	0.0	0.1	0.8
24.64	0.75	5.97	3.85	-2.28	0.2	1.1	0.8	-0.7	6.8	0.2	0.6	1.8
1.46	-0.13	0.10	7.89	-2.11	-0.1	0.4	16.5	-0.7	-1000.0	-0.2	-0.2	-0.2
1.44	-0.01	0.09	6.71	-2.21	0.7	1.3	0.0	-2.0	6.7	-0.1	1.1	0.6
0.25	0.03	0.02	8.55	-2.56	0.7	1.6	-3.2	-2.3	7.7	0.0	-0.3	-2.8
0.00	0.10	0.04	-7.40	-2.67	0.5	1.2	-2.0	-2.4	5.6	0.1	0.1	-2.4
11.37	0.02	2.39	-1.14	-2.54	0.4	1.0	-3.2	-2.6	3.7	0.3	-0.5	-3.9
12.63	0.05	0.62	-1.47	-3.25	0.1	0.5	1.4	-4.0	6.5	-0.4	1.1	2.4
7.69	0.24	1.17	-1.42	-2.08	0.2	1.0	-1.6	-0.8	6.7	0.0	-0.1	-1.5
15.41	2.10	4.05	0.69	-2.37	0.0	0.6	-0.3	-0.7	5.0	-0.2	0.1	-0.4
16.91	3.29	4.48	-1.40	-2.41	0.3	1.2	-0.2	-0.7	6.6	0.0	0.2	0.1
5.06	0.34	0.30	-13.42	-2.41	0.0	0.7	-0.8	-0.7	6.3	0.0	-0.1	-0.5
0.01	0.28	0.03	-9.17	-2.15	0.7	1.3	-3.7	-1.8	8.5	-0.2	-0.3	-2.4
0.40	0.18	0.00	-11.47	-2.87	0.2	0.9	-2.1	-3.4	9.1	-0.4	0.0	-0.7
-0.30	0.13	0.03	-11.93	-3.22	0.2	0.6	2.0	-3.3	6.8	-0.1	1.2	3.0
9.03	0.02	1.04	-1.26	-2.71	0.4	1.2	3.0	-5.2	6.7	0.1	1.9	5.8
8.58	0.05	0.91	-1.14	-2.11	0.4	1.4	-0.1	-2.1	5.2	-0.3	0.5	1.2
6.31	0.02	0.48	-0.94	-2.45	0.2	1.0	-0.3	-0.7	5.4	-0.5	0.1	0.1
6.57	0.02	0.59	-0.70	-2.34	0.4	1.4	-1.2	-0.7	4.5	-0.3	-0.1	-1.2
9.11	0.29	1.77	-0.68	-2.34	0.4	1.5	17.8	-0.7	-1000.0	0.1	0.2	-0.5
2.51	-0.06	0.07	-1.38	-2.34	0.2	1.0	-0.8	-0.7	5.5	-0.1	0.0	-0.5
-0.38	-0.06	-0.10	-15.36	-2.46	0.6	1.5	-2.6	-4.5	6.8	-0.1	0.3	-1.6
0.65	0.03	-0.02	-0.06	-2.79	0.3	1.2	-2.9	-3.5	6.1	-0.5	-0.2	-2.9
-0.33	0.00	-0.08	-7.09	-3.38	0.1	0.5	1.7	-4.1	7.2	-0.5	1.3	2.7
11.21	0.12	0.53	-1.43	-2.96	0.1	0.7	1.9	-3.5	7.8	-0.2	1.3	3.4
13.14	0.51	1.38	-0.07	-2.26	0.1	1.0	-0.8	-0.8	6.5	-0.7	0.2	-0.6
10.14	0.47	2.15	0.68	-2.23	-0.2	0.3	17.5	-0.7	-1000.0	-0.6	0.3	0.5
13.52	1.19	7.13	2.28	-2.44	0.1	0.9	0.4	-0.7	7.7	-0.3	0.5	0.9
16.18	1.03	1.39	-2.46	-2.42	0.2	1.0	-0.5	-0.7	8.7	-0.1	0.2	0.2
0.39	0.09	0.01	-1.86	-1.94	0.6	1.3	17.8	-1000.0	21.6	-0.7	0.7	-0.8
1.34	0.02	0.06	10.82	-2.22	0.4	1.6	-2.2	-3.3	7.2	-0.4	0.5	-1.8
1.30	-0.02	0.00	2.32	-2.49	0.1	0.8	0.6	-2.8	8.8	-0.4	1.0	2.1
0.18	0.04	-0.03	3.23	-2.22	0.4	1.4	-2.6	-1.0	5.8	0.0	-0.5	-2.6
8.70	0.03	0.85	-0.80	-2.14	0.2	1.2	-0.4	-0.8	7.2	0.0	0.3	0.2
6.93	0.03	0.42	-0.04	-2.21	0.3	1.3	-0.2	-0.7	6.5	0.0	0.3	0.1
9.09	0.26	1.54	0.04	-2.09	0.2	1.0	-1.2	-0.7	6.6	-0.1	0.0	-0.8
11.25	0.53	2.05	-0.17	-2.07	0.2	1.0	-0.4	-0.7	7.5	-0.1	0.3	0.5
2.43	-0.02	0.44	-4.45	-2.03	-0.1	0.4	-0.4	-0.7	7.0	-0.6	0.2	0.3
-1.92	-0.28	-0.18	18.46	-2.45	0.5	1.8	-2.5	-4.9	6.6	-0.3	0.5	-1.8
-1.86	-0.27	-0.12	4.11	-2.46	0.6	1.9	-1.2	-5.0	7.0	-0.3	0.8	-0.1
-1.65	-0.25	-0.09	15.62	-2.79	0.4	1.1	1.3	-4.5	7.8	-0.4	1.4	3.0
11.51	0.03	0.71	-0.72	-2.40	0.6	1.9	-1.7	-0.9	8.4	0.1	0.1	-1.6
12.08	0.02	0.00	-0.95	-2.58	0.4	1.5	1.0	-0.7	7.6	0.0	0.4	2.2
15.08	0.53	2.90	2.62	-2.47	0.1	0.9	0.5	-0.7	7.4	-0.2	0.5	0.9
4.41	-0.08	0.29	8.87	-2.32	0.1	0.8	0.9	-0.7	7.0	-0.1	0.5	1.7
0.10	-0.20	-0.02	-1.11	-2.24	0.4	1.4	0.2	-0.7	7.1	0.4	0.4	0.9
N/A	N/A	N/A	N/A	-2.00	0.7	1.2	-0.9	-1.8	7.1	0.0	0.8	-0.3
N/A	N/A	N/A	N/A	-2.41	-0.5	-0.4	-9.0	-0.6	4.6	-2.6	-2.5	-10.6
N/A	N/A	N/A	N/A	-3.24	0.3	1.2	-8.8	-0.6	4.1	-1.7	-2.5	-11.3
N/A	N/A	N/A	N/A	-3.46	0.5	1.6	-7.6	-0.6	4.5	-1.8	-2.0	-10.0
N/A	N/A	N/A	N/A	-3.53	0.6	1.7	-7.3	-0.6	1.5	-1.7	-2.1	-10.4
N/A	N/A	N/A	N/A	-2.71	0.1	-0.7	-5.9	-1.8	5.4	-1.1	-1.2	-6.5
N/A	N/A	N/A	N/A	-2.93	0.4	0.0	-5.4	-2.6	4.1	-2.0	-0.8	-6.2
N/A	N/A	N/A	N/A	-2.78	-0.2	-0.9	-3.7	-2.3	4.9	-1.5	-1.3	-2.0

Appendix 4 – Lithology ERT profiles

This section shows the lithological classes and model uncertainty of the ERT profiles where the y-axis represents the depth relative to sea-level and the x-axis the distance along the profile. The lithological classes and model uncertainty are colour coded according the legend below where the lithological classes show the highest probable lithological class and the model uncertainty shows the percentage of uncertainty.

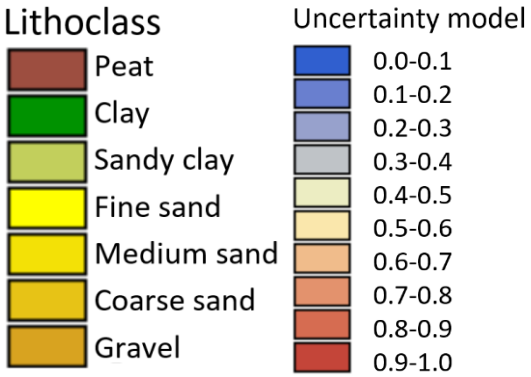

Profile II

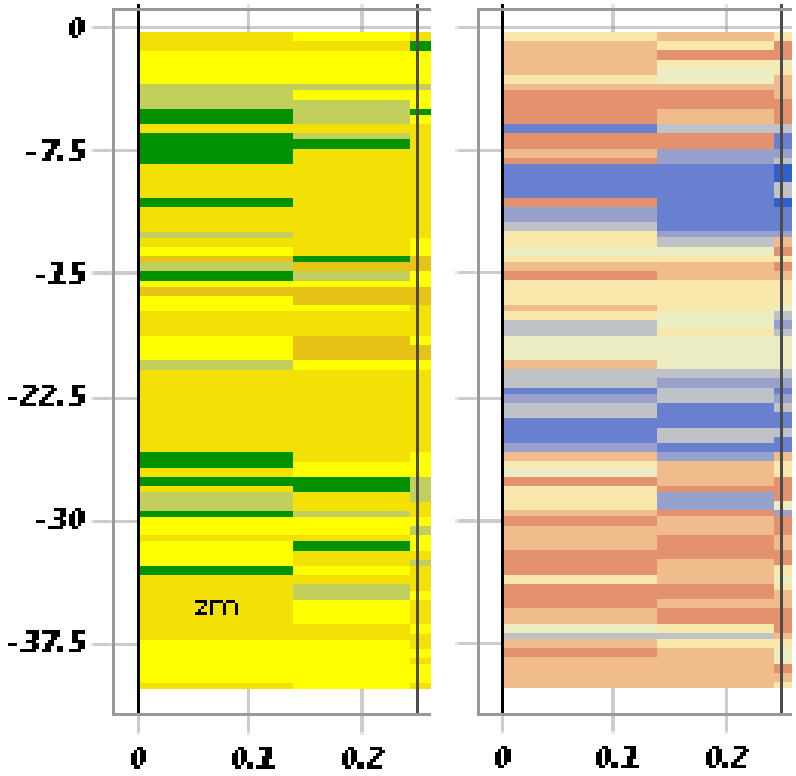

Profile VII

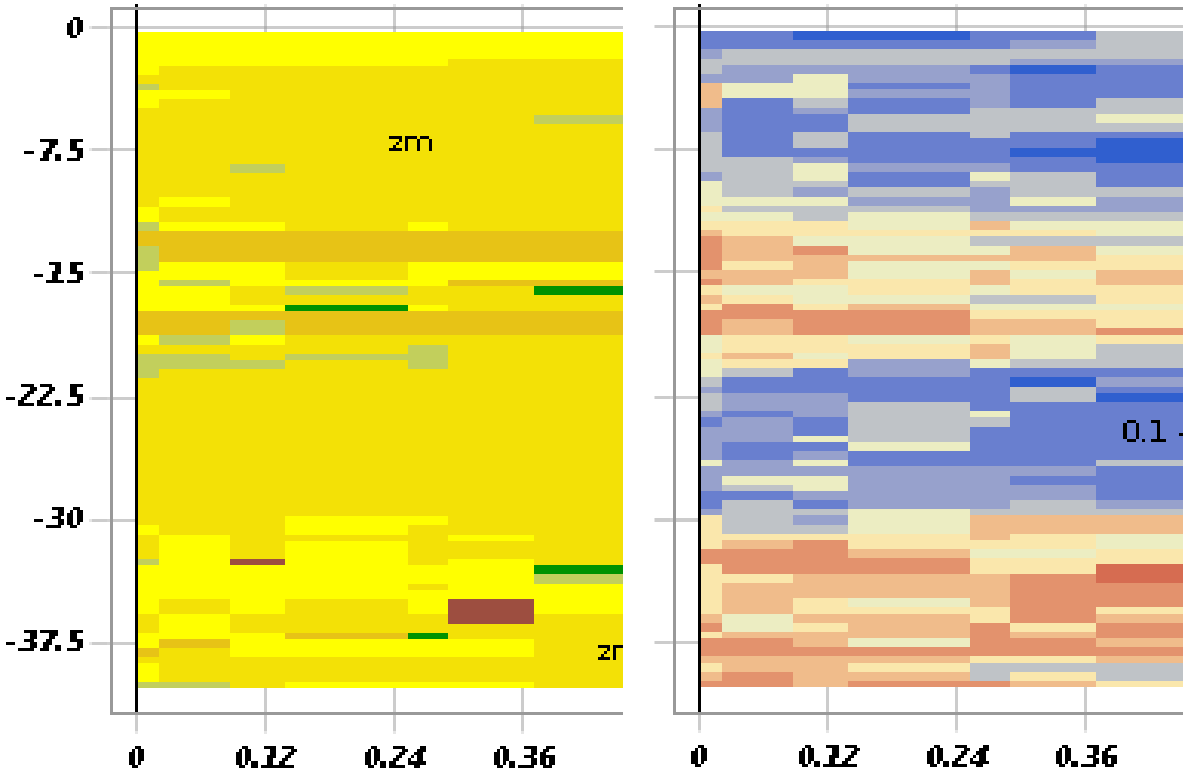

Profile V

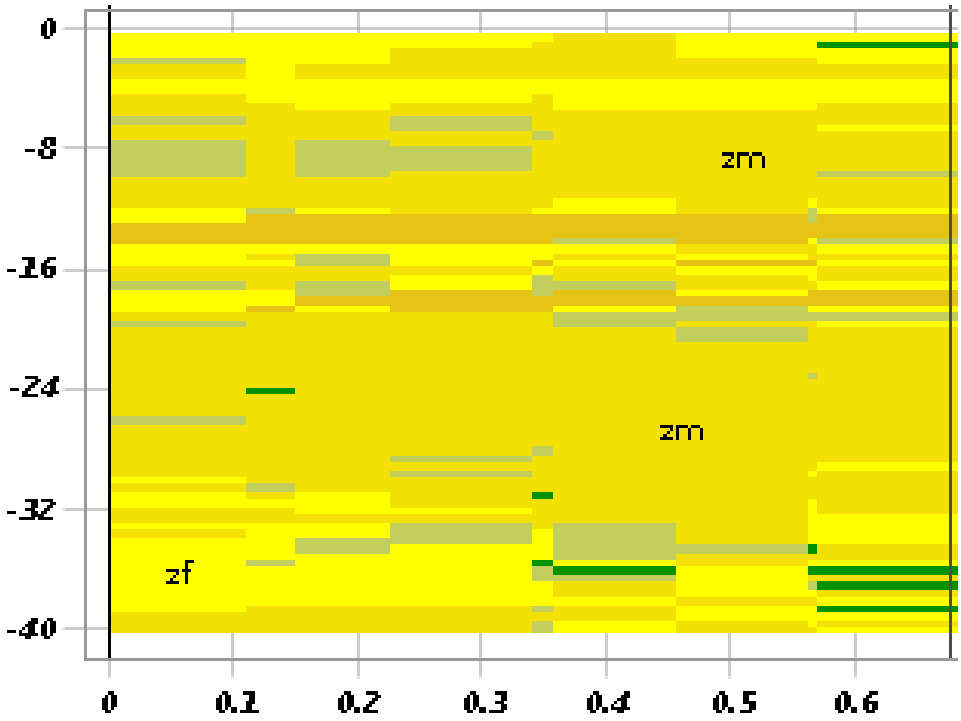
0
-8
-16
-24
-32
-40
0
0.1
0.2
0.3
0.4
0.5
0.6
zm
zm
zf

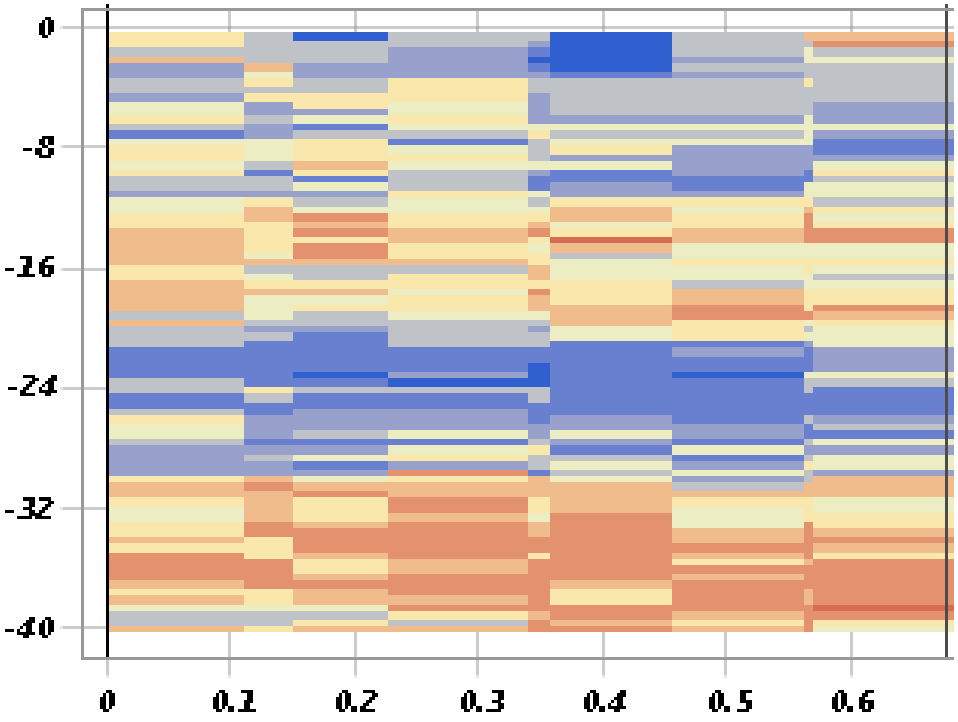
0
-8
-16
-24
-32
-40
0
0.1
0.2
0.3
0.4
0.5
0.6

Profile X

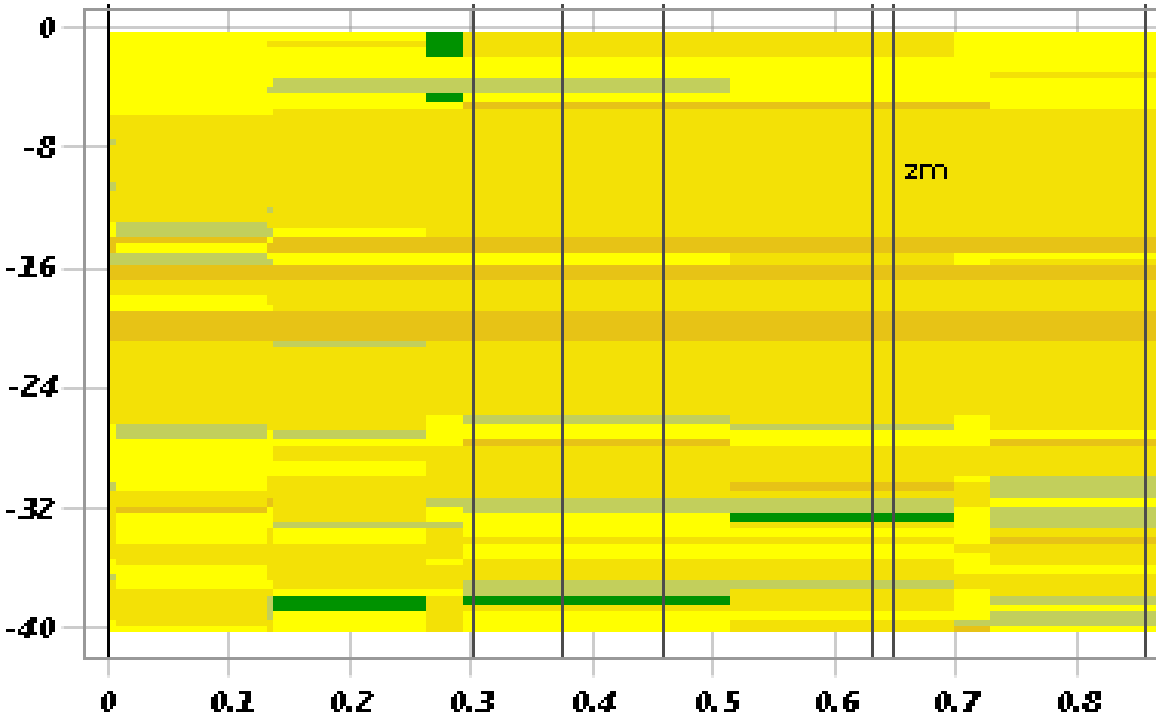
0
-8
-16
-24
-32
-40
zm
0
0.1
0.2
0.3
0.4
0.5
0.6
0.7
0.8

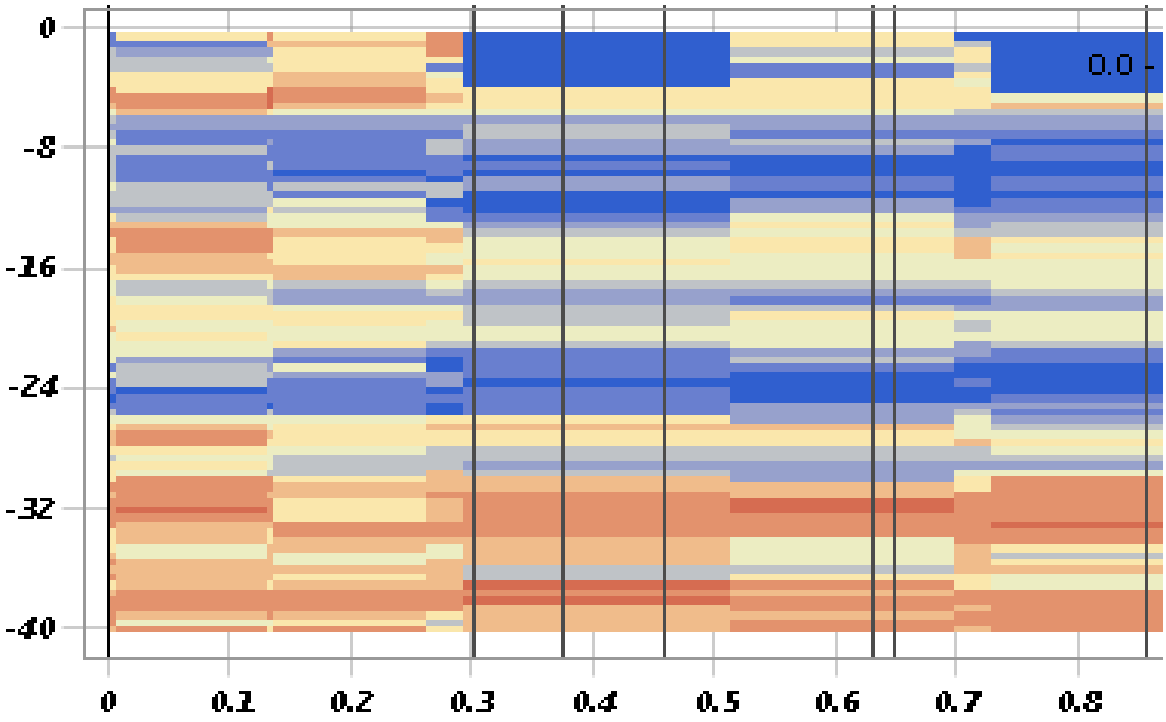
0
-8
-16
-24
-32
-40
0.0
0
0.1
0.2
0.3
0.4
0.5
0.6
0.7
0.8